LIQUID-LIQUID SYSTEMS IN A CONTINUOUS TAYLOR-COUETTE REACTOR: UNDERSTANDING TRANSITIONS AND USE IN APPLICATIONS

A Thesis

Presented to the Faculty of the Graduate School

of Cornell University

In Partial Fulfillment of the Requirements for the Degree of

Master of Science

by

Mayank Jhalaria

August 2016

ABSTRACT

Developing ways to enhance the mixing of two liquids is an industrially important topic because of limitations on mass transfer especially imposed by immiscibility. Applications of immiscible liquids in commercial settings generally include that of liquid-liquid extraction, formation of emulsions and use in reaction systems. A Taylor-Couette system could help resolve mixing problems and enhance mass transfer by maximizing the interfacial area between the immiscible liquids. This work looks at liquid-liquid Taylor-Couette flows, the development of its instability and use as an emulsifier to create silica microcapsules from microemulsions.

The first objective was to characterize the development in the dynamics of the flow in the system and understanding how the flow develops with changes in the operating parameters is important to know how to design an efficient reactor. The primary flow transitions are studied for several model systems, with varying physical parameters of the liquid, in an effort to quantify these transitions. How the addition of surfactants to depress the interfacial energy affected the system was also studied. We also looked at how converting the process into a continuous process by inducing axial flow affects these instabilities for different Reynolds Numbers. Finally, an attempt is made to predict primary flow transitions for a given pair of liquids based on the interfacial energy of the two liquids.

Secondly, we looked to apply these concepts to a reaction system. Silica microcapsules are an efficient way of storing sensitive materials due to their

high mechanical strength and their resistance to chemical treatment. Current methods for preparing these capsules require high-energy inputs due to the use of sonicators for emulsification as well as the inability to formulate a continuous process using such methods. Using the Taylor-Couette reactor as an emulsifier to generate microcapsules is studied. The sizes of the particles are characterized by two length scales that reflect the dispersed phase length scales expected in the system.

BIOGRAPHICAL SKETCH

Mayank Jhalaria was born in Nagpur, India in 1992 and spent most of his life in Mumbai, India. During his school years, Mayank was a participant in several quiz competitions and won or reached the final rounds of several district, state and national level events. He attended the Indian Institute of Technology (IIT), Gandhinagar for an undergraduate degree in Chemical Engineering from 2010 to 2014.

While at IIT Gandhinagar, he interned at Bharat Petroleum (BPCL) for a period of 1 month in the summer of 2012 and was stationed at their refinery in Mumbai. His project while there involved estimating operational and theoretical efficiency for box fired furnaces at the Catalytic Reforming Unit (CRU). In the summer of 2013, he spent his summer at the University of Saskatchewan in Canada working under Prof. Ajay Dalai. While in Canada, he estimated the life cycle emissions for green diesel (dehydrogenated vegetable oil) and biodiesel and compared the two to determine.

After wrapping up his undergraduate degree, Mayank moved to Ithaca, NY to pursue his Master of Science in Chemical Engineering at Cornell. He worked under the guidance of Prof. Y. L. Joo to complete his master's thesis and will be graduating in the month of August of 2016.

To my parents - Kishor and Renu Jhalaria

ACKNOWLEDGMENTS

I would like to thank my committee chair, Prof. Yong L. Joo from the department of Chemical engineering for his advice, guidance and support throughout the duration of this project, Prof. Mingming Wu for agreeing to be on my committee and for the discussion on the project that I had the chance to have with her.

I would also like to thank Prof. Margaret Frey for allowing me access to laboratories at the department of Human Ecology, Xia Zeng for teaching me how to operate the equipment used in those laboratories, CCMR (NSF DMR-1120296) for also providing access to their numerous facilities present across the campus at Cornell University.

Lastly, I would like to thank Mohammad Aljishi for his initial discussions and introduction to this project, Clement Wei Kang Sim for his help on the project while working on this for his Masters of Engineering project, other Joo group member for their valuable inputs and my family and friends for being there for me.

TABLE OF CONTENTS

LIST OF FIGURES

LIST OF TABLES

LIST OF ABBREVIATIONS

Re	Reynolds Number
Ta	Taylor Number
We	Weber Number
Ca	Capillary Number
TC	Taylor Couette
Ta_c	Critical Taylor Number
SEM	Scanning Electron Microscopy
DLS	Dynamic light scattering
TEOS	Tetraethoxyorthosilane

LIST OF SYMBOLS

ω	Rotation Rate
σ	Surface Energy
R_1	Internal Diameter
R_2	Outer Diameter
d	Gap width
η	Ratio of inner to outer radius
ν	Kinematic Viscosity
ρ_c	Continuous phase density
ρ_d	Dispersed phase density
μ_c	Continuous phase viscosity
μ_d	Dispersed phase viscosity
$\dot{\gamma}$	Shear rate
g	Gravitational attraction
ϵ	Energy dissipated
L_C	Reactor length
V_R	Volume of Reactor
T	Aspect Ratio
$\cos(\theta)$	Contact Angle
d_p	Droplet Size
ϕ	Volume fraction

λ_c	Wavelength
a_c	Wavenumber
f	Friction factor
Q	Flowrate
κ	Effectiveness factor
τ	Shear stress

CHAPTER 1

INTRODUCTION

1.1 History

Geoffrey Taylor's seminal paper in 1923 [1], which explored the stability of a viscous fluid in an annulus between two rotating cylinders forms the cornerstone for research on instabilities in Taylor – Couette flows. The theory and initial experiments done by Taylor in the non-turbulent regime have enabled researchers to build upon the idea of using such flows for various applications. Such a device was earlier used by Maurice Couette [2] to measure the viscosity of fluids and hence the name for unstable flows between rotating cylinders came to be known as Taylor-Couette flow.

The initial motivation behind Taylor's work came primarily from work done by Hopf, Mallock, Rayleigh and Couette. [2-5] Lord Rayleigh described the scenario for which stable flows would tend to become unstable due to the differing effects of centrifugal forces on differing fluid layers in the annulus. And thus mathematically Rayleigh's criterion [3] could be written as

$$\frac{d}{dr}(r^2 * \Omega)^2 < 0$$

Early experiments by Couette [2] and Mallock [4] had a fixed inner cylinder and an outer cylinder that could be rotated at various speeds, which thus satisfied Rayleigh's criterion for all possible values of rotation and therefore the flow, would always remain unstable. Experiments performed by Taylor were more generalized and were able to find transition points from stable to unstable flow as well for rotations in the same direction and disproving Rayleigh's criterion for the case when cylinder rotations were in opposite directions.

The form of Taylor's experiments have been generally adapted for all future research in the field of Taylor – Couette flow, with the possibility of having both the inner and outer cylinders rotating or only having the inner cylinder rotation and the outer cylinder fixed.

1.2 Introduction to Taylor- Couette Flow

Taylor couette flow is induced due the hydrodynamic instabilities in a cylindrical annulus through the application of rotation on the inner and/or outer cylinder of a coaxial cylinder system. The hydrodynamic instabilities are caused by the centrifugal forces within the system generated by the rotation of at least one of the coaxial cylinders. The advantages of any such potential system is that the rotation rates and residence times can be accurately

controlled through stepper motors and peristaltic pumps respectively and therefore reproducibility of results as well as conditions is possible. Although the initial purpose of such an apparatus was to measure the viscosity of reference liquids, such flow has found several other applications also over the years, such as Emulsion Polymerization [6,18], Nucleation and monodisperse particle synthesis [7-9], Heterogeneous catalysis [10-11], Liquid-liquid extraction [12], Particle Coating [53], Membrane separation [13], filtration [14], precipitation [15-17], three-phase encapsulation [19], and agglomeration [20].

From a mathematical viewpoint, such flow can be characterized as a symmetrical disturbance of an inviscid fluid in an annulus as was done by Taylor [1]. Taylor solved the equations of motion for the system and determined the characteristics of the system, initial development of disturbance as well as provided a dimensionless number that characterizes the flow. This number is called the Taylor Number and transitions to critical flow happen after a certain thresholding number is crossed.

$$Ta = \frac{2\omega^2 R_1^2 d^4}{\nu^2 (R_2^2 - R_1^2)}$$

$$Ta_c = 1896 \; for \; \eta = 0.9$$

Different flow structures are generated for different rotation rates and transition usually occurs at a critical rotation rate that is a function of the physical

properties of the fluid as well as properties of the Couette Cell. This transition point reflects the transition from Laminar Taylor Flow to Turbulent Taylor Couette flow. There have been several studies on understanding the transition mechanism as well as measuring the transition points for the various possible flow regimes for such a system [21-30]. The transitions are gradual and are accompanied by enhancements in fluid mixing as we move further down the chain. The phase space for a single fluid system has been studied in depth and Figure. 1 describes the entire explored phase space for all possible cases

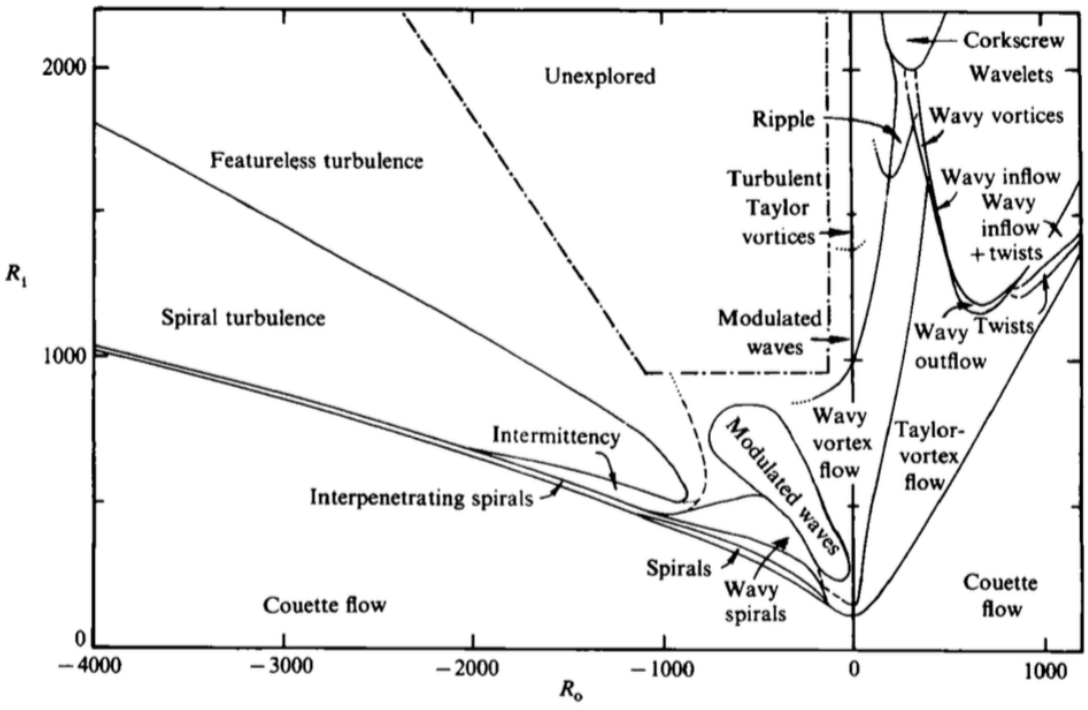

Figure 1. Phase space diagram for a single-fluid in a Couette Cell. Image taken from Andereck et al. [23]

Single-phase transitions reflect the change in regime of the fluid from laminar stable flow to turbulent unstable flow. Moving up the chain from laminar to turbulent is accompanied by a variety of different flow structures that also reflect their different mixing enhancements. When there is no co-rotation and only the outer cylinder rotates – laminar couette flow first transitions to vortex flow and then to wavy vortex flow and subsequently to modulated wavy vortex flow. These transitions reflect a change in inter-vortex mass transfer and as well as intra-vortex structuring. A general rule of thumb is – the more turbulent the flow higher is the inter-vortex mass transfer and therefore better is the mixing.

Transitions are categorized according to their relation to the Taylor Number and the Azimuthal Reynolds Number of the system. These numbers, along with the wave number can completely characterize the flow in the system and makes it possible to quantize the laminar to turbulent transitions. There have been several studies, experimental and theoretical, to measure the critical Taylor Number for transition from laminar to turbulent flow. Chandrashekaran [32] and Snyder [33] have the earliest literature on this topic and have been used as the basis for future works on the topic. The Reynolds Number and Wave Number is described below

$$Re_\theta = \frac{\omega R_1 \rho d}{\mu}$$

$$a_c = \frac{2\pi}{\frac{\lambda_c}{d}}$$

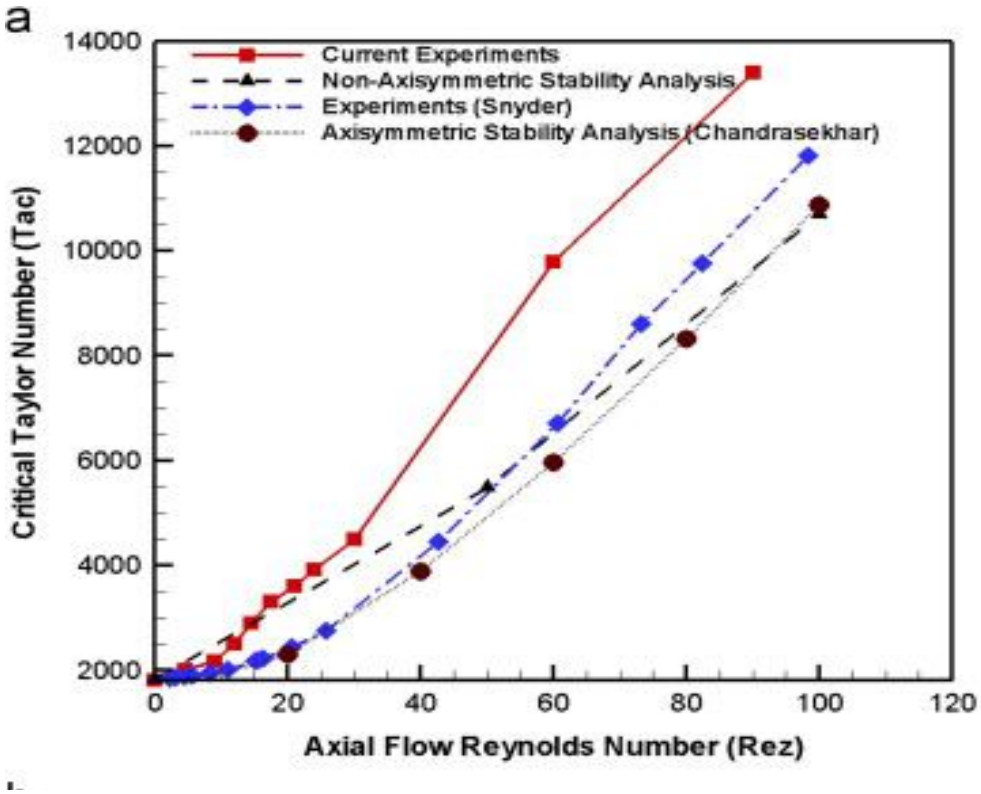

Figure 2. Effect of annular axial flow on the critical Taylor Number for a single-phase system. Image taken from Aljishi et al. [7]

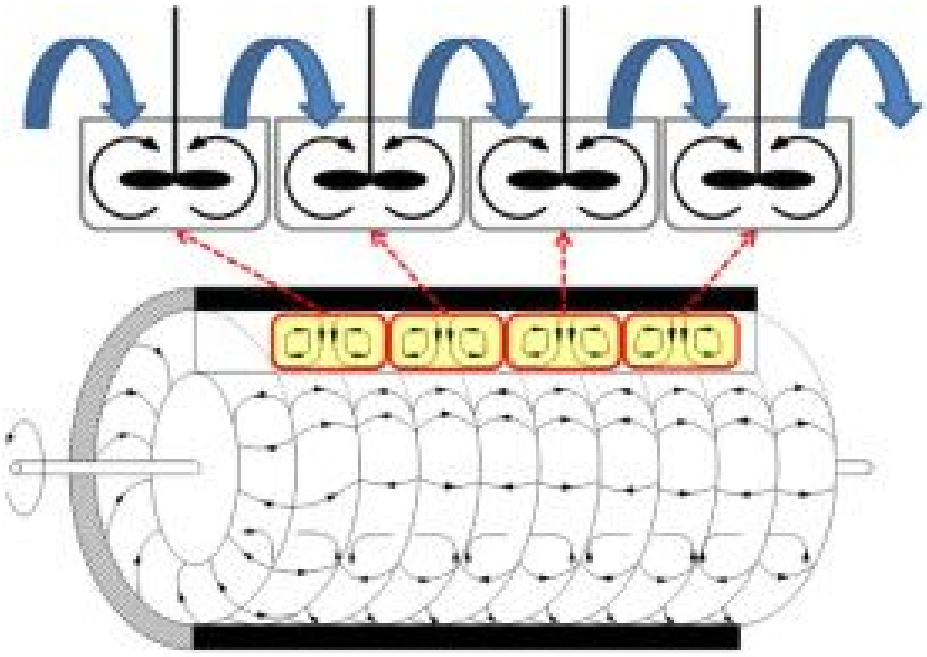

Figure 3. Development of vortices in a Couette cell and their model as a series of CSTR's. Taken from [20]

A fluid undergoing Taylor Vortex Motion in a Couette cell could be modeled to represent a series of micro stirred tank reactors with high mixing coefficients, which reflected the mixing enhancement, expected in the system. Microscale CSTR's reflect an individual vortex in the system and how each vortex can perfectly mix its contents. The diffusion layer between each counterrotating pair of vortices behaves like an ideal plug flow reactor with uniform mixing in the radial direction. This was shown earlier by Kataoka et al. [33]

The systems studies for understanding transition between the flow regimes are usually simple single-phase liquid systems and are studies by either visual measurements or laser-based measurement techniques. Earlier studies are all exclusively visual studies but the development of techniques such as Particle Image Velocimetry (PIV) and Planar Laser Induced Fluorescence (PLIF) have helped develop a better understanding of these systems.

1.2.1 Planar Laser Induced Fluorescence

Planar laser induced fluorescence is done by creating a laser sheet for examining a specific cross section of the flow. Flow through and in the cross section illuminated by the laser sheet can be visualized by doping one of the phases with a fluorescent dye that is excited when the laser sheet is imposed on the system. A schematic for such a set up in a Taylor Couette system is provided below and illustrates how the laser sheet could be used to visualize spatial orientations within the system.

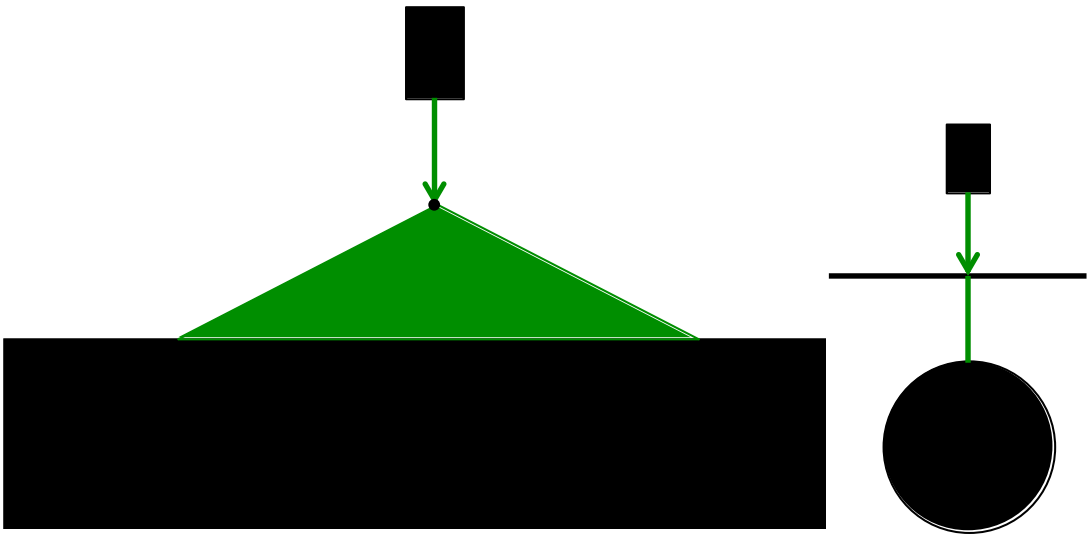

Figure 4. Schematic of laser induced fluorsecence imaging as used in this work. First image is the front view and second image is the side view.

Planar laser induced fluorescence helps us understand the spatial distributions of the vortices and other things within the system. The choice of fluorescent dye is critical and should be done keeping in mind – the solubility and compatibility with the test fluid, excitation at the chosen laser wavelength and it's chemical inertness to all else within the system.

1.2.2 Particle Image Velocimetry

Particle image Velocimetry [34] is an important tool that helps researchers measure the instantaneous fluid velocity at spatially different points as well as other fluid properties in the system of interest. Seeding the fluid with small isotropic particles that follow the streamlines developed within the fluid is the key behind the PIV technique. It enables researchers to develop two-dimensional as well as three-dimensional flow field structures for systems of interest. A standard PIV apparatus consists of – a high-speed and resolution camera, a laser illuminating a small region of flow and a synchronizing trigger.

1.3 Industrial Significance

The possibility of implementing such Couette systems industrially could be especially key in areas where mixing is a critical aspect of how reactions or other chemical interactions take place. Such systems provide the possibility of converting low throughput processes with high-energy consumption to high-throughput processes with low-energy consumption.

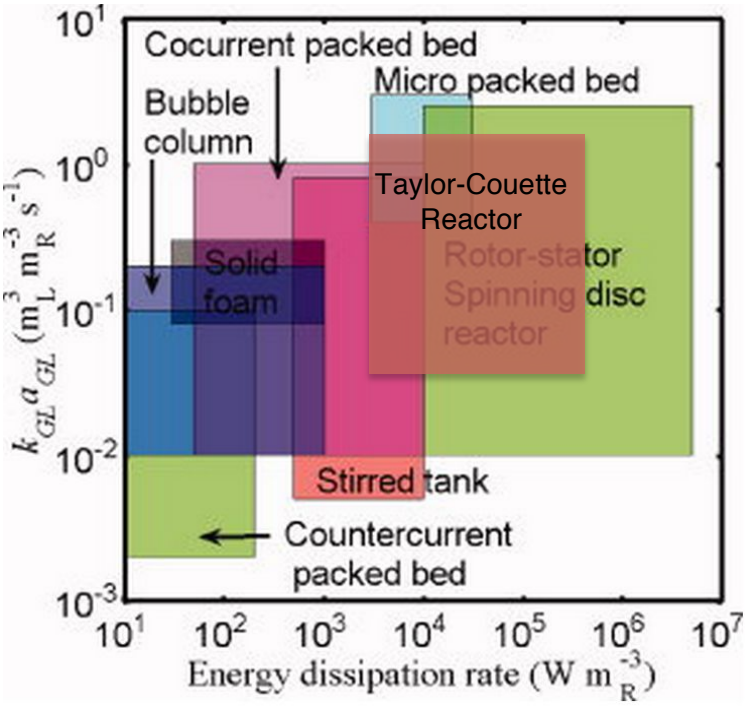

Figure 5. Volumetric mass transfer coefficient as a function of energy dissipation, for a variety of multiphase reactors. Image taken from [35] and modified to include a hypothetical position for a Taylor-Couette contactor

A hypothetical position for the Taylor-Couette reactor is also provided in the schematic that compares it with other applicable multiphase contactors. A Taylor Couette contactor will have an order of magnitude better mass transfer coefficient than a conventional stirred tank reactor while maintaining the possibility of achieving high throughputs that are the advantages of stirred tank systems. Methods such as Ultrasonication or Acoustic Wave emulsification, which have many orders of magnitude higher energy dissipation rates, are not included in this analysis.

The physical properties of the vortex structure also help enhance mass transfer by maximizing surface area and by reducing aggregation through turbulence. Aljishi et al. [7] showed that for crystallization and precipitation studies in such a system, monodisperse distributions are obtained within the system as there is no effective boundary layer within the system and all particles in the system spend an equal amount of time in the annulus after the flow reaches the unstable regime.

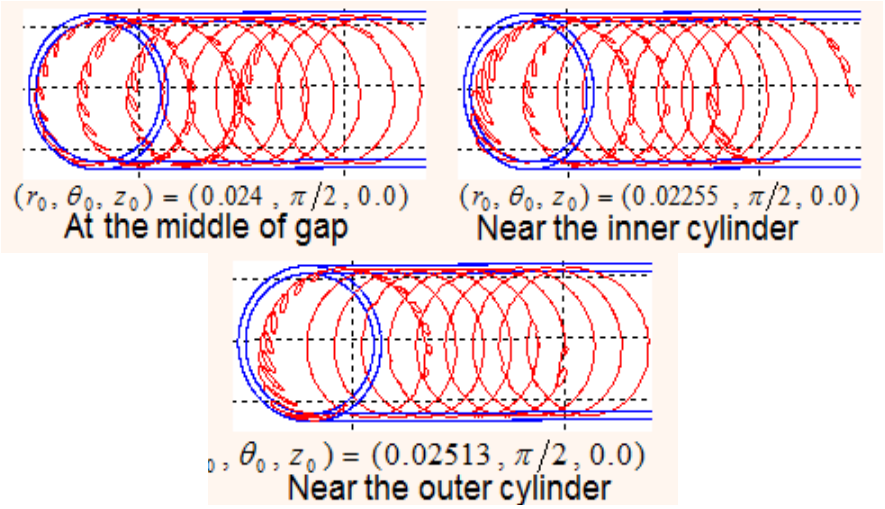

Figure 6. Particle trajectory analysis for particles at different spatial positions in the annulus. Taken from Aljishi et al. [7]

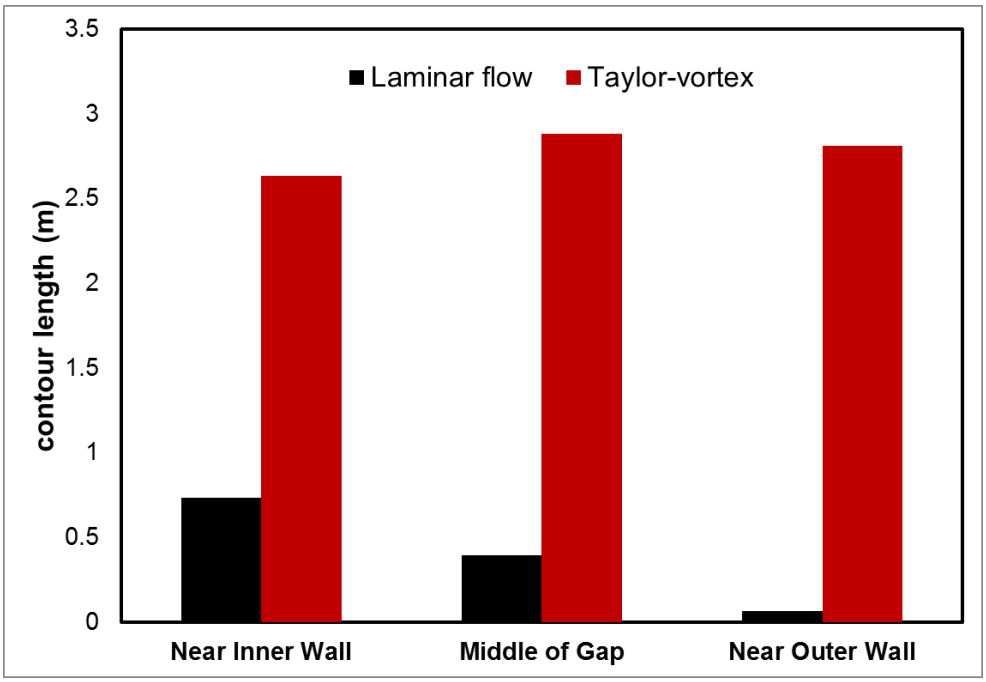

Figure 7. Contour length analysis for different particles in the annulus. Image taken from Aljishi et al. [7]

1.4 This Work and existing work in the field

This work focuses primarily on the flow induced when the system contains 2 immiscible liquids as compared to the body of work that is based on the flow of a single fluid. We are looking at the conditions that influence the first and second transitions of flow and therefore work with lower rotation rates. Finally, we want to study an application of these flows to a real life system.

There has not been much in terms of work done to understand the dynamics for flow in immiscible liquids apart from a few works that form the basis for the work done in this thesis. Different orientations of the system produced different results and there is published literature for both horizontal and vertical orientations. In terms of applications, stratified flows for contactors are used in liquid-liquid extraction and dispersed flow of liquids within the field of reaction engineering.

In the earliest case, Joseph et al. [36] investigated the numerical stability of centrifugal stratification and proposed the following relation for global stability

$$J_i = \frac{(\rho_2 - \rho_1)\omega^2 R_i^3}{\sigma}$$

For J_i > 4, global stability is achieved for such flows and liquids could be stratified with instabilities present in each phase. Joseph and co-workers [37] also explored the phase space for immiscible liquid Taylor-Couette flow with a stationary outer cylinder and a rotating inner cylinder. The modes observed were – a) A homogenous emulsion, b) Rollers involving axisymmetric blobs of the oily phase attached to the inner cylinder and the water undergoing vortical motion, c) Banded flow.

Baier and Graham [38] studied the case of centrifugally stratified fluids in a Taylor-Couette contactor, where both the inner and outer cylinders could be co-rotated to achieve such a configuration. They showed that stratified flows where the denser liquid lies above the lighter liquid are prone to Kelvin-Helmholtz instabilities, which precede and dominate over the effects of the Taylor-Couette instability. They also formulated the linear theory for such configurations for the prediction of stability and velocity profiles.

Since we were more interested in droplet based flows of immiscible liquids rather than centrifugal stratification, these papers provided an interesting reference point for predicting properties of our systems.

PA Haas [39] looked at dispersion of aqueous droplets in the organic liquids and proposed a droplet size correlation that is widely used to predict the size

of droplets in the annulus for multi-phase flows. The correlation is shown below and Sathe et al. [40] showed it to be sufficiently accurate by measuring droplet sizes using optical techniques.

$$\frac{d_p}{D} = 150We^{-0.65}Re^{-0.2}\left(\frac{\mu_d}{\mu_c}\right)^{0.5}\left(\frac{d}{R_1}\right)^{0.5}$$

Where the parameters reflect the general trend followed through this thesis.

Campero and Vigil [41] studied flow structures with liquid-liquid Taylor-Couette-Poisuelle flow with very weak axial flow rates being induced within the system. They observed 3 different flow states for their operating range of parameters – alternating vortices that translate at a velocity different from the bulk velocity, a phase inversion where the kerosene phase became the continuous phase with no spatial variations in the vortex structures and one where the vortex structure alternated between the banded and homogenous inverted phase described above. An interesting observation made by the authors of the paper was the periodic propagation of a phase inversion that would create a homogenous emulsion within the system.

Zhu and Vigil [42] described the conditions that lead to banded flow and homogenous emulsions for flows involving two liquid systems. They looked at the characteristic time scales of droplet migration from vortex cores due to

eddy diffusivity and the effect of centrifugal force on the systems and defined a ratio of these two quantities. The transition happened when the value of the ratio was close to 1 as described below. The physical properties of the fluid and annulus dimensions were critical to this explanation but there were certain flaws in the reasoning, which did not encompass all possible combinations of fluids. Their reasoning for the origin of homogenous flow does not hold when the dispersed phase is heavier than the continuous phase.

Zhu and Vigil [43] also showed that inter-vortex diffusivity depends on the flow pattern of the system and showed that this value only increases after a certain critical Reynolds Number threshold is reached. This correlates to a change of laminar vortices to turbulent vortices, which promote such inter-vortex mass transfer.

Sathe et al. [40] studied the evolution of different flow regimes in a vertical Taylor-Couette reactor for a two-phase system. A complete analysis using a combination of PIV, PLIF and CFD was done to explain the origin of flows in such a systems. Since all experiments were done using an equal volume fraction of the organic and aqueous phase, the evolution of instabilities for different volume fractions was not analyzed for the given system, which is what separates this thesis from most of other papers out in the field. They also compared a theoretical droplet size prediction with their own measurements

from experiments for turbulent flow and found that there is a sufficient fit from experimental data for the correlation to be valid for vertical systems as well. They showed that for vertical systems, centrifugal forces due to inner cylinder rotation are the dominant forces within the system at higher rotation rates and are the origin for banded flows within the system.

Flow in couette cells has also been used to suppress coalescence in surfactant-stabilized emulsions in shear flow induced by rotation of an inner cylinder. A paper published in 1999 by Nandi et al [44] who looked at transient development of particle sizes in a shear-stabilized couette cell system showed this. They showed that below critical transitions, couette flow could stabilize emulsions and prevent coalescence much better than a quiescent or stirred system. A combination of droplet break up and coalescence suppression are the key factors for this observation.

CHAPTER 2

EXPERIMENTAL SETUP, MATERIALS AND METHODS

2.1 Experimental Setup

The experimental setup used for all experiments performed in this project is a Taylor-Couette cell with horizontal orientation; no experiments were done with a vertical orientation of the reactor. The physical dimensions of the reactor are provided in Table 1 and the ratio of the inner and outer cylinders for all experiments was fixed at ~ 0.9. The outer cylinder of the reactor was constructed from plexiglass while the inner cylinder was constructed from aluminum. None of the materials used in the experiments interacted chemically with the construction materials and therefore all results are purely a function of physical interactions. The large aspect ratio ensured that end effects were neglected within the system and the primary instability was the Taylor-Couette or in some cases the Kelvin-Helmholtz instability.

The rotation rate of the inner cylinder was controlled with a Hyundai Stepper Motor, which had a resolution of 1 RPM and had a minimum of 30 RPM and maximum of 1700 RPM. The stepper motor was not completely accurate and had an error of +/- 5 RPM at higher rotation speeds. Since most data points are also reported with a similar error and it's effect on transitions decrease with increasing rotation rates, this variation was deemed to be irrelevant.

Axial flow was induced in the system using a Watson Marlow Peristaltic Pump having a double motor. Pre-mixed liquid was introduced using a 3/16" diameter with a wall thickness of 1/16", PVC tubing into the reactor from the top of the reactor setup and had an operating range of 30-880 mL/min for the tubing diameters used in the setup. The peristaltic pump had an internal error of $\pm 2.7\%$ which is not considered significant for the system.

The temperature at which the system operated was fixed at room temperature for all experiments, and energy dissipated within the reactor did not contribute greatly to any increase in the temperature. As the setup was installed in a fume hood, any energy generated was quickly dissipated into the atmosphere.

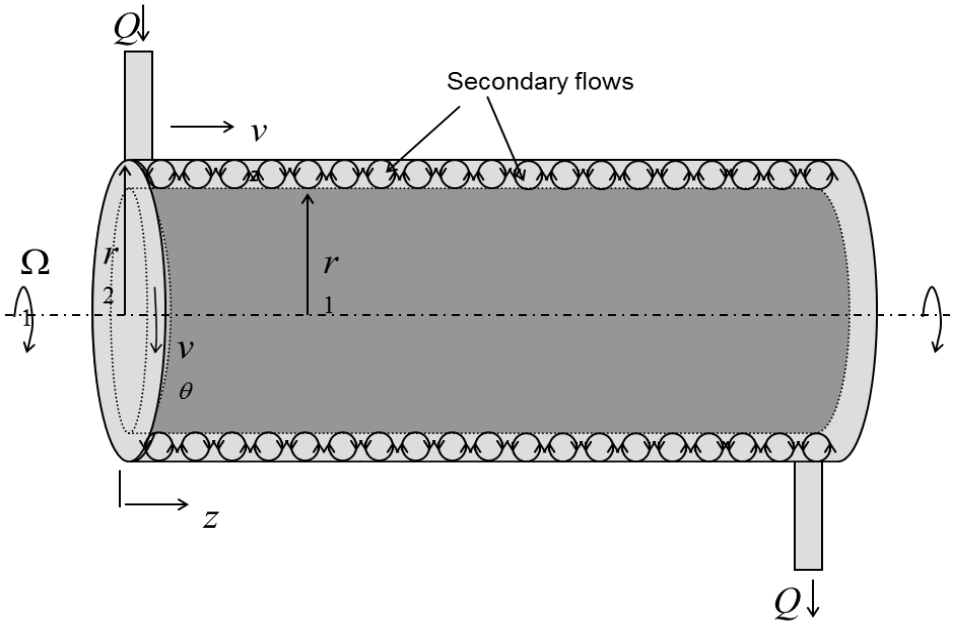

Figure 8. General Schematic for the Taylor-Vortex setup used for all experiments within this thesis.

$\boldsymbol{L_C}$	$26.6 \pm 0.1\ cm$	$\boldsymbol{R_2}$	$2.537 \pm 0.01\ cm$
$\boldsymbol{R_1}$	$2.279 \pm 0.01\ cm$	$\boldsymbol{d}$	$0.258\ cm$
$\boldsymbol{\eta}$	0.898	$\boldsymbol{T}$	103.1

Table 1. Physical parameters of the Couette cell used for all flow visualization and characterization experiments

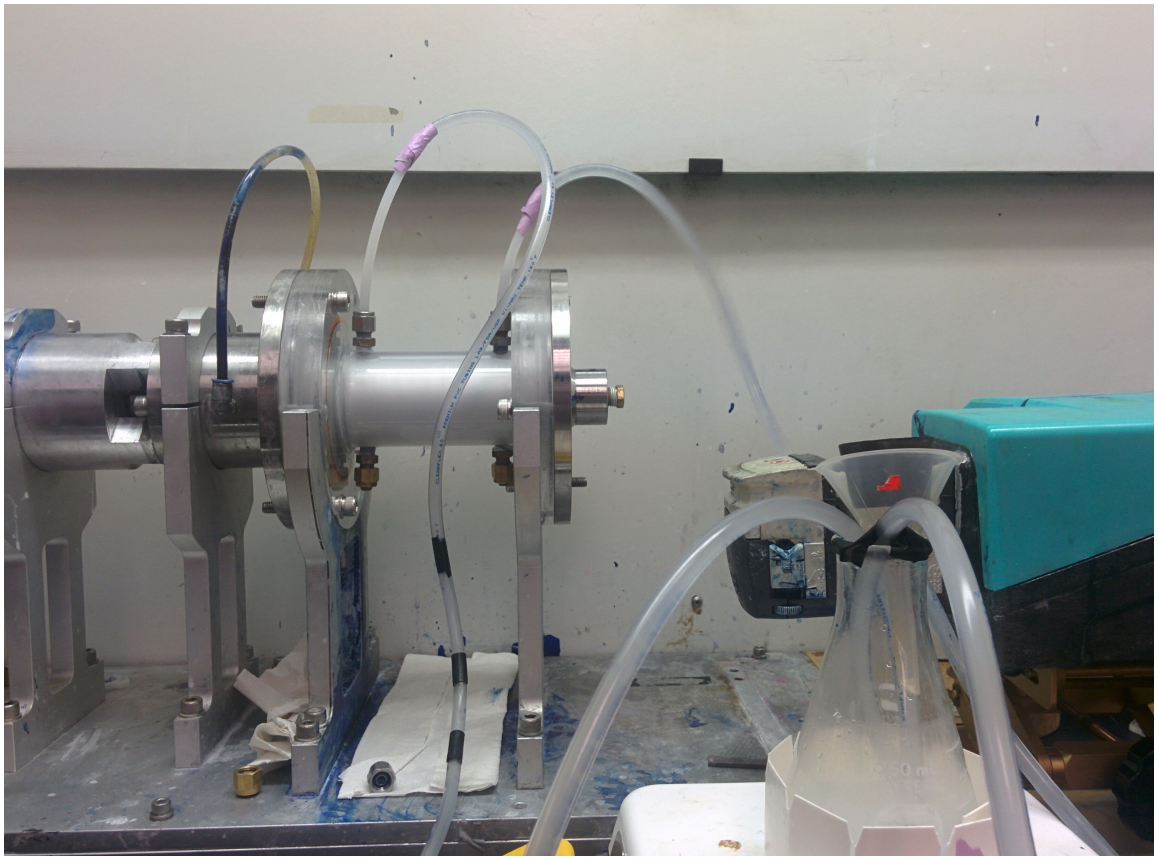

Figure 9. Experimental setup used in actuality.

The large aspect ratio T prevents longitudinal instabilities in the system and prevents end effects. The optimal value of the aspect ratio is $T > 20$**.** (ref)

2.2 Chemicals Used

All chemical used in this work were at the very least analytical grade. Deionized water was used for all experiments. Kerosene (4L, low odor) was purchased from Baker Inc. Sodium Iodide (ACS Grade) was purchased from BDH, VWR Analytical Corp. Hexadecane (> 99%), Tetraehtylorthosiliacte (TEOS, 98%), 3-Methacroloxypropyltrimethylsilane (97%), Rhodamine-B (> 97%), Cetyltrimethylammonium Bromide (CTMA-Br, >98% powder), Methylene Blue and Oil-Red O were purchased from Sigma-Aldrich Inc. Flamenco Super Pearl was purchased from BASF Co. Benzene (99%) was purchased from EMD Millipore Inc. Glycerol (liquid, > 99.5%)was purchased from Macron Chemicals Inc. Triton X-100 (liquid, > 99%) was purchased from Amresco Chemicals.

2.3 Methods and Characterizations

2.3.1 Flow Visualization

It was important to stain at least one of the liquids used in the system with a dye to enable optical detection. Water was stained with Methylene Blue at a concentration of 0.3 g/L and Kerosene could be stained with Oil-Red O at a concentration of 0.1 g/L. For laser induced fluorescence experiments, the aqueous phase was stained with Rhodamine B at a concentration of 100 mg/L. Addition of tracers was also done to both phases depending on the

application being studied. The concentration of the solid tracers (Flamenco Super Pearl) was 500 mg/L irrespective of the phase in which the tracer was being added.

2.3.2 Centrifuging

Figure 10. Bench scale centrifuge used for separation of solids from suspensions. The system had a maximum operating speed of 6500 RPM.

Centrifuging was done to separate the modified tracers from its suspension. A VWR Clinical 100 centrifuge with a maximum speed of 6500 RPM was used for the separation. Samples were placed in 15 mL holder tubes manufactured by VWR from Polypropylene, before being placed in the centrifuge. Samples

were usually centrifuged for 30 minutes at 6500 RPM. Centrifuging exploits density differences between the different materials and forces the denser material downwards to settle at the bottom and the lighter material upwards.

2.3.3 SEM and EDS

SEM and EDS was done using Tescan Mira3 FESEM installed with a Bruker QUANTAX EDS system. EDS data was analyzed using the ESpirit software provided by Bruker that collects, interprets and presents data that could be easily understood. SEM images were captured using the InBeam setup, with a standard working distance of 4 mm and an accelerating voltage of 10 kV. Some images were taken using higher accelerating voltages as well i.e. 20 kV and 30 kV. Scanning electron microscopy uses a focused beam of electrons to scan the image and signals detected post interaction with the sample provides details about the surface topography and elemental composition on the surface. This provides a powerful tool for looking at surface properties at the micro and nanoscale.

A beam of electrons on interacting with the sample generates a wide variety of signals – secondary electrons, backscattered electrons, diffracted backscattered electrons, photons and heat. The secondary electrons are the primary source of information for the morphology and topology of the samples.

2.3.4 FTIR (Fourier Transform Infrared Spectroscopy)

Fourier Transform Infrared Spectroscopy (FTIR) is used to obtain the infrared spectrum of emission and absorption for a sample. The final data is only obtained after subjecting the raw data to a Fourier Transform and hence the name. A Nicolet Mattson 5020 spectrometer with a KBr splitter and DTGS detector is used for FTIR measurements. Liquid samples were analyzed using a holder for the system. Infrared measurements were done between 600 – 4000 $cm^{-1.}$

FTIR measures the intensity of infrared beams after passing through or being reflected by the material being studied. Different molecular phenomenon and bonds interact differently with the infrared beam, which give rise to characteristic signals that correspond to specific phenomenon. The interaction frequencies for the bonds are known as the resonant frequencies.

2.3.5 TGA (Thermogravimetric Analysis)

Thermogravimetric analysis is used to quantify the weight of additional material or measure weight loss at different temperatures of different samples. The weight loss is associated with possible secondary bonded molecules to the primary sample or impurities in the sample. TGA analysis was done using a TA Instruments Q500 V20.10 Thermogravimetric analyzer at a heating rate of 10^{o}C/min up to a temperature of 550 ^{o}C.

2.3.6 DLS (Dynamic Light Scattering)

Figure 11. A Malvern Zetasizer Nano ZS used for hydrodynamic radius measurements.

Dynamic Light Scattering measurements for determining particle size distributions were done using a Malvern Zetasizer Nano ZS, which had a hydrodynamic particle measurement range from .6 nm to 6 um. The scattering light had a wavelength of 532 nm, and a clear disposable cuvette was used to store the sample. The measurements reported in this thesis correspond to the intensity-averaged particle sizes for the suspension.

When particles interact with the laser beam, they undergo Rayleigh scattering and form a speckle pattern that represent how the light was diffracted by each particle. As particles undergo Brownian motion, there is a time scale associated with their movement within the sample. Autocorrelating speckle patterns with this timescale can provide information on the size of the particles and their polydispersity based on the size distribution of the particles.

2.3.7 Refractometry

For effective visualization using laser-induced fluorescence, it became necessary to match the refractive indices of the components using extra additives. Refractive index measurements were done using a Abbe refractometer that is usually used to measure sucrose concentration in sugar extracts from cane. The light used for measuring the refractive index was sourced from the ambient environment and the refractometer could be adjusted to correct for dispersion. Refractive indices up to 1.6 could be measured accurately using this refractometer and therefore was an appropriate instrument for the liquids used in this study. The test liquid was sandwiched as a thin layer between the collection plate and the aperture for the light source for such a refractometer.

Fluid	Refractive Index
Water	1.333
Glycerol	1.4735
Kerosene	1.4225
60 wt% Sodium Iodide solution.	1.48
Water, Sodium Iodide and Glycerol 28.57 wt% Sodium Iodide 28.57 wt% Water 42.85 wt% Glycerol	1.458
Mineral Oil	1.47

2.3.8 High Speed Imaging

To capture images of the flow dynamics, high speed imaging was an important tool used. Imaging was done using a MotionPro HS-3 Camera connected to a laptop running Motion Studio x64. A Nikkor AS-F lens attached to a 2x teleconverter and apertures varying from f/22 to f/2.8 were used to capture images. Motion Studio x64 allowed us to vary the exposure time from 1.6 us to 33300 us and the number of frames captures per second from 30 to 1500 depending on the exposure time set.

High Speed imaging cameras like this one, have sensitive films with a rapid turnover time that allow fast capture of images. All images captured were in Black and White keeping in line with the capabilities of the high-speed camera used.

2.3.9 Ultrasonication

Ultrasonication was done using a Branson 500 W Ultrasonicator at an amplitude of 60% and pulse of 30s with a rest phase in between of 10s. Ultrasonication involves the use of sound waves to agitate the liquid to mix homogenously or to create emulsions. When sound waves > 20 kHz are used it is referred to as Ultrasonication. A lot of heat and sound energy is also generated during the process, which is why it becomes important to immerse the sample in an ice bath during the process. The ice bath absorbs most of the heat generated thus helping keep the temperature of the mixture down.

2.3.10 Laser Sheet Visualization

Developing a holistic understanding of how the two liquids behave, laser sheet visualization is an important tool to study flow structures in the gap between the inner and outer cylinder. A laser sheet perpendicular to the flow through the gap is required for such optical visualization. This is done by passing a laser beam through a thin cylindrical glass rod, which splits the beam into a sheet of light. The light is used to excite a fluorescent dye in one of the phases and reflect off anisotropic tracer particles in the other phase, thus giving a

picture of the spatial distribution of the phases with respect to the inner and outer cylinders.

2.4 Surface Tension Measurement

An important scope of this study is the how surface tension between liquid pairs affects transitions between different flow structures. Varying liquid pairs gives us the possibility of constructing a possible phase diagram for transitions and the effect of surface tension on these transitions. Surface Tension (or Surface Energy) between two liquids was measured using a method described by Rashidnia et al. [45]. This method was based on a capillary rise measurement method due to surface forces between two liquids.

$$\sigma_{12} = \sigma_{1a} * \left(\frac{\cos(\theta_{1a})}{\cos(\theta_{12})}\right) + \frac{\rho g r}{2\cos(\theta_{12})}(h_1 + h_2 - L_1)$$

The first step involves measuring the surface tension between air and the liquid that is to be in contact with air i.e. the lighter phase. This forms a basis for the calculation of the interfacial tension between two immiscible unreactive liquids using the capillary rise method.

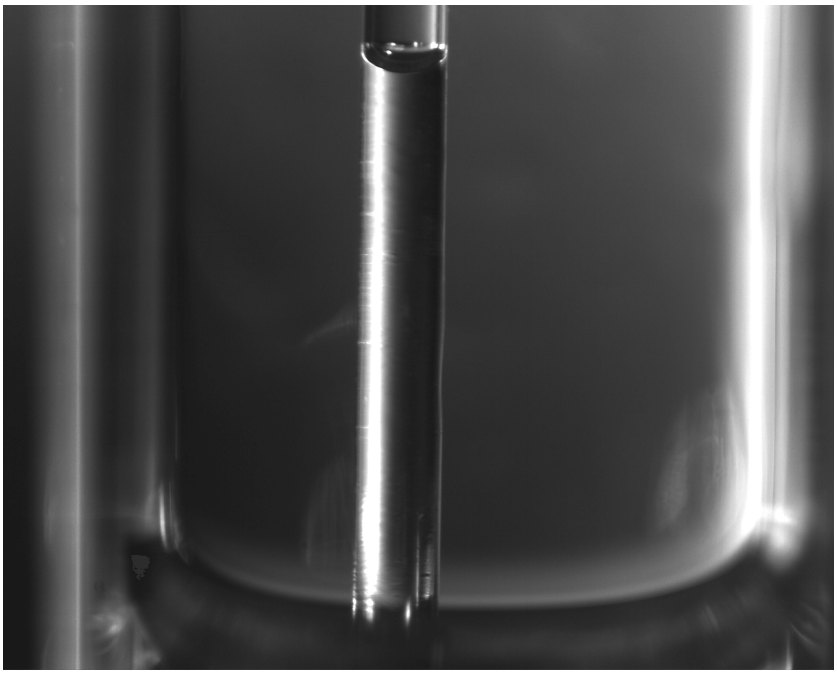

Figure 12. Contact angle and capillary length measurement for calculating the surface tension at the Air-Liquid Interface

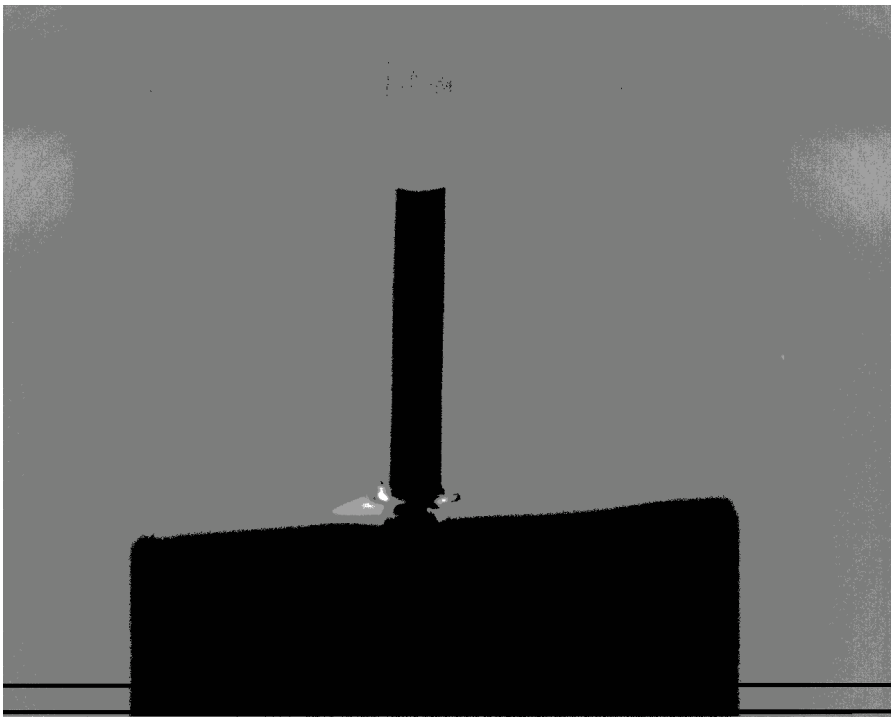

Figure 13. Contact angle between two liquids for calculating interfacial tension

Phase 1	Phase 2	Surface Tension (mN/m)
Kerosene	Water	29.7
Hexadecane	Water	22.3
Mineral Oil	Sodium Iodide/Water/Glycerol	22
Kerosene	Water w/Surfactant (0.1 g/L)	19.9
Kerosene	Water w/Surfactant (0.5 g/L)	17.2
Kerosene	Water w/Surfactant (1 g/L)	.78

Table 2. Calculated values of surface tension pairs for the test liquids used in this work

All values of surface tensions calculated using this method are approximate values and small changes in Contact Angle measurements have a substantial effect in surface tension values. Therefore all values are treated with a tolerance limit of $\pm$ 10 %.

2.5 Amphiphilic Tracer Particles

Amphiphilic Tracer particles were prepared for flow visualization experiments. Most tracers that are traditionally used in flow visualization experiments are hydrophilic and therefore show preferential treatment to the water-based phase. The advantage of using partially modified tracers in these experiments is for their ability to arrange themselves on the boundary of the water-organic interface. This is very important for identifying the spatial positions of the organic phase in the gap for the cases where the continuous phase is the water-based phase. This method was based on the method described by Nur et al. [46] who synthesized catalysts this way.

The tracers used in these experiments were TiO_2 modified Mica flakes, sold under the trade name Flamenco Super Pearl by BASF. The Titanium moieties on the surface contribute to the hydrophilicity and provide an avenue for the modification of the particles using Organosilanes. 1g of the tracer was mixed with 0.5 cm^3 of Water and mixed well with a Spatula to ensure even mixing. 0.124g of 3-Methacroloxypropyltrimethylsilane (Sigma Aldrich, 97%) mixed with 10 mL of Benzene (EMD Millipore, 99%) and stirred for 10 minutes. The mixture was centrifuged to separate the solid and washed with ethanol twice.

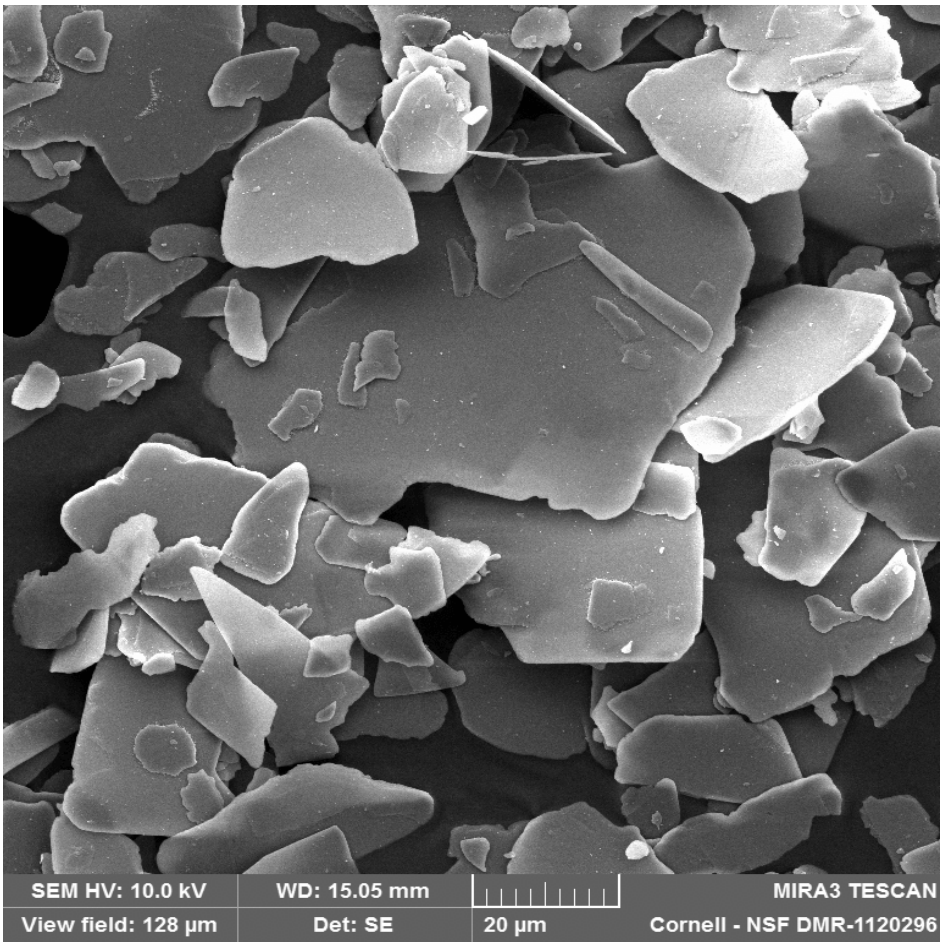

Figure 14. SEM Image of the hydrophobic tracer used in the experiments. A large aspect ratio is observed from the images.

The resultant wet solid was dried at 110 ℃ for 1 hour before it can be used as a tracer. The powder was characterized using SEM, EDS and FTIR, which confirmed adhesion of the organosilane on the surface. Adding premeasured quantities of the powder to a Water-Kerosene mixture showed an arrangement in the organic phase and the liquid-liquid interface, which confirmed its partial amphiphilicity and hydrophobicity.

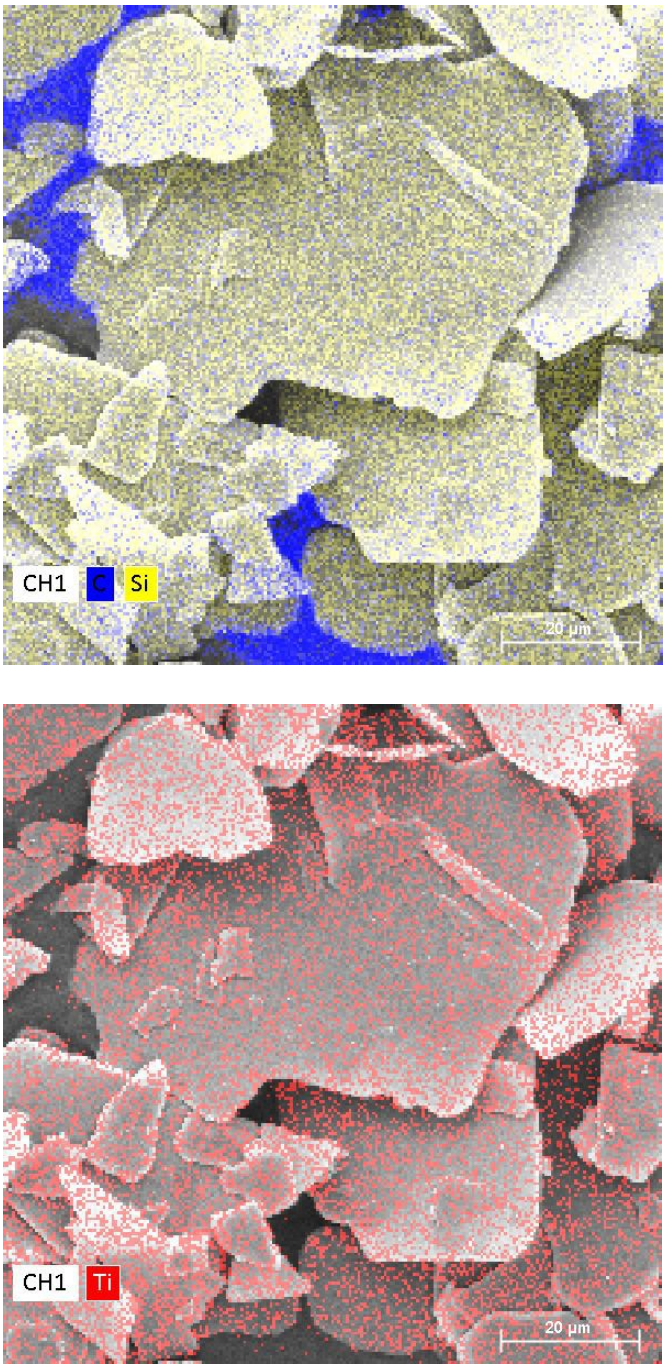

Figure 15. EDS Images for the modified tracer particles. Presence of silica and carbon on the surface indicates successful grafting of the organosilane on the surface.

CHAPTER 3

FLOW VISUALIZATION AND CHARACTERIZATION

3.1 Introduction

The purpose of flow visualization is to understand how flow characteristics can be used to determine most favorable conditions for a variety of applications. Interactions between the two immiscible liquids become increasingly important as well as their spatial orientation and effective mass transfer area depending on the application in question. The aim of these experiments was to understand how flow dynamics affect these properties and how primary transitions happen for this type of flow. This thesis looks at the two initial primary transitions that span the transition from laminar to turbulent flow as well as how fluid dynamics affects the dispersion of the minor phase in the continuous phase of the liquid.

For a liquid-liquid system there are several parameters that could be modified to change the system dynamics. The parameters that are varied for the experiments done in this thesis are listed below

1. Volume Fractions of the Organic Phase: 0.1, 0.2, 0.3, 0.4, 0.5, 0.7, 0.9
2. Rotation of the inner cylinder: 30 – 1500 RPM

3. Axial Flow Rates: Residence Times in the column: 1 minute, 30 seconds and 15 seconds
4. Fluid pairs with varying densities, viscosities and interfacial energies.
5. Fluid pairs with identical densities and viscosities and varying interfacial energies.

3.2 Observed Flow States

Through the course of flow visualization experiments, three primary flow states were observed that characterize the system for the flow rates studied in this thesis. Phase diagrams were subsequently constructed that tracked the transitions between these flow states for different volume fractions of the organic and aqueous phases. The three primary flow states for which transitions were tracked through the course of experiments. It also becomes important to understand which forces dominate within each flow regime, as these forces determine the spatial distribution of the dispersed phase within the continuous phase. The primary forces that are acting on the fluids are – centrifugal forces, gravitational force, interfacial tension and shear forces due to vortical motion. A balance on the forces provides the theoretical understanding for how this distribution takes place, while laser induced fluorescence visualization provides experimental evidence of this.

Stratified Flow

Stratified flow is the primary flow state observed for really low rotation rates. This regime is characterized by a continuous boundary between the two immiscible liquids. The surface between the two is not broken to induce droplet based flow, but each fluid is individually chaotic if the rotation rate is beyond the critical rotation rate for that liquid.

Segregated flow

Segregated flow is characterized by the breakup at the surface of the two liquids and the formation of non-continuous surfaces between the two liquids. Large macroscopic droplets with no definite streamlines are the characteristics of this flow. This flow state is always observed after the stratified state and the primary transition for these flows is reflected by dropletization of the dispersed phase.

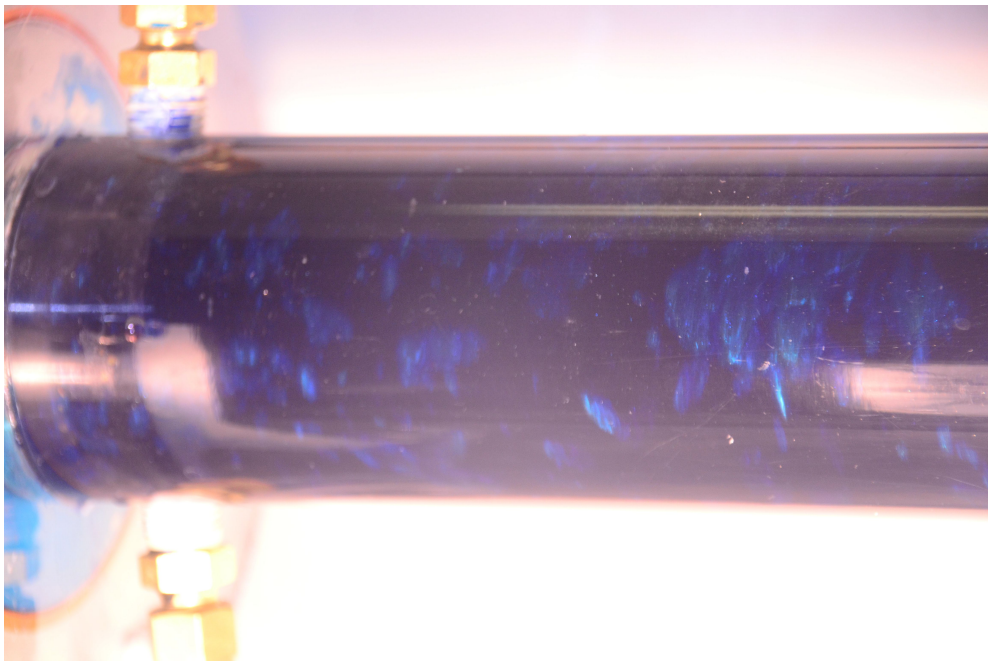

Figure 16. Image of the column during segregated flow characterized by large slugs of the dispersed phase flowing the annulus.

Banded Flow

Banded flow is characterized by the formation of bands at the inflow and outflow boundaries of the vortices that give the representation of alternating phases of fluids. The bands are usually richer in the dispersed phase than the rest of the mixture, while the other parts of the flow are leaner in the dispersed phase. The bands are formed when the shear force breaks the droplets into length scales that can be easily influence by the vortical motions. This gives rise to the lighter fluid moving to the boundaries of the vortices.

On the addition of axial flow, the bands start translating in the direction of the axial flow but not at the same axial velocity as that of the induced flow.

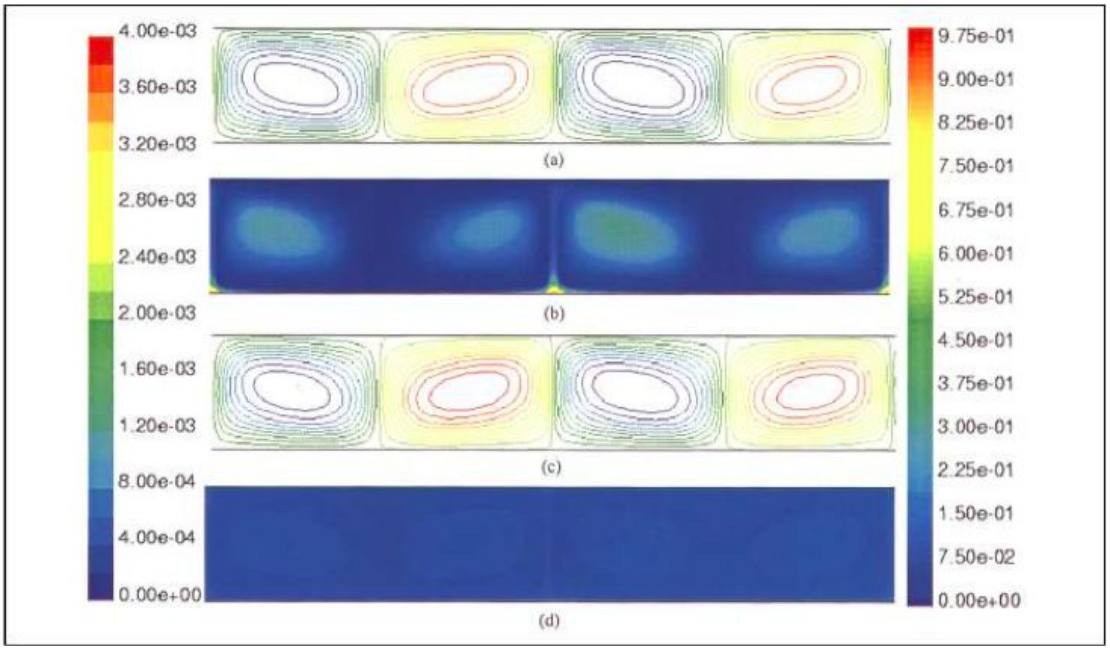

Figure 17. Fluid dynamic simulations of the origins of banded flow in Liquid-liquid Taylor Couette flows. The dispersed phase arrange themselves on the outflow boundaries of the vortices and in the core of the vortices thus explaining the observed structure. Taken from Zhu and Vigil [42]

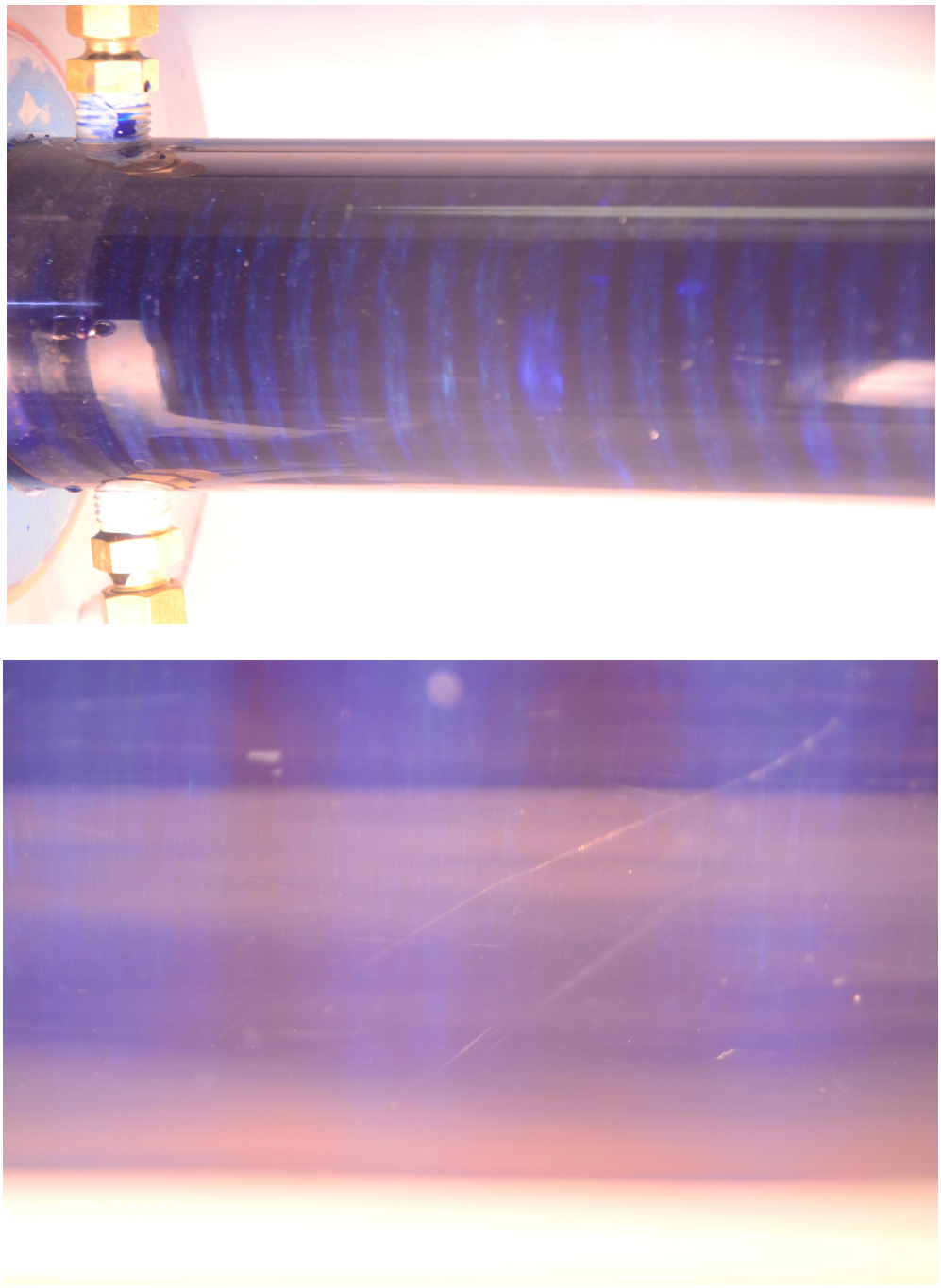

Figure 18. Bands propagating in the column (with no axial flow) and b) a close up of the bands in the column.

Travelling Modes of Flow

On the addition of axial flow to the system, another flow state is observed in which bands translate in a direction opposite to the direction of the induced axial flow. This forms one of the primary traveling modes observed on the addition of any axial flow to the system. The origin of these modes is hitherto unknown and has not been explored further in this thesis.

3.3 Other Phenomenon

No emulsified state

No conditions were observed for regular parameters where the flow was completely emulsified. Zhu and Vigil [42] developed a theory, which explains the conditions that lead to the formation of these emulsions. The underlying principle behind the idea is the neutrality of spatial positions of droplets. It should be equally probable that droplets reside either within a vortex of on the boundary of a vortex. When this condition is satisfied the flow exists in a emulsified state.

$$\tau_c = \frac{9\mu_c}{8(\rho_c - \rho_d)u_\theta^2}\left(\frac{d}{d_p}\right)^2$$

$$\tau_t = \frac{D^2\rho_c}{16\mu_t}$$

$$\frac{\tau_c}{\tau_t} = \frac{18\mu_c\mu_t}{(\rho_c - \rho_d)\rho_c d_p^2 u_\theta^2}$$

The term τ_c and τ_t reflect the time scales of transport of a droplet from the vortex periphery to the vortex core and vice versa respectively and therefore a ratio of these two parameters would define the importance of one mode of transport over the other.

For the range of parameters used in these experiments, the value of this quantity lies between the values of 0.2 – 0.5 and hence we don't observed a well characterized homogenous flow.

Hysteresis

An interesting phenomenon also observed over the course of the experiments was that of hysteresis. Depending on the direction of approach i.e. either going low from a higher rotation rate or going higher from a lower rotation rate, the form of flow formed at a certain speed persists even though it falls on the other side of the transition boundary. It's a form of Hopf bifurcation where the current state persists for a while before reverting to the most stable state at that particular rotation rate.

For the purpose of their thesis, all experiments were done where the rotation rate was increased (and not decreased) and therefore the phenomenon of hysteresis was neither encountered nor studied during the course of this work. Some papers have analyzed such bifurcations [47,48].

3.4 Chaos in stratified flow

At low rotation rates, the flow remains completely separated from each other. A continuous boundary that separates the two liquid phases characterizes the system. At low rotation rates even though each individual liquid phase undergoes transition to it's unstable form of Couette flow. Based on a critical Taylor number of 1896 [7] for single phase fluids undergoing transition from stable to unstable flow in this setup, the critical rotation rates for the experimental fluids used in this thesis is shown below. Sathe et al. [40] observed similar phenomenon even for vertical oriented columns for liquid-liquid Taylor Couette Flow and therefore the appearance of such phenomenon for horizontal columns is not unexpected.

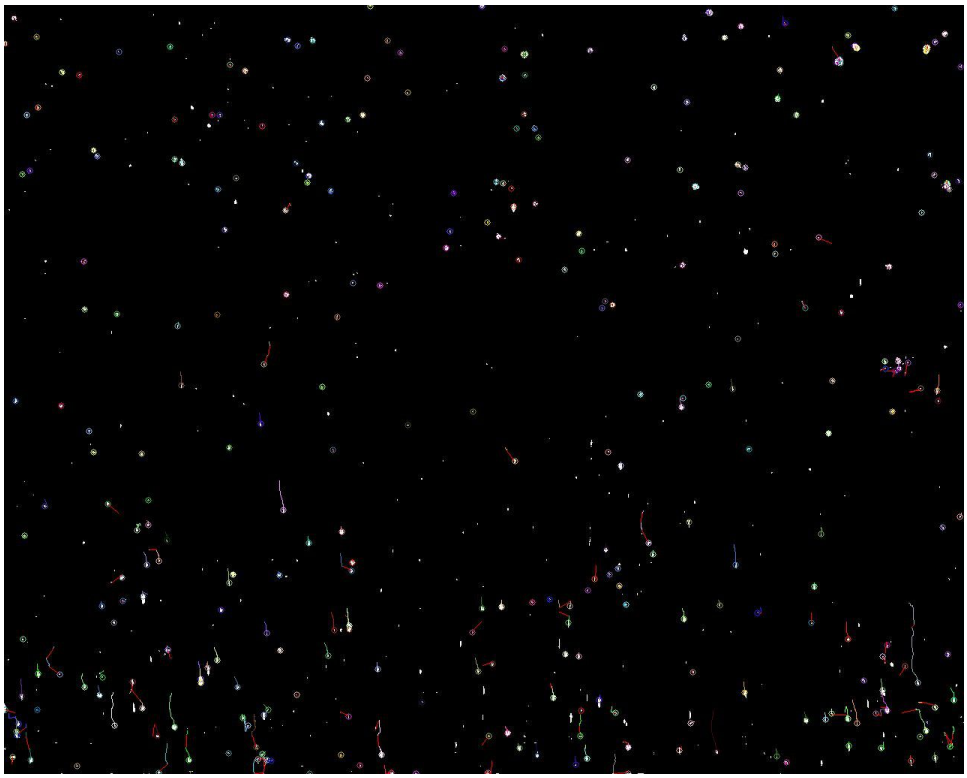

Figure 19. Streamlines show particles moving randomly into the plane of the image, downwards in the plane of the image and in random brownian motion. This image was taken at 57 RPM for a Kerosene-Water System, with kerosene having a volume fraction of 0.2

Liquid	Density (kg/m^3)	Viscosity (kg/m s)	Critical Taylor Rotation Rate (RPM)
Water	1000	0.001	21
Kerosene	800	0.00164	43
Hexadecane	780	0.00364	100
50 wt% Glycerol (aq.)	1120	0.006	115

Table 3. Critical Rotation rates for the onset of instability for individual liquids used in the study.

Even though the mixture of fluids don't become unstable in the Taylor regime, they exhibit individual chaotic flow above the critical rotation rate with tracer visualization showing tracking of particles with time of these proving this. 4 consecutive frames show particles appearing and disappearing randomly as they move in and out of the plane of the fluid as well as settling in the gravitational field and moving with the direction of the flow in other parts of the annulus. Thus chaos and therefore some amount of mixing is present even in the stratified form

To display the motion of tracers in the fluid while stratified, a hydrophilic tracer was added to the water phase and the motion of the tracers was tracked over time. A particle tracking software, MOSAIC [49] was used to track the motion of the particles with a displacement cutoff of 10 pixels per particle per frame. Tracking was done using Fiji, an ImageJ implementation developed at NIH. [50]

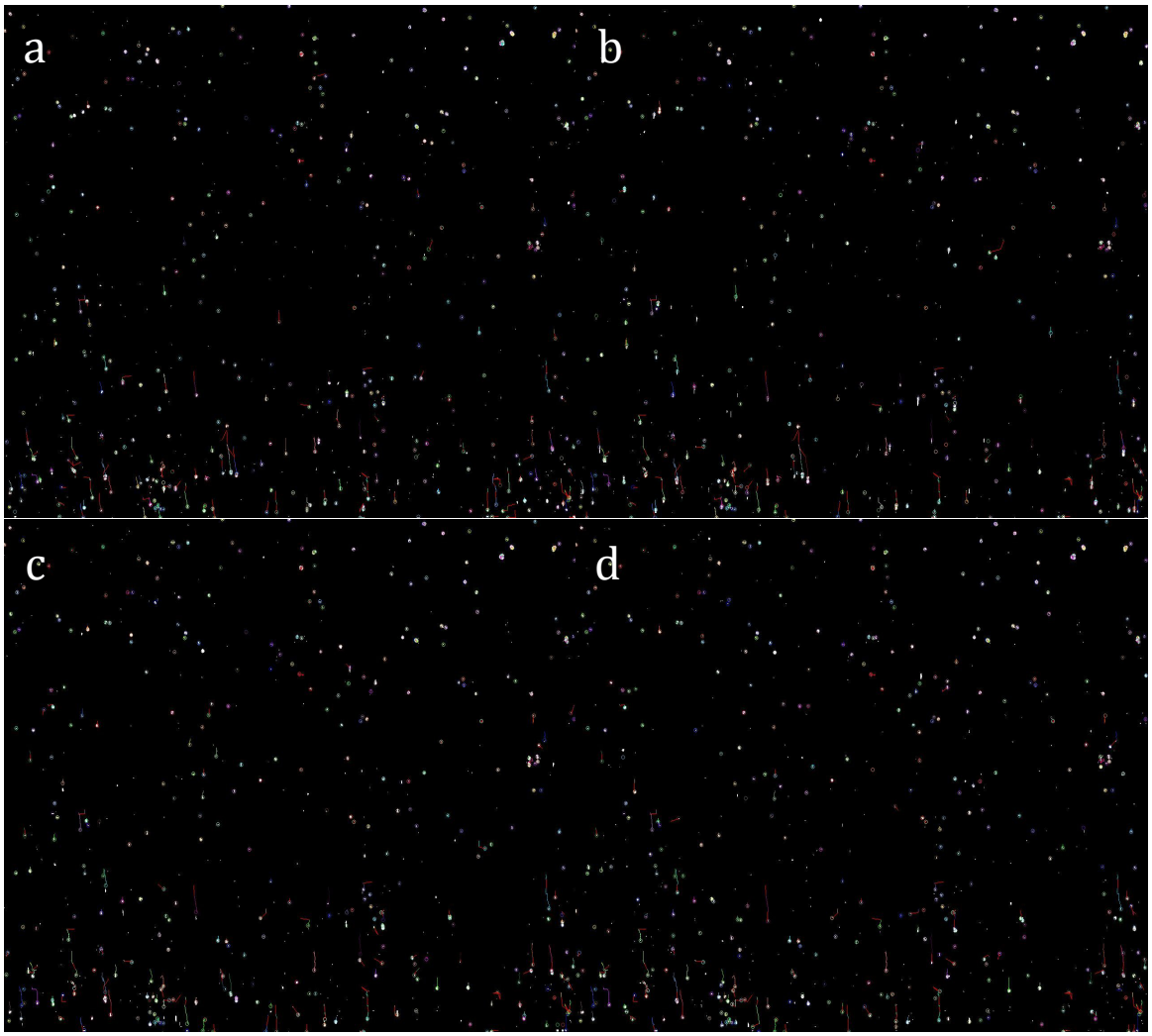

Figure 20. Figures a,b,c and d show 4 consecutively captured frames of the tracers in one of the stratified phases. Particles appear and disappear at random positions indicating the presence of a chaotic flow

3.5 Spatial distribution for segregated flow

How droplets position themselves in the case of segregated flow was looked at during the course of the experiments. The two primary forces that act on these droplets are centrifugal and gravitational forces. The effect of vortical forces and other shear forces are not large enough to affect the droplets in this current state. The length scale associated with turbulent vortices is dictated by the Kolomogrov microscale and is much smaller than the size of the droplets, which are on the order of the annular size of the system. The physical orientation of the droplets with respect to the annulus is dictated by the physical properties of the system and the dominant force field within the system. Keeping this in mind, the Ekman and Froude Numbers are able to describe how this spatial orientation develops in the system.

$$Fr = \frac{R_i \omega^2}{g}$$

$$Ek_j = \frac{\mu_j}{2\rho_j \omega d^2}$$

The Froude number is the ratio of inertial forces in the system with an external force field, which in this case is gravity. The Ekman number describes a relation between the physical properties of the system i.e. the viscosity and density of the fluid and rotational parameters of the Couette cell.

Laser Sheet Visualization experiments

Laser sheet visualization experiments were done to assess dispersed phase spatial distribution within the gap. The continuous phase used was the refractive index matched solution of Sodium Iodide, Glycerol and Water whereas the dispersed phase used was mineral oil. The continuous phase was doped with Rhodamine B, a fluorescent dye that has an absorption maxima near the wavelength of the laser used i.e. 532 nm. The concentration of Rhodamine B in the continuous phase was 100 mg/L and the dispersed phase had no additional additive that could reflect light or emit fluorescence in it. The volume fraction of he dispersed phase in the visualizations was $\phi = 0.2$.

All experiments were done by a stepwise increase in the rotation rate to insure that there is no influence of hysteresis on the system.

Images were taken using an IDT high-speed camera fitted with a Nikkor AF-S Lens and a 2x teleconverter. The aperture used on the cameras was f/2.8 and the exposure time for each frame was 33000 us. A total of 30 frames were recorded each second, which was the limit for the exposure time used.

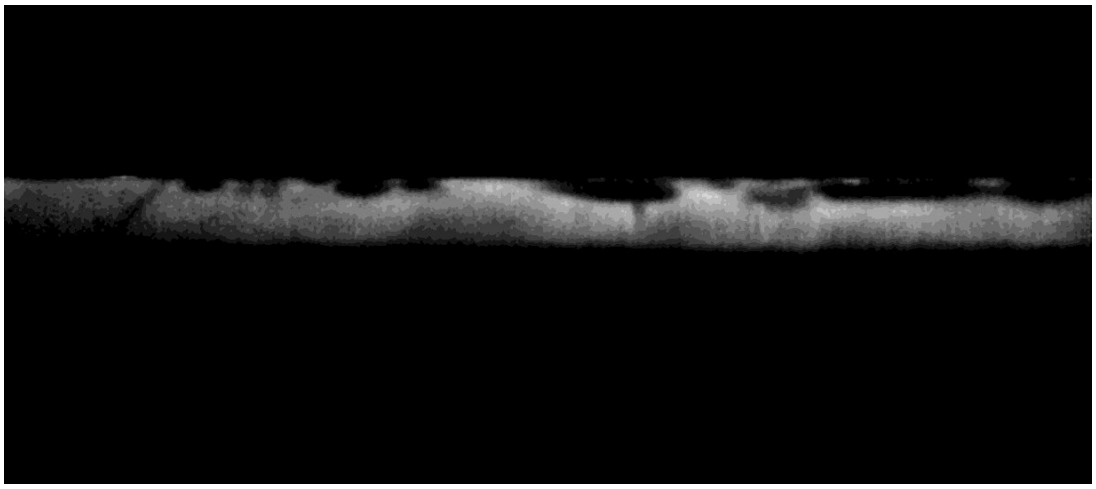

Figure 21. Spatial distribution of the dispersed phase in the gap at 70 RPM. The dispersed phase is hexadecane in a modified aqueous system

At a small rotation rate of 70 RPM, the flow develops into segregated flow and therefore large slugs of the dispersed phase can be seen moving through the gap. The dominant force on the system will dictate how the slugs distribute themselves within the gap. Based on the physical properties of the two and the properties of the system, gravitational forces dominate the centrifugal forces forcing the lighter liquid to the top and the heavier liquid to the bottom. The Froude number for this system is $Fr = 0.125$ while the Ekman Numbers for the individual fluids are $Ek_{dispersed\ phase} = 0.047$ and $Ek_{continuous\ phase} = 0.076$.

4 consecutive frames from this system also prove that the slugs indeed do move in the gap and are not trapped in the current orientation indefinitely due

to forces in the azimuthal direction not being strong enough to induce segregated flow.

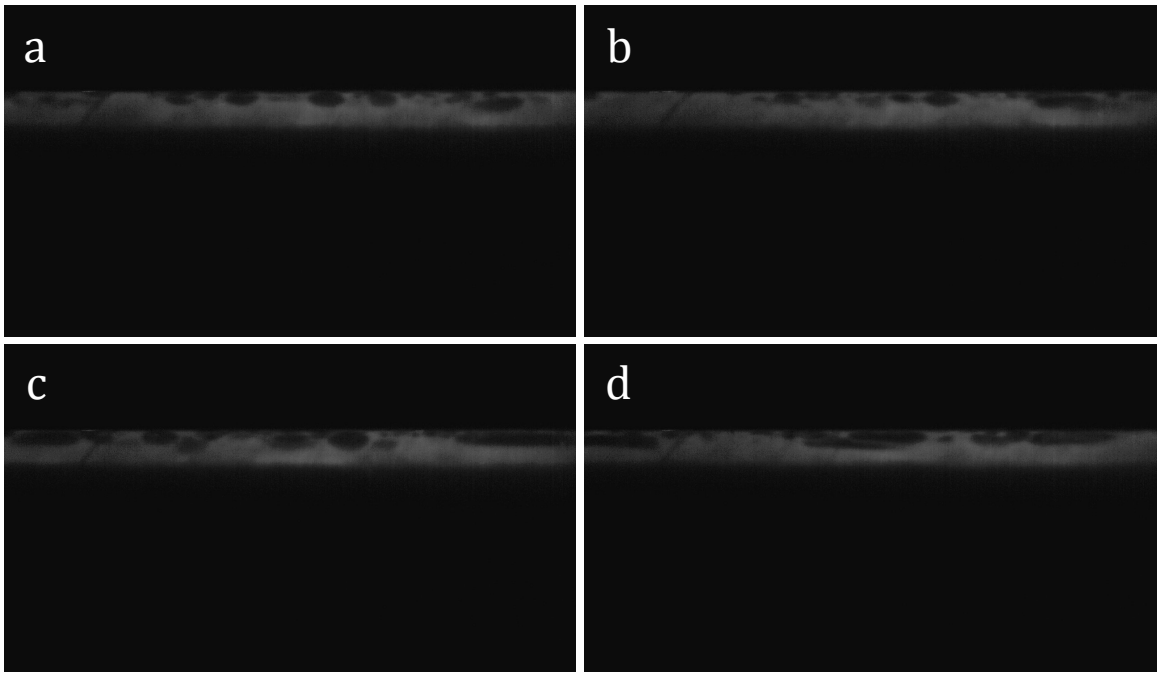

Figure 22. 4 consecutive frames showing the movement of slugs through the gap for a rotation rate of 70 RPM.

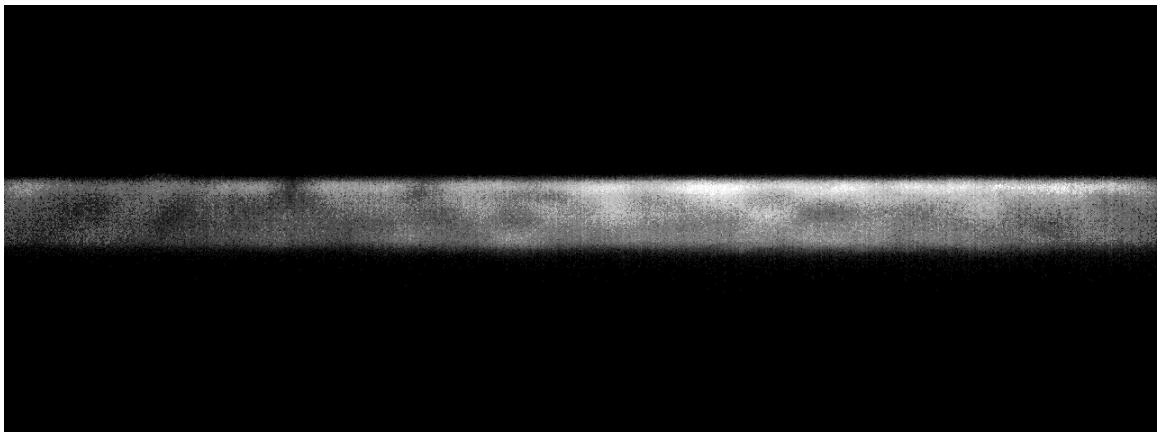

Figure 23. Spatial distribution of the dispersed phase in the gap at 250 RPM. The dispersed phase is hexadecane in a modified aqueous system.

The rotation rate for which the Froude Number, $Fr = 1$, is the point where both the gravitational and centrifugal forces acting on the system is the same and therefore the system will exhibit properties of buoyancy of the dispersed phase within the continuous phase. This would lead to spatially well-distributed droplets of the dispersed phase within the system if the Ekman numbers were nearly the same for both. The above system at a rotation rate of 250 RPM exhibits this phenomenon where the fluids are neutrally positioned through the gap with a greater preference for the upper half of the gap.

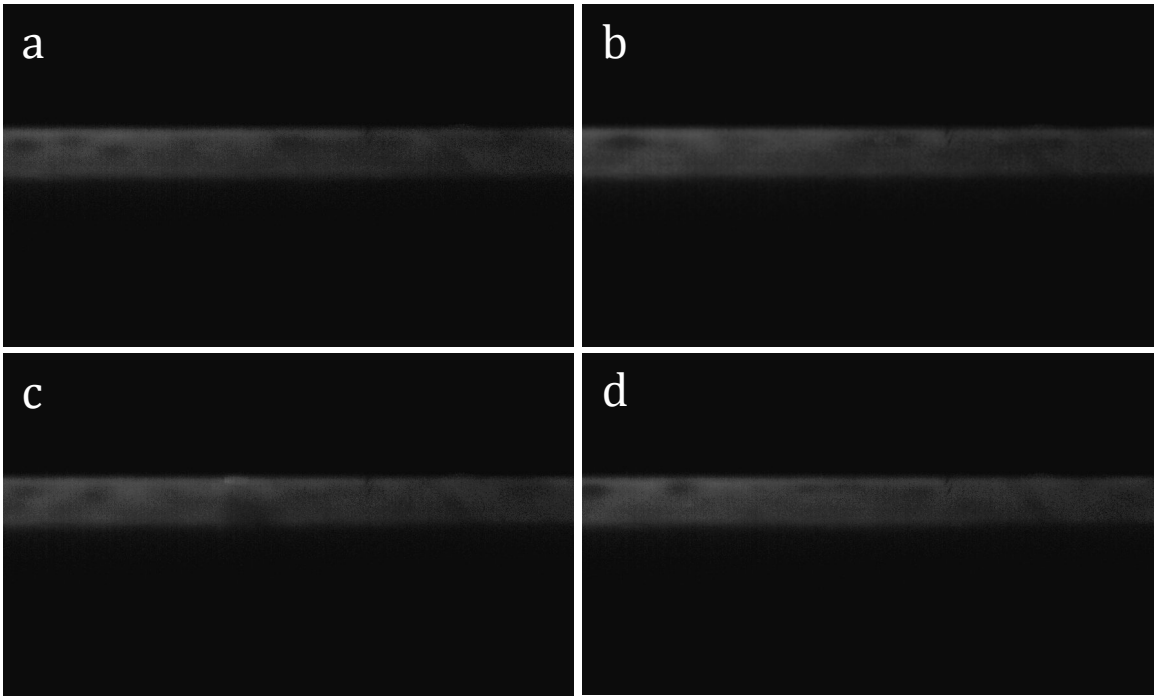

Figure 24. 4 consecutive frames showing the movement of droplets through the gap for a rotation rate of 70 RPM.

The limiting case for such a system is when 1 fluid in the system has a density and viscosity much lower than of the dispersed phase used currently. For that purpose we replaced the organic phase with air as it fulfilled these criteria. Taylor-Couette flow with air in the system showed that air still occupied the area closest to the outer cylinder even though centrifugal forces should be dominant in the system at the rotation rates studied for the air-water system as Fr >> 1. This indicates that physical parameters of the fluid are as important to the spatial distribution as the forces acting on a small droplet of the fluid in the system.

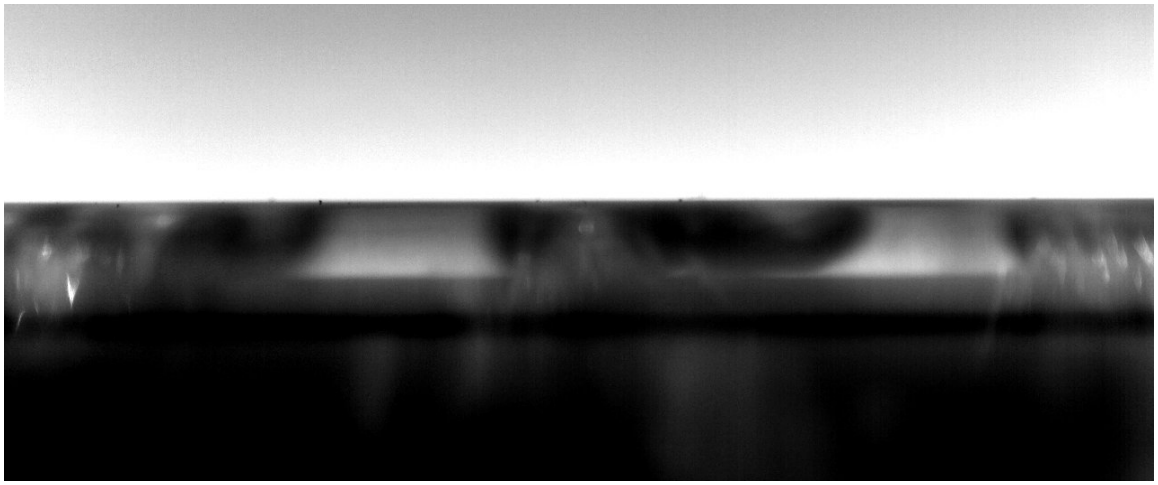

Figure 25. Droplet distribution in the gap for an air-water system at 700 RPM and the volume fraction of air is 0.2.

3.6 Model systems

Most flow characterization experiments were done using kerosene as the organic phase and water as the aqueous phase. Water was dyed with Methylene Blue when it was the continuous fluid and kerosene was dyed with Oil Red O when it was the continuous fluid. This allowed us to obtained some resolution on the separation between the two fluids and therefore it became easier to characterize the flows. The organic phase was also seeded with the modified amphiphilic tracer particles that enable better visualization especially when the organic phase was dispersed in the aqueous phase. Initial batch scale experiments were performed by loading the reactor with the requisite volume fraction of the fluids based on the total volume of fluid that could be accommodated within the reactor. Since there was no inlet or outlet to the reactor, the volume fraction remained constant through the period of reactor operation and all data points were collected for that volume fraction.

Unlike previous experiments of this kind, we looked at identifying the primary transitions for these forms of flow and possible ways of controlling or understanding the transitions for these flows. For the case where no axial flow was induced in the annulus, the three primary flow states of – stratification, segregation and bandedness was observed. The phase diagram across various different volume fractions is shown below

For calculating parameters that could be associated with the transition, it was necessary to calculate mixture properties i.e. the viscosity and density of the mixture and not of the individual components of the system. Averaging both by the volume fraction of each component accomplished this

$$\mu = \mu_1^{\varphi} \mu_2^{1-\varphi}$$

$$\rho = \phi\rho_1 + (1-\phi)\rho_2$$

The different metrics used to identify transitions points for the system are the – Azimuthal Reynolds Number, the Taylor Number, the Capillary number, the Weber Number and the Ohnesorge Number. These five numbers associate the three primary forces within the system with each other thus providing a powerful tool of estimating the possible transition points and mechanisms of the flow. The five numbers used are defined below

The Taylor Number relates centrifugal forces to viscous forces, the Weber Number relates inertial forces to interfacial forces, the Reynolds Number relates all inertial forces to viscous forces and the Capillary Number relates the viscous forces to surface forces and the Ohnesorge Number relates all three forces.

$$Ta = \frac{2\omega^2 R_1^2 d^4}{\nu^2 (R_2^2 - R_1^2)}, the\ Taylor\ Number$$

$$Re_\theta = \frac{\rho \omega R_1 d}{\mu}, Azimuthal\ Reynolds\ Number$$

$$We = \frac{2d\omega^2 R_i^2 \rho_c}{\sigma}, Weber\ Number$$

$$Ca = \frac{\mu \omega d}{\sigma}, Capillary\ Number$$

$$Oh = \frac{\mu}{\sqrt{\rho \sigma d_p}}, \quad the\ Ohnesorge\ Number\ or\ \ La = \frac{1}{Oh^2}\ , the\ Laplace\ number$$

3.6.1 Kerosene-Water

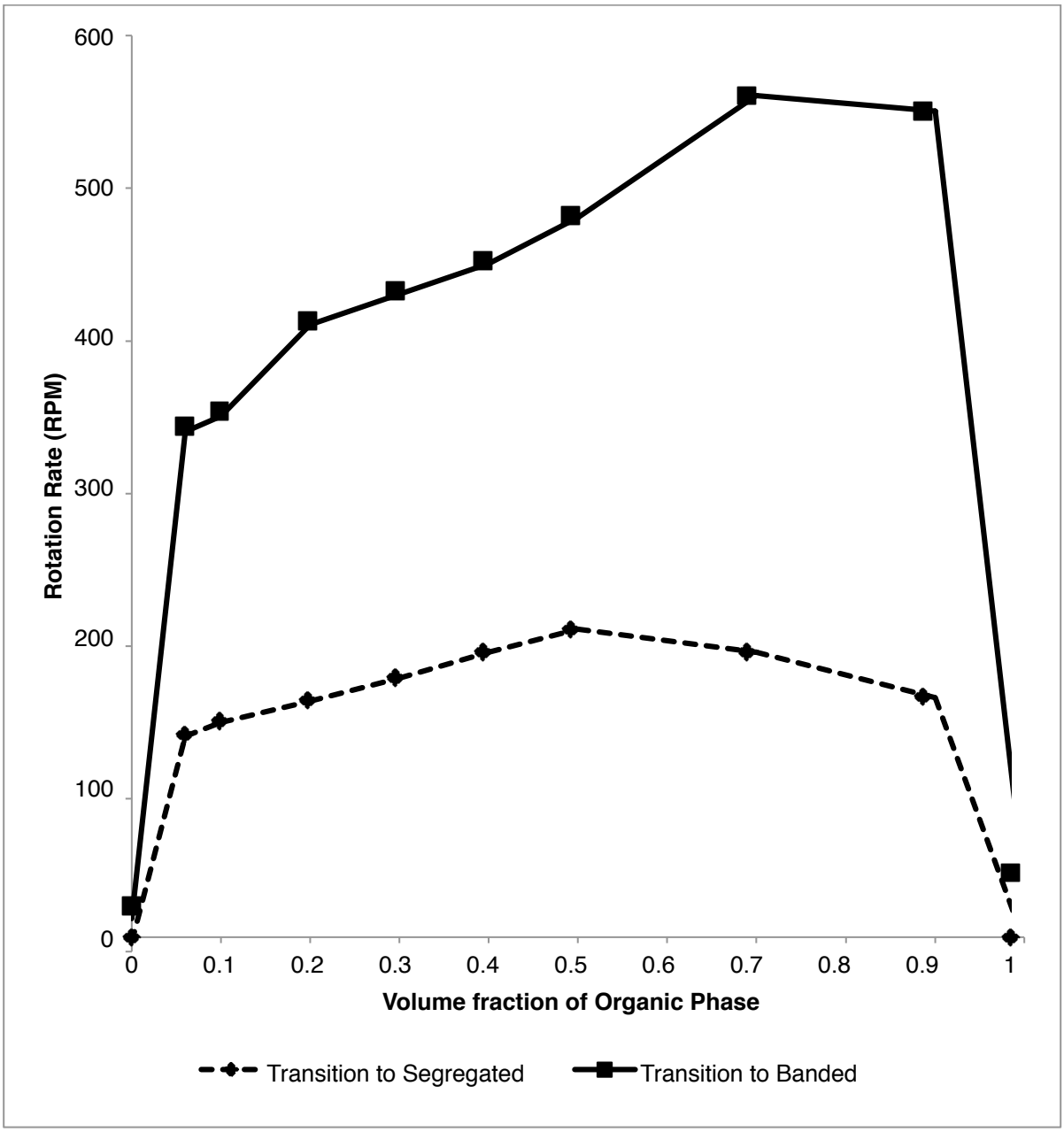

Figure 26. Phase Diagram for a kerosene-water system with no axial flow at different volume fractions. Shown are the transitions from stratified to segregated flow and from segregated to banded flow.

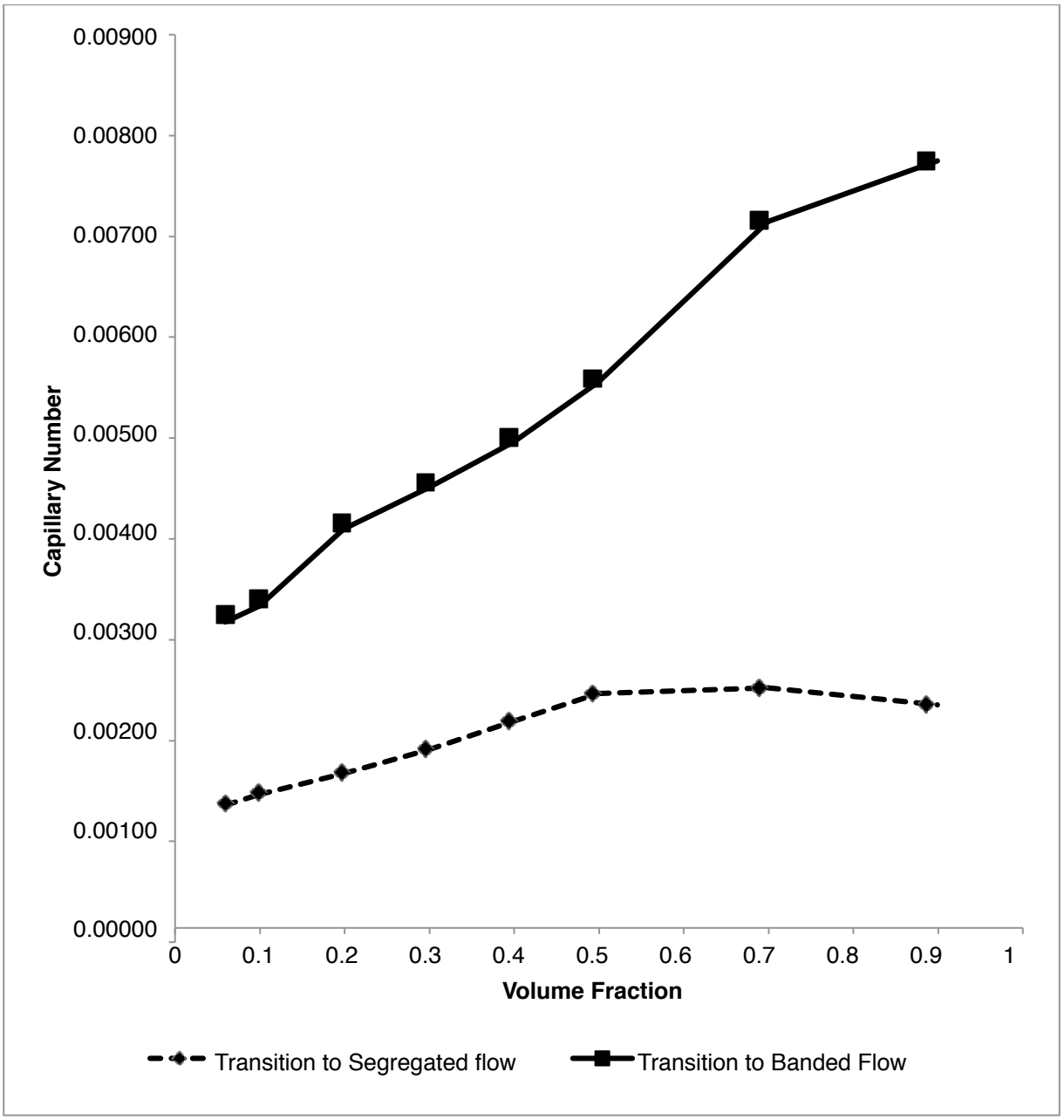

Figure 27. Phase diagram for a kerosene-water system with no axial flow at different volume fractions. The transitions are shown for different Capillary Numbers

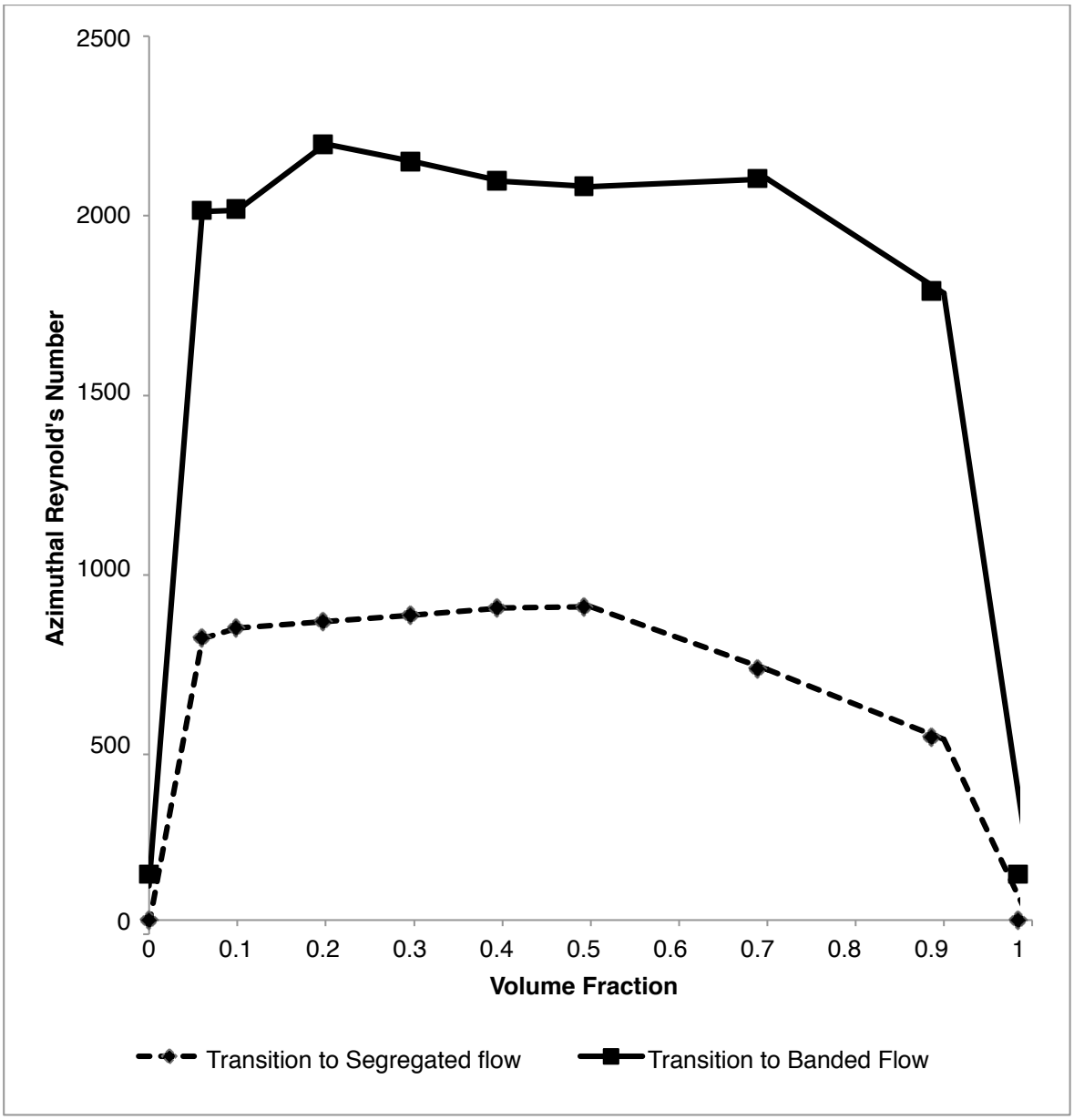

Figure 28. Phase Diagram for a kerosene-water system with no axial flow at different volume fractions. Shown are the transitions from stratified to segregated flow and from segregated to banded flow at different azimuthal Reynolds numbers.

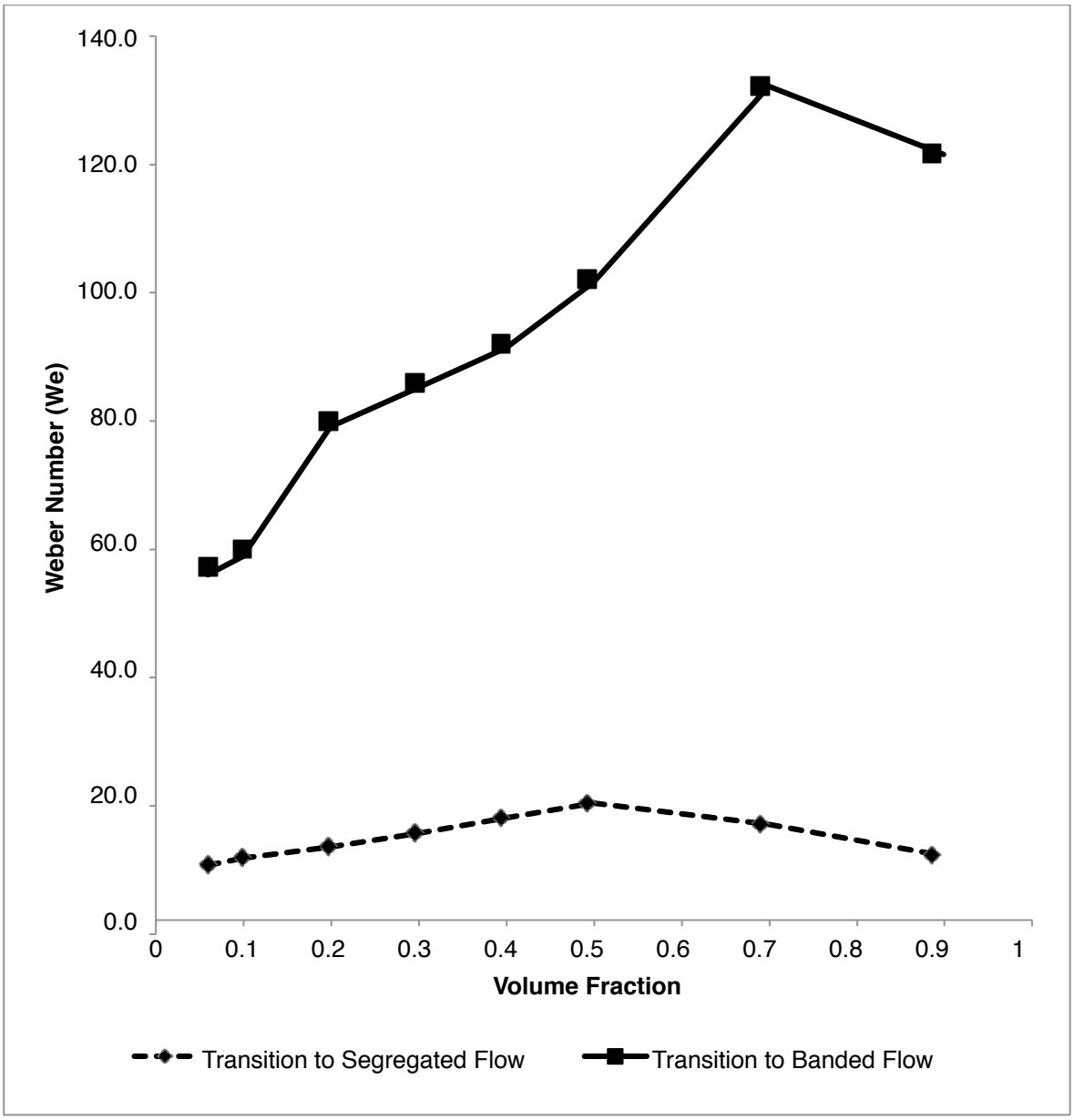

Figure 29. Phase Diagram for a kerosene-water system with no axial flow at different volume fractions. Shown are the transitions from stratified to segregated flow and from segregated to banded flow at different Weber Numbers.

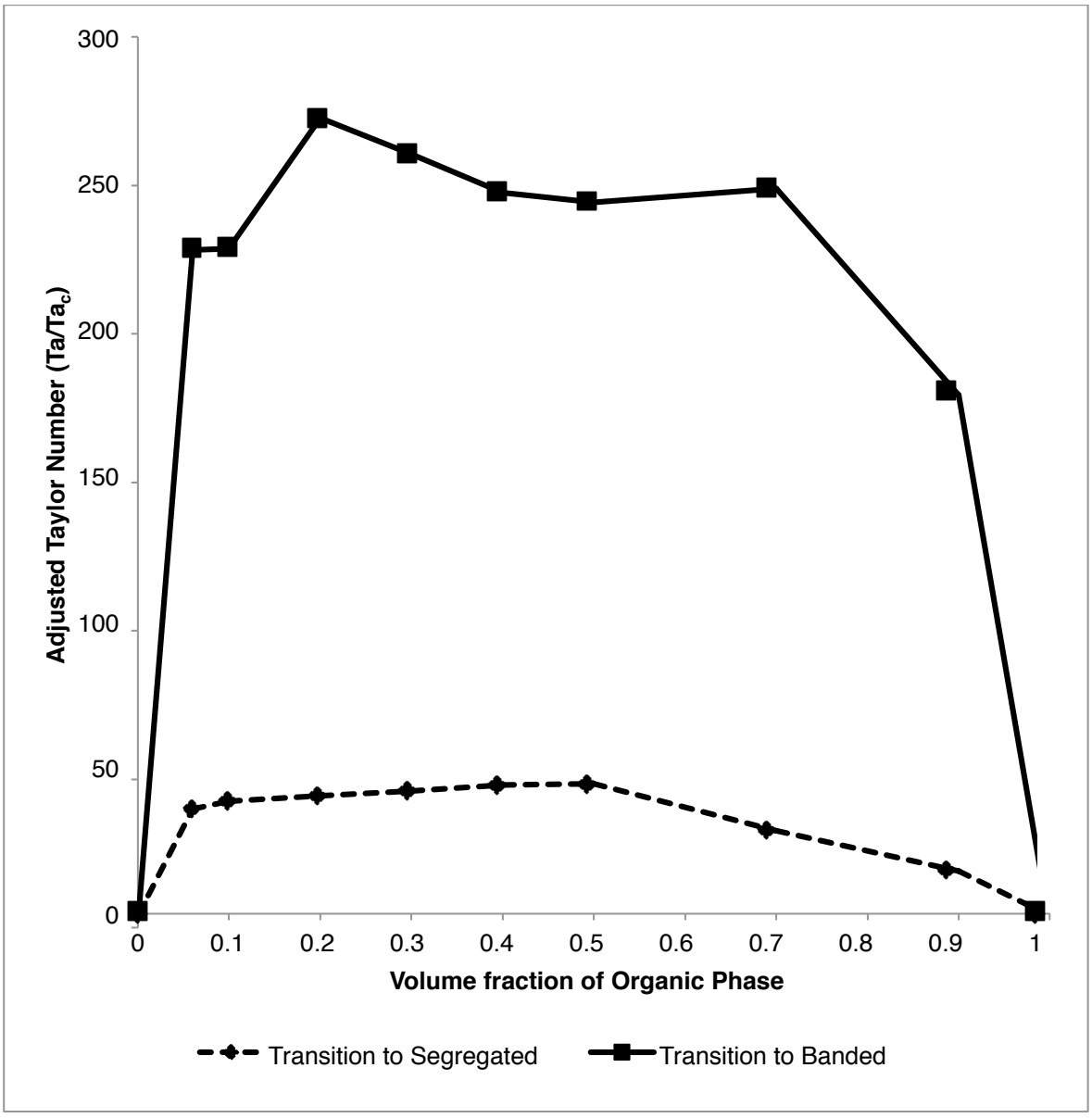

Figure 30. Phase Diagram for a kerosene-water system with no axial flow at different volume fractions. Shown are the transitions from stratified to segregated flow and from segregated to banded flow at different Taylor Numbers. All Taylor Number's are normalized using the single phase critical Taylor Number, $\boldsymbol{Ta_c = 1896}$

The azimuthal Reynolds number that dictates the transition from one flow state to the other remains nearly the same across all volume fractions after adjusting for their mixture viscosity and mixture density, within a small error range. This means it could be possible to link the interfacial energy and the effects of viscous and inertial forces to understand how all three together parameters could dictate flow transitions. All other parameters vary depending on the volume fraction of the system and therefore are not suitable for understanding the transitions. For all graphs hereafter only the variance and dependence with the Reynolds Number is shown.

3.6.2 Hexadecane-Water

Replacing Kerosene with Hexadecane allows us to look at how the flow develops when a more viscous liquid with a similar density to that of Kerosene is used in the system instead of the less viscous one that is Kerosene. Experiments were done using Hexadecane as the dispersed phase in an aqueous solution. The continuous phase was dyed blue with Methylene Blue and the organic phase was left blank. Hexadecane has a viscosity of 3.64 cP compared to that of 1.64 cP of Kerosene but has a lower interfacial energy with water – 22.3 mN/m vs 29.7 mN/m for a Kerosene-Water system. As densities of the two organics are nearly equal, the effect of inertial forces across both the system remains nearly the same with only viscous forces and energetic forces enforcing possible changes in flow dynamics.

A mini phase diagram for a hexadecane water system is shown below, with 3 volume fractions studied i.e. 0.2, 0.3 and 0.4.

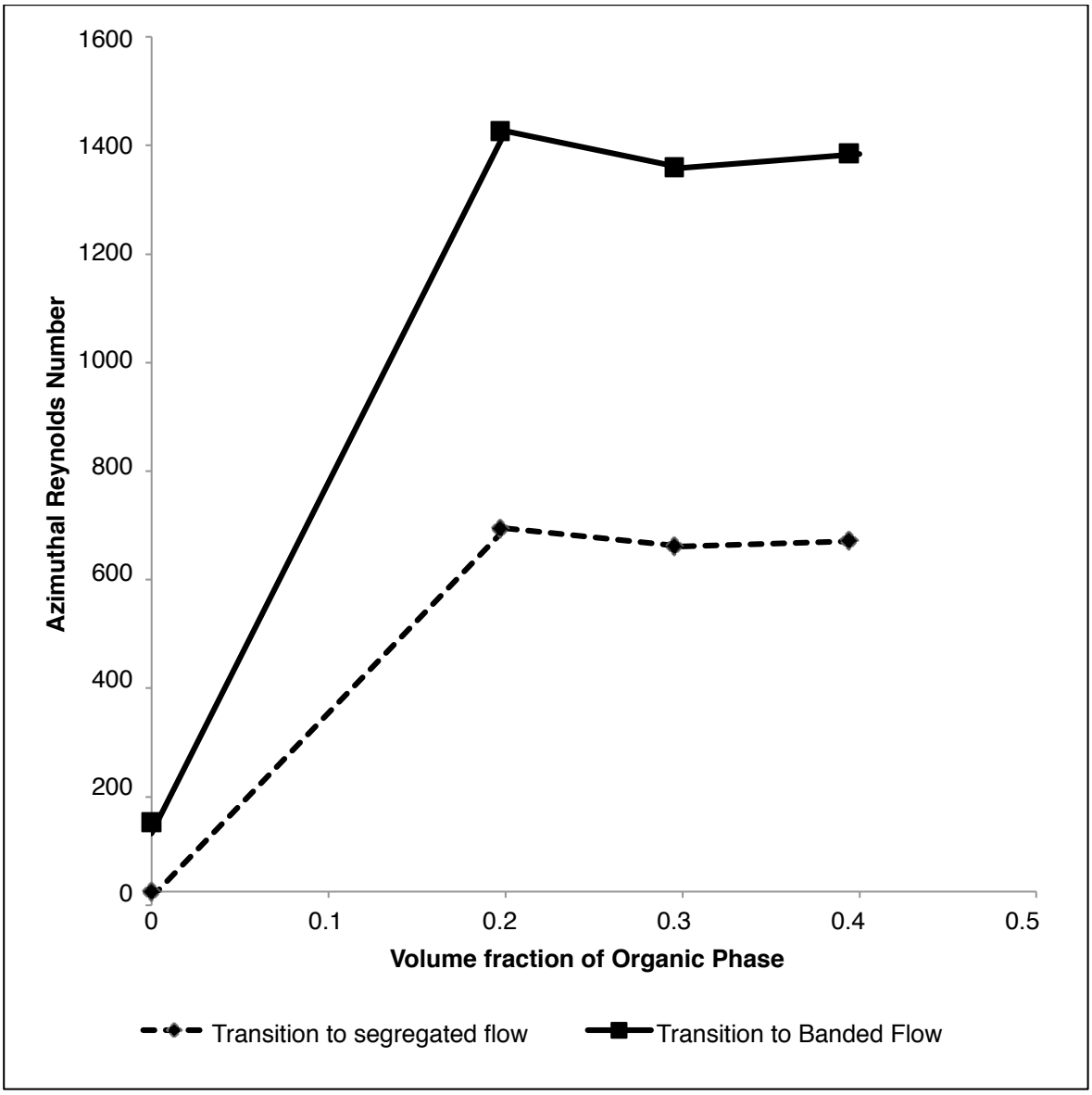

Figure 31. Phase Diagram for a hexadecane-water system with no axial flow at different volume fractions. Shown are the transitions from stratified to segregated flow and from segregated to banded flow at different azimuthal Reynolds numbers.

3.7 Effect of Surfactants

Isolating the effect interfacial tension between the fluid pairs is important to understand how critical this parameter is to the development of flow dynamics in the system. The other possible physical parameters that could be varied were the density and viscosity of the fluids as well as the volume fraction of the dispersed phase. The simplest way of achieving this goal was to add a certain amount of surfactant to the continuous phase that would alter the interfacial tension between the two liquids. All experiments were done using a Kerosene-Water system and a surfactant was added to the continuous aqueous phase.

The surfactant used for experiments was Triton X-100 and three different concentrations were studied – 0.1, 0.5 and 1 g/L, in the aqueous phase. All experiments were performed with the volume fraction of kerosene held fixed at 0.2 for these experiments and the transition from stratified to segregated and segregated to banded flows was studied.

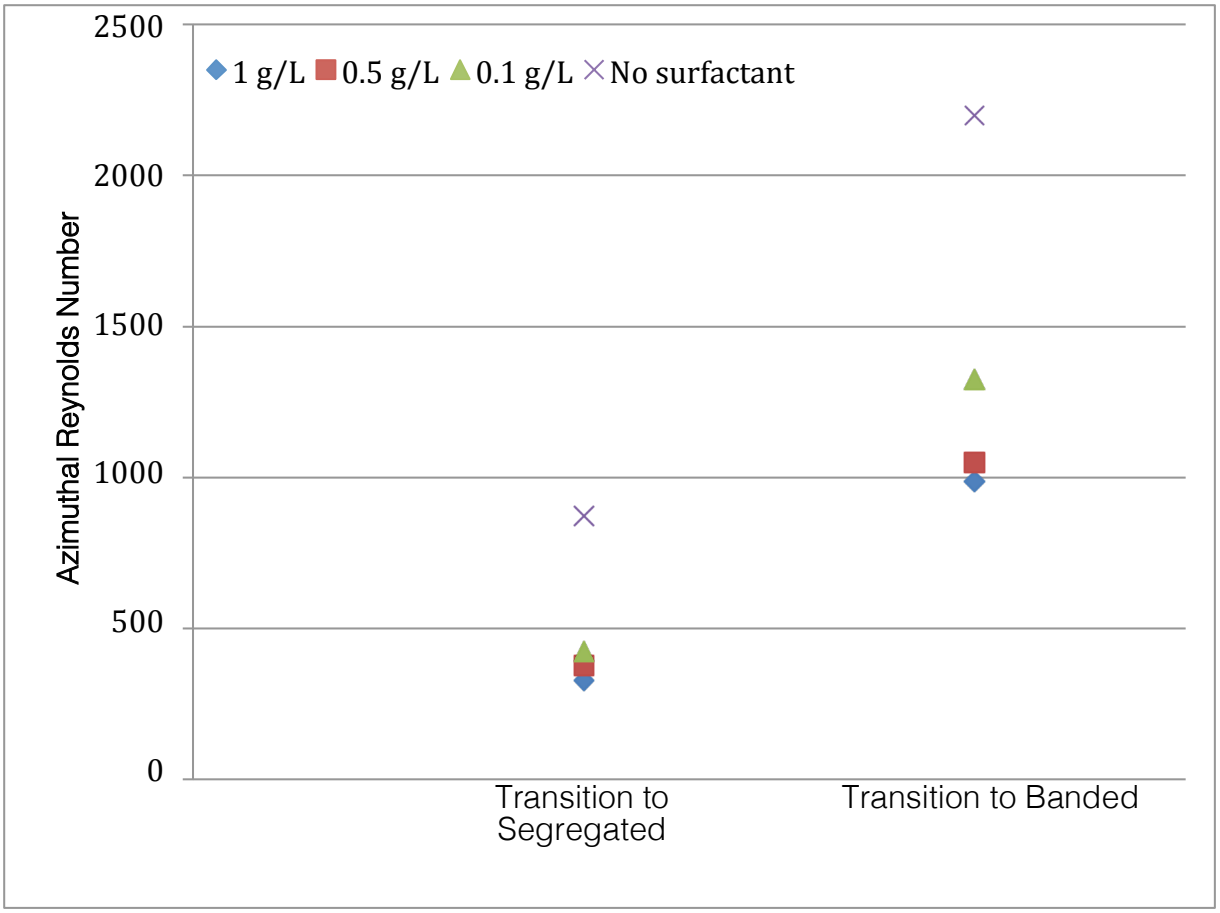

Figure 32. Increasing surfactant concentration in the liquid depresses the transitions from 1 flow state to the other.

Transitions happen at different azimuthal Reynolds numbers indicating that changes in interfacial tension are the primary cause of the depressions in these transitions. Trying to understand how this interfacial energy affects transitions between these three primary flow states is looked at further in this thesis.

3.8 Effect of Axial Flow

Most of the previous studies on Taylor-Couette-Poisuelle flow had weakly induced axial flows in the system with Reynold's Numbers less than 1**.** The motivation behind using weak axial flows was to not disrupt the vortex structure developed in the flow. But, for applications at larger scales and to increase throughput, it would become necessary for such a system to display similar properties at much lower residence times as well. To test the effect that axial flow has on the system, we chose 3 different axial flow rates with column residence times of – 1 minute, 30 seconds and 15 seconds. How the flow developed on the addition of such strong axial flows was seen through the phase diagrams developed for the three different flow rates.

All experiments were done using the model Kerosene-Water system with the aqueous continuous phase dyed with methylene blue and kerosene left untouched. What we noticed was that for different volume fractions, on increasing axial flow through the column – transitions were accelerated and happened much earlier when compared to the system with no Poisuelle flow.

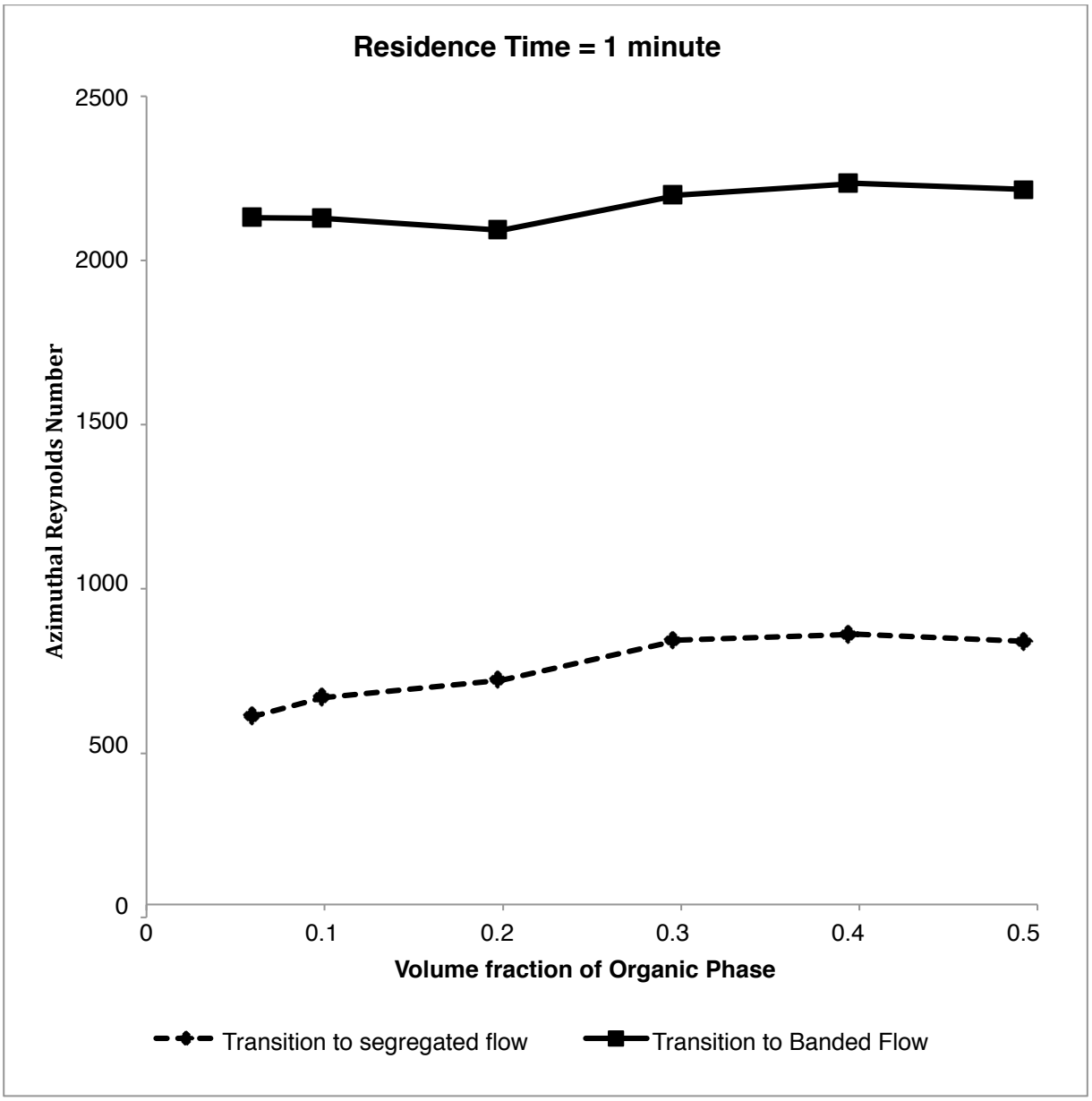

Figure 33. Phase Diagram for a kerosene-water system with a column residence time of 1 minute. Shown are the transitions from stratified to segregated flow and from segregated to banded flow at different azimuthal Reynolds numbers.

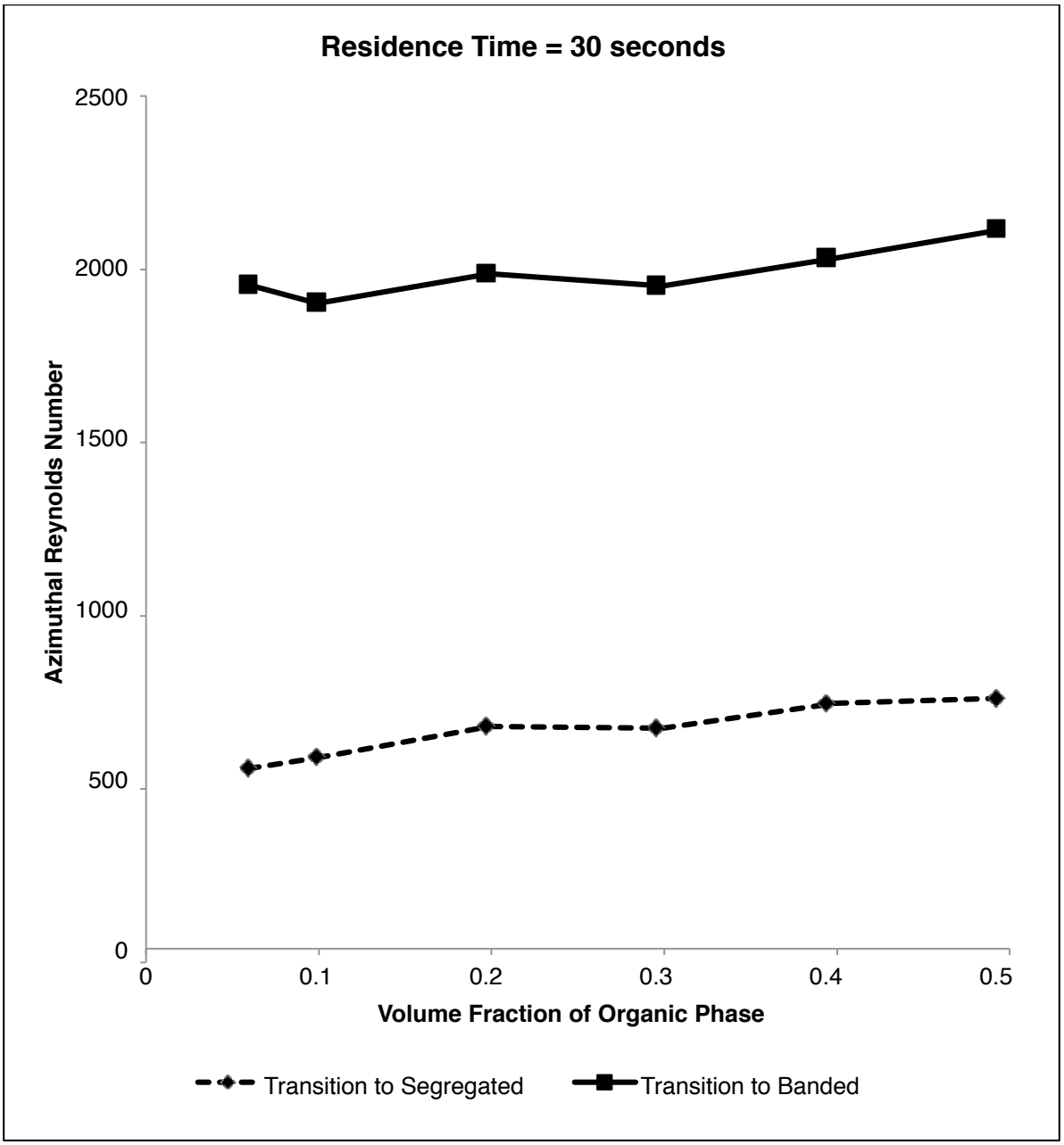

Figure 34. Phase Diagram for a kerosene-water system with a column residence time of 30 seconds. Shown are the transitions from stratified to segregated flow and from segregated to banded flow at different azimuthal Reynolds numbers.

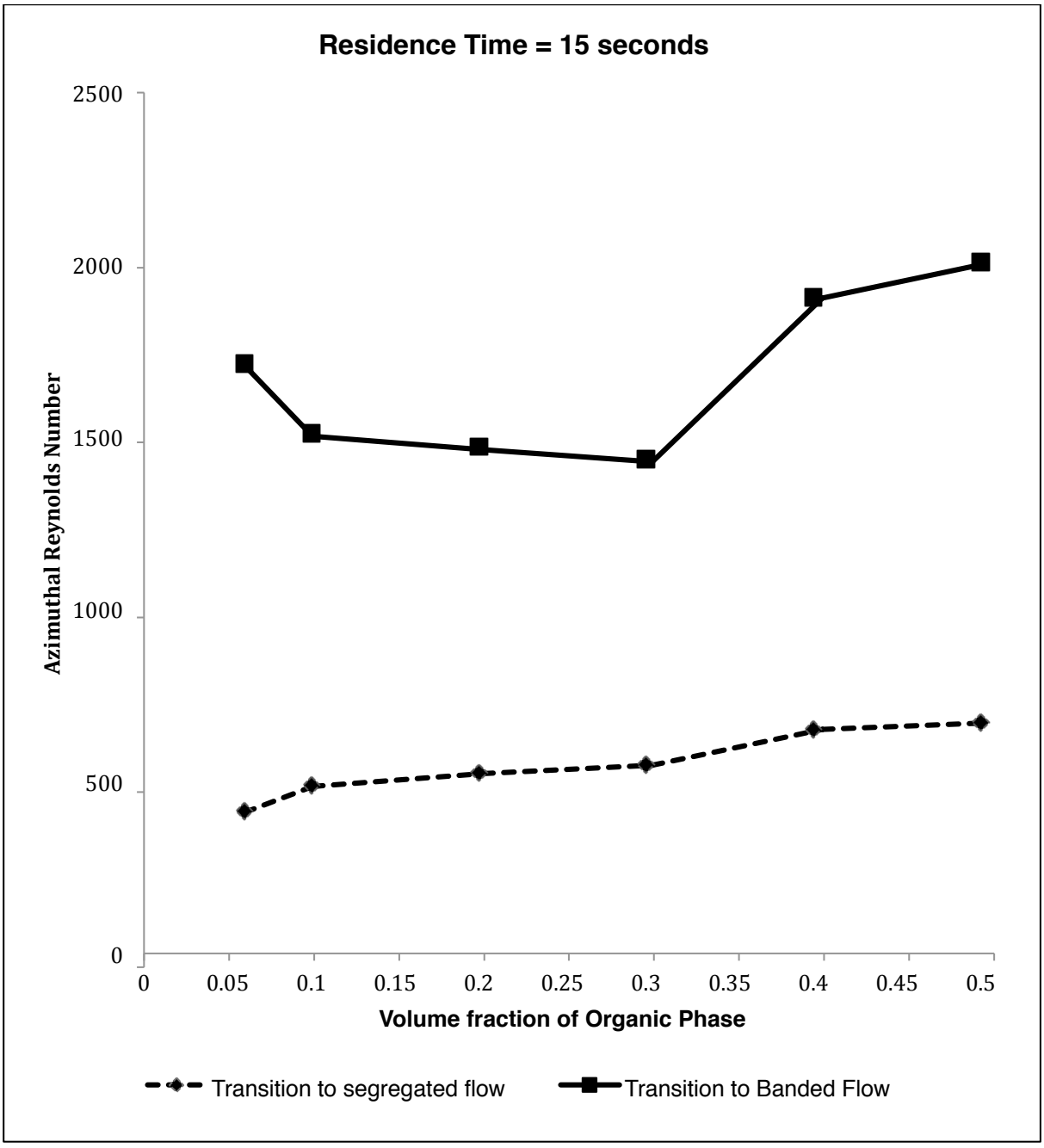

Figure 35. Phase Diagram for a kerosene-water system with a column residence time of 15 seconds. Shown are the transitions from stratified to segregated flow and from segregated to banded flow at different azimuthal Reynolds numbers.

Transitions at higher axial flows (Residence Time = 15 seconds) does not seem to follow any form of Reynolds Number trend, with transitions for lower volume fractions happening later than transitions at higher volume fractions, unlike other flow rates studies. This may be due to the vortex structure being strained because of the high axial flow rate and therefore not being able to maintain the proper Taylor Vortex structure.

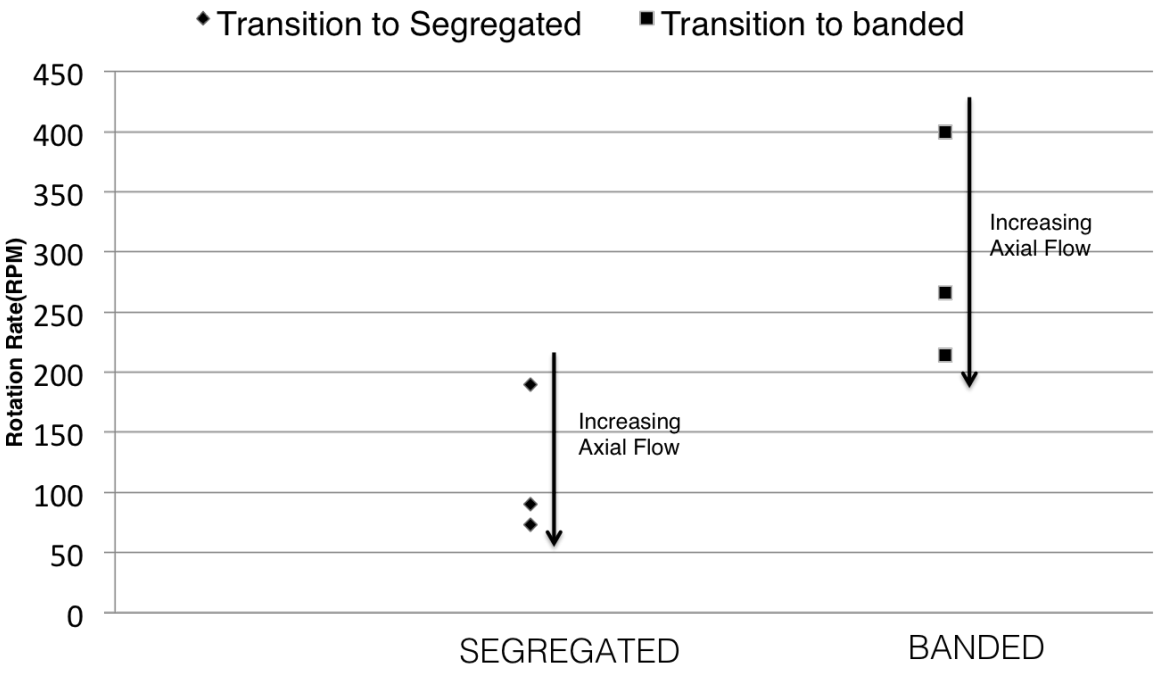

Figure 36.. Acceleration of transition to segregated and banded flow on increasing axial flow in the system. These data points correspond to a volume fraction of 0.3

This observation is the reverse of what is observed for single fluid Taylor-Couette-Poisuelle flow, where the axial flow stabilized the vortices and delays the onset of instability to higher rotation rates. The critical Taylor Number for transitions for those systems increases exponentially with induced axial flow rate. The graph below taken from Aljishi et al. [7] shows the relation between critical Taylor Numbers

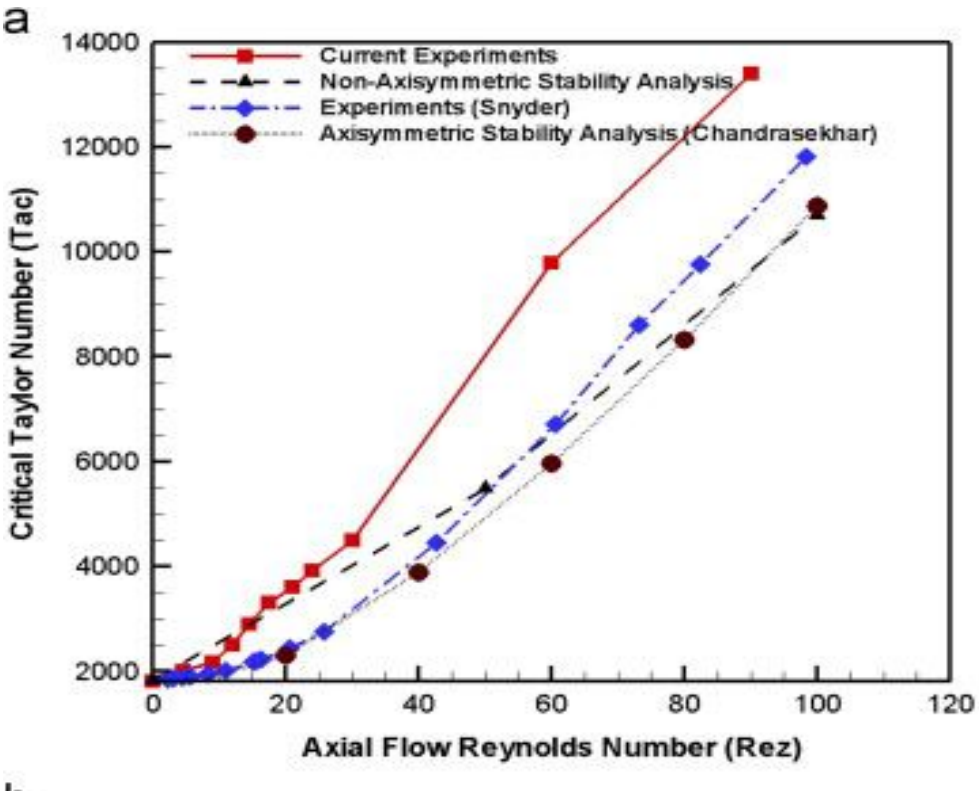

Figure 37. Dependence of Critical Taylor Number on the induced axial Reynolds number for single-phase systems. Taken from Aljishi et al. **[7]**

With increase in axial flow for two-phase systems, there is an acceleration to the onset of instability as compared to the delay observed for single-phase flows. As shown previously, stratified flow is individually chaotic irrespective of if the entire system undergoes a transition to its first unstable state. This implies that the framework is already present for the development of Taylor vortices even at lower rotation rates and some mechanism is needed to accelerate this onset. The primary reason for this delay is due to the interfacial energy between the fluid pair, which provides an energy barrier that the

system must overcome before reaching instability. The barrier for single-phase flows is much lower due to the absence of this additional energetic phenomenon and therefore each phase individually becomes chaotic after crossing its threshold of critical rotation rate.

Our hypothesis is that energy dissipation due to frictional forces contributes to the onset of instability by providing energy to stabilize the interfacial energy between the two phases and subsequently provide enough energy to break the surface between the two. The total energy dissipated in a couette cell can be calculated using the following formulas – the total energy dissipated due to rotation, the wall shear stress and the friction factor. Taken from [16]

$$\epsilon = \frac{\pi L_c R_i^4 \omega^3 f}{V_R}$$

$$\tau_{shear} = \frac{f \rho R_i^2 \omega^2}{2}$$

$$f = 0.80 \left(\frac{d}{R_i}\right)^{0.35} Re_\theta^{-0.53}, \quad for\ Re\ \geq Re_c$$

$$Re_c = 41.2 \left(\frac{d}{R_i}\right)^{-0.5} + 27.2 \left(\frac{d}{R_i}\right)^{0.5} + 2.8 \left(\frac{d}{R_i}\right)^{1.5}$$

Here ϵ is the total energy dissipated per unit mass of the reaction mixture, f is the friction factor and all other units follow the general trend used through this

thesis. On the addition of axial flow there will be an additional frictional additive term due to friction in the direction of the axial flow. This additive term can be calculated by estimating the friction factor in the z-direction i.e. the direction of the flow

Based on the flow, friction factor can be the laminar friction factor or the turbulent friction factor

$$f = \frac{16}{Re}, for\ laminar\ flow$$

$$\frac{1}{f^{\frac{1}{2}}} = -4.0 \log_{10}\left(\frac{\frac{\epsilon}{d}}{3.7} + \frac{1.256}{Re_z f^{\frac{1}{2}}}\right), the\ Colebrook\ equation$$

The additional energy dissipated due to axial flow in the annulus can be written as

$$\epsilon_{a\square ial} = \frac{\mu \bar{v} L_c V_R}{1000(D_2^2 - D_1^2)}$$

$$\bar{v} = \frac{Q}{2.448(D_2^2 - D_1^2)}$$

The axial flow Reynolds number is quite low and therefore the flow can be assumed laminar in the z-direction of flow hereinafter.

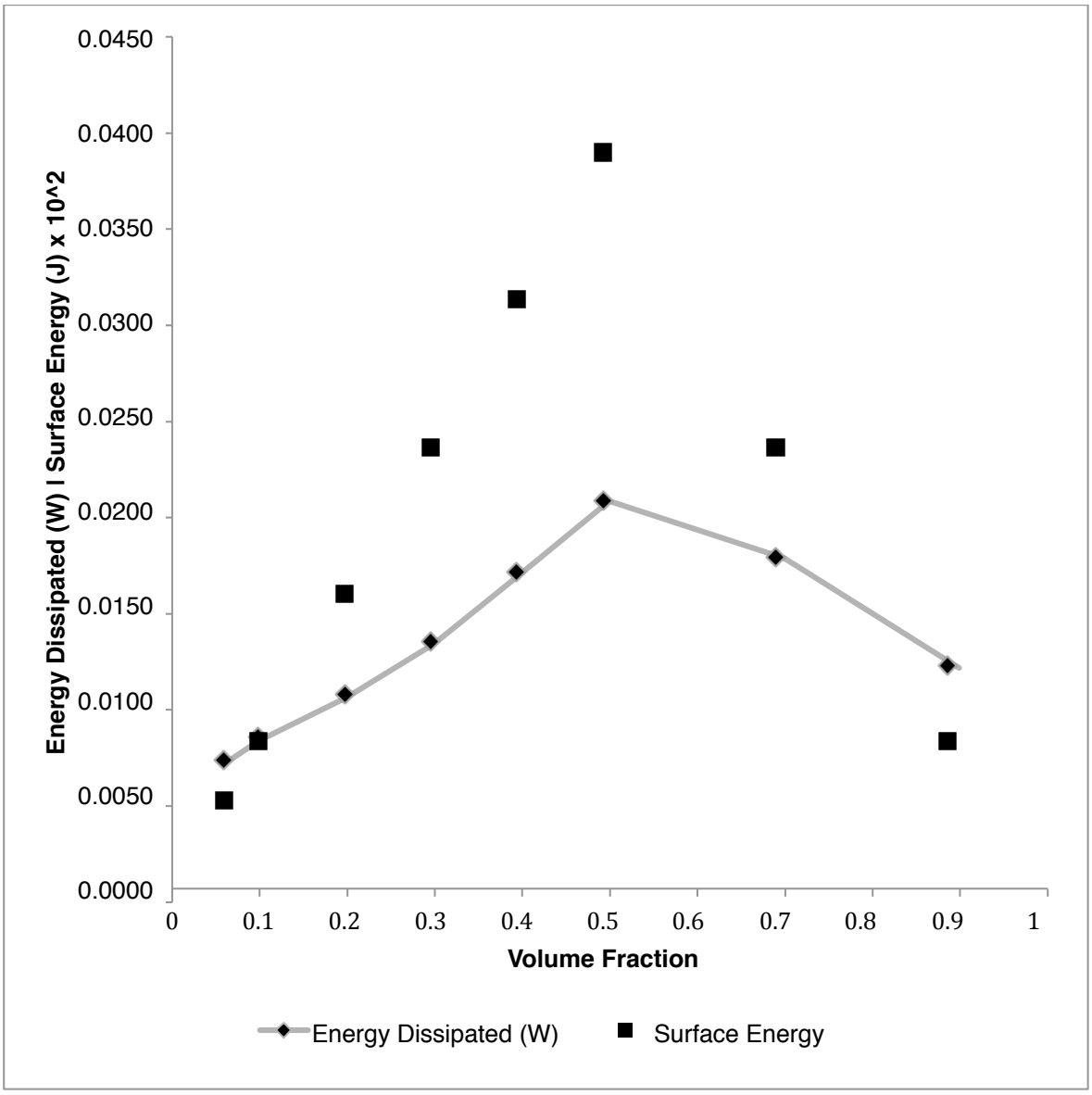

Figure 38. Trends of total surface energy and energy dissipated in the column at the transition rotation rates. Surface Energies are multiplied by 100 to ensure they are on the same order of magnitude as the energy dissipated.

As energy dissipated would convert to several forms of energy, there still exists a definite similar trend between the total energy dissipated and the total surface energy of the system. Also on addition of axial flow, the total energy dissipated increases and the trend with corresponding transitions points.

3.9 Modeling transitions with interfacial energy

Collecting information from several liquid pairs, a trend was observed where transitions happened much later for liquid pairs having a higher interfacial energy. As all three of the primary forces would affect any primary flow transitions, it became important to understand and identify if there was any trend present that would explain the transitions. The three primary numbers that interrelate the forces with each other were the – Taylor Number, Reynolds Number and Weber Number. Due to fact that the transitions at different volume fractions for the same system had nearly identical Reynolds numbers, it better explained how the inertial and viscous forces acted on the system and correlating this value to the interfacial energy seemed to be the way forward. Fluids with identical properties apart from their interfacial energy, showed different flow transitions and highlighted the importance of surface energy of the system. An effort has been made to qualitatively and statistically study the correlation between the azimuthal Reynolds Number and the interfacial energy of the system.

Also, as there is a certain amount of error in the mixture density, viscosity and measured transition rotation rate, all values lie within the error range of the phase space measurements.

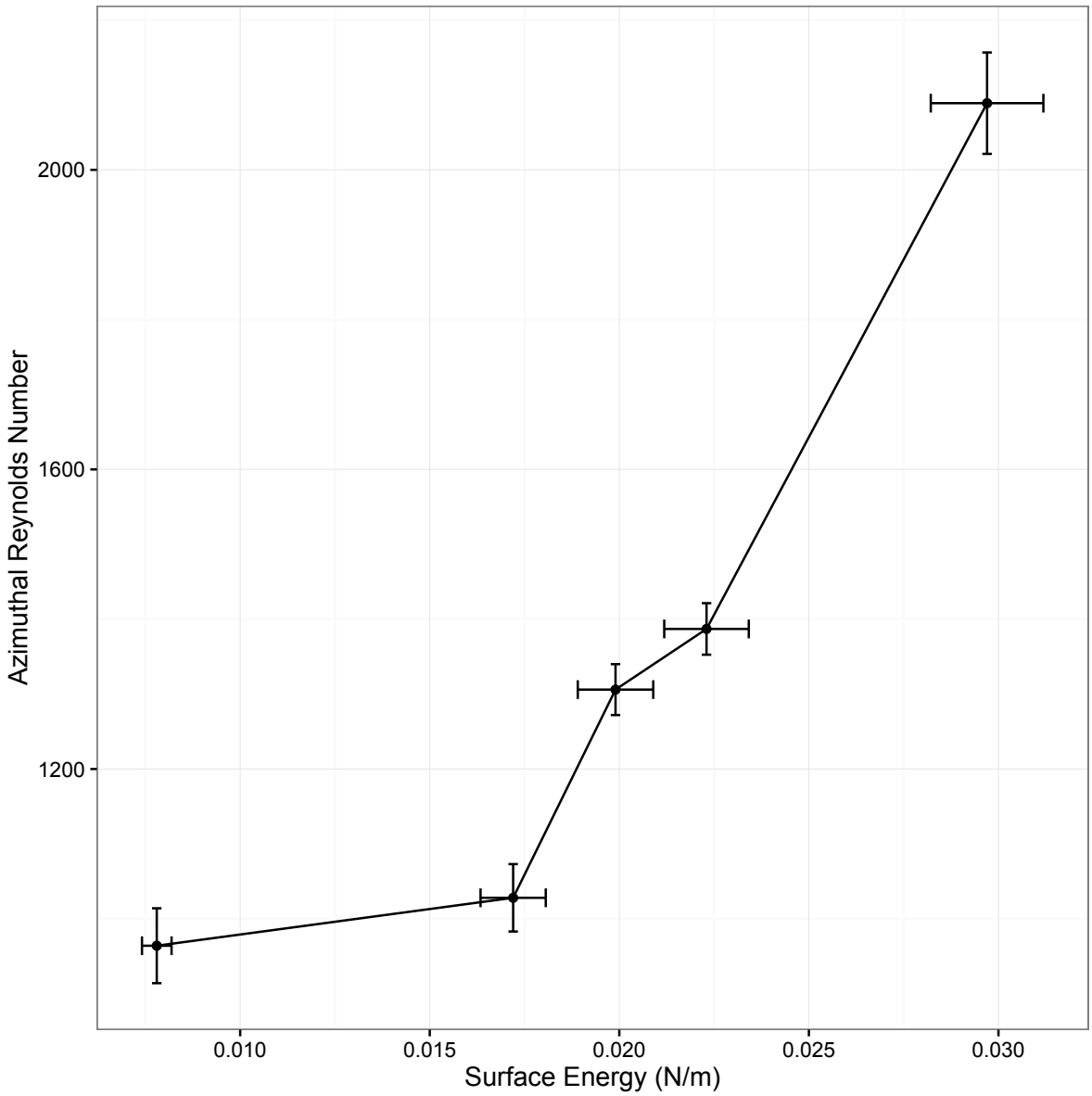

Figure 39. Azimuthal Reynolds Number for transition from segregated to banded flow with respect to the surface energy for the liquid pair. As seen above there is a possible equation that could capture the influence of all three forces on the system.

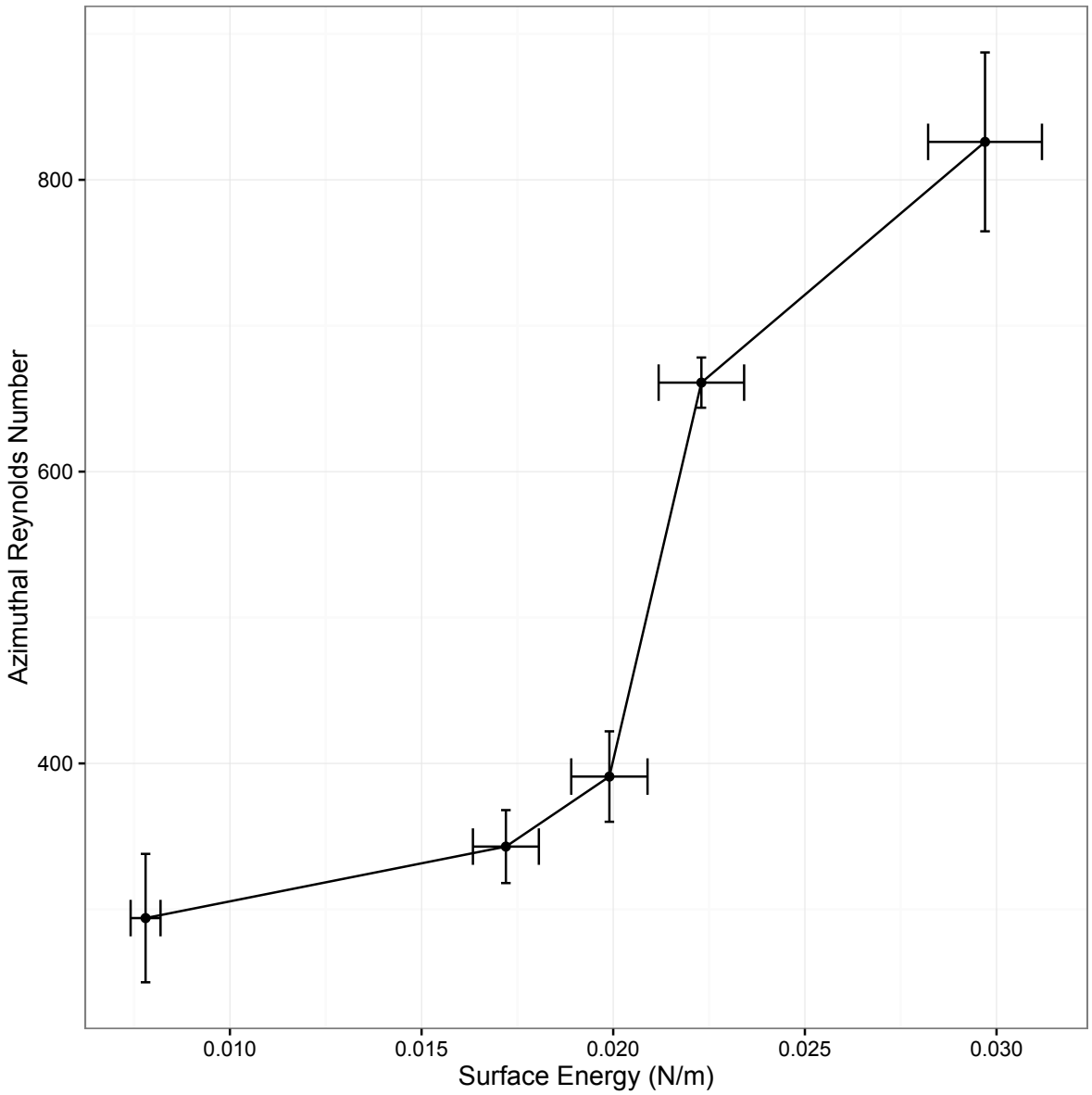

Figure 40. Azimuthal Reynolds Number for transition from segregated to banded flow with respect to the surface energy for the liquid pair. As seen above there is a possible equation that could capture the influence of all three forces on the system.

Performing a non-linear regression on both the datasets searching for an equation of the form $y = ax^b$, where y is the Reynolds number for transition and x is the interfacial energy between the fluid pair.

For transition from segregated to banded flow

$$Re_{transition} = 10136\sigma^{0.5}$$

And for transition from stratified to segregated flow

$$Re_{transition} = 9067\sigma^{0.74}$$

5 data points are not enough to make a good estimate on the prediction of transition points depending on the Reynolds Numbers but the coefficient of the interfacial energy shows that effects of surface energy affect transitions more during the first primary transitions rather than the second transition i.e. the transition from segregated flow to banded flow. The initial energy barrier is higher for breaking the most stable state i.e. the stratified state and thereinafter the energy barrier can be easily overcome through energy dissipation within the reactor.

CHAPTER 4

APPLICATION OF TAYLOR COUETTE FLOW: SILICA MICROCAPSULES

4.1 Introduction

Silica nanocapsules are advantageous containers for any materials due to their superior mechanical and thermal properties over other popular materials, which are usually some forms of polymers. There are several ways of making these capsules that usually involves templating using a two liquid phase suspension. Using the advantageous mixing platform afforded by the Taylor-Couette reactor as a mechanism for generating miniemulsions that form the initial templates for the capsules. The idea proposed here is the mechanism for using a Taylor-Couette cell as the primary means of forming a stable suspension that would then subsequently enable the capsules to be formed over time with minimal coalescence. Smoluchowski [51] studied coalescence initially and he gave the following equation

$$C_s(v, v') = \frac{\gamma}{\pi}\left((v)^{\frac{1}{3}} + (v')^{\frac{1}{3}}\right)^3 n(v)n(v')$$

When surfactants are used as templates for the formation of these emulsions the coalescence rate is much lower due to minimized interactions between the droplets due to them being covered by surfactant micelles.

Traditional methods of preparing capsules usually involve using either sacrificial template that is later dissolved out or through the formation of microemulsions using larger amounts of surfactants.

For the purpose of encapsulation in this work, we used surfactant-induced emulsions as the templates for the formation of such capsules. Fickert et al. [52] showed the formation of nanocontainers with either Grubb's catalyst or dicyclopentadiene being stored inside the silica shells. The mechanism used for generating emulsions in this paper was by Ultrasonication using a Branson 450 W ultrasonicator and letting the condensation reaction occur overnight thereafter. The primary silica precursor used for their experiments was Tetraethoxysilane (TEOS) with some amounts of 3-mercaptopropyltrimethoxysilane (MPTES) and 3-aminopropyltriethoxysilane (APTES) being used at times.

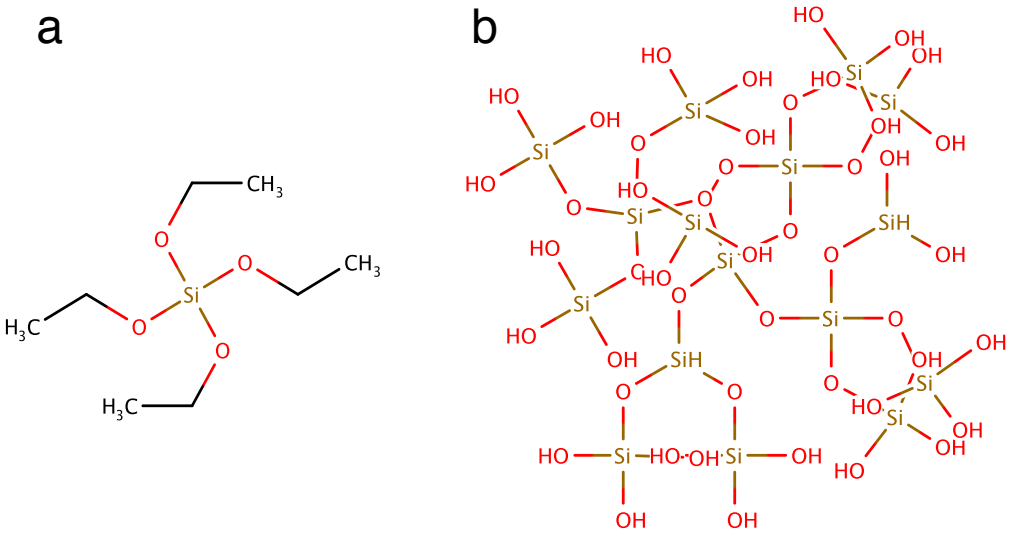

Figure 41. Silica precursors used (a) and Siloxane linkages (b) that leads to the formation of silica shells.

4.2 Reference Experiments and characterization

Two sets of reference experiments were done for comparing results to that obtained after emulsification in a Taylor Couette cell – through conventional stirring with a magnetic stir bar and with emulsion being done using an ultrasonicator. Emulsions were prepared using a 30 mL surfactant solution with a concentration of 1 mg ml^{-1} of CTMA-Br. The emulsified material was a mixture of 2g of TEOS and 0.66.g of Hexadecane.

Emulsification in the ultrasonicator was done at amplitude of 60%, and a pulse of 30s with a quiet time of 10s in between for 3 minutes. The solution was subsequently kept and stirred overnight for the silica condensation reaction to complete.

Emulsification using only the stir bar was done using the same compositions as described above without processing the solution in the ultrasonicator. The mixture was once again left overnight to complete the silica condensation reaction.

Dynamic light scattering for the silica capsules was done assuming standard physical parameters of silica – a refractive index of 1.46 and an optical absorption of 0.01, values taken from Wang et al. [54]. The intensity-averaged sizes have been displayed below, with the data collected from the DLS

software. Measurements for the experiment standard done using Ultrasonication showed particle sizes of $135\,nm \pm 48\,nm$, a very monodisperse distribution.

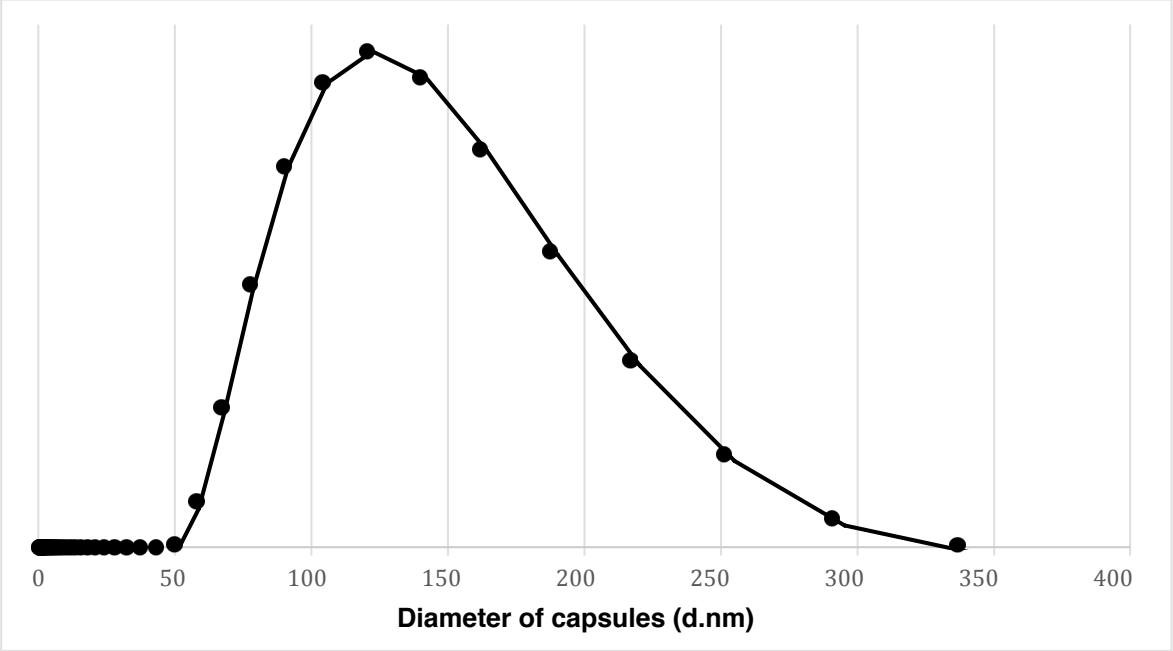

Figure 38. Diameter of capsules prepared using Ultrasonication with 60% Amplitude and a 30s pulse.

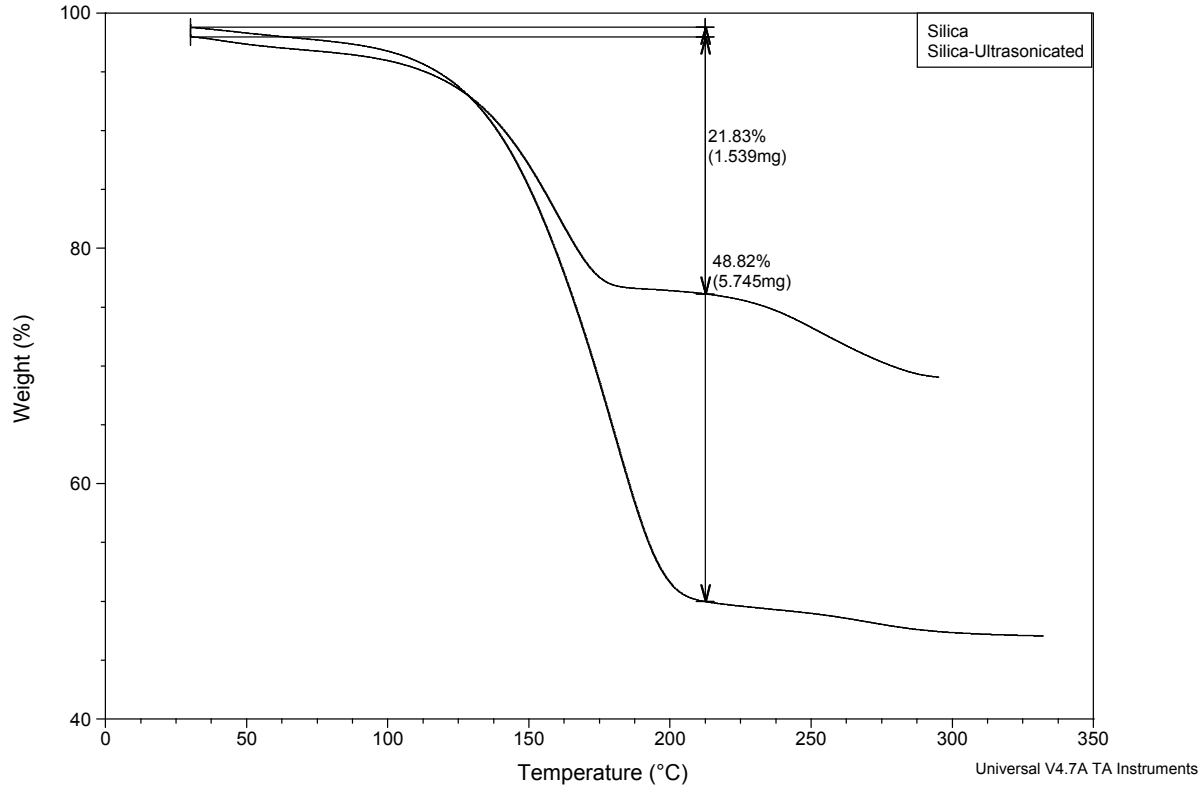

Figure 42. TGA shows a 27 wt% encapsulation of Hexadecane.

Samples that were stirred continuously with a magnetic stirrer showed no particles under the size of 6 μm and were of much larger size than the capsules obtained through emulsification via ultrasonication. Counting particles from SEM images of the same provides us with a distribution of the particle sizes in that system.

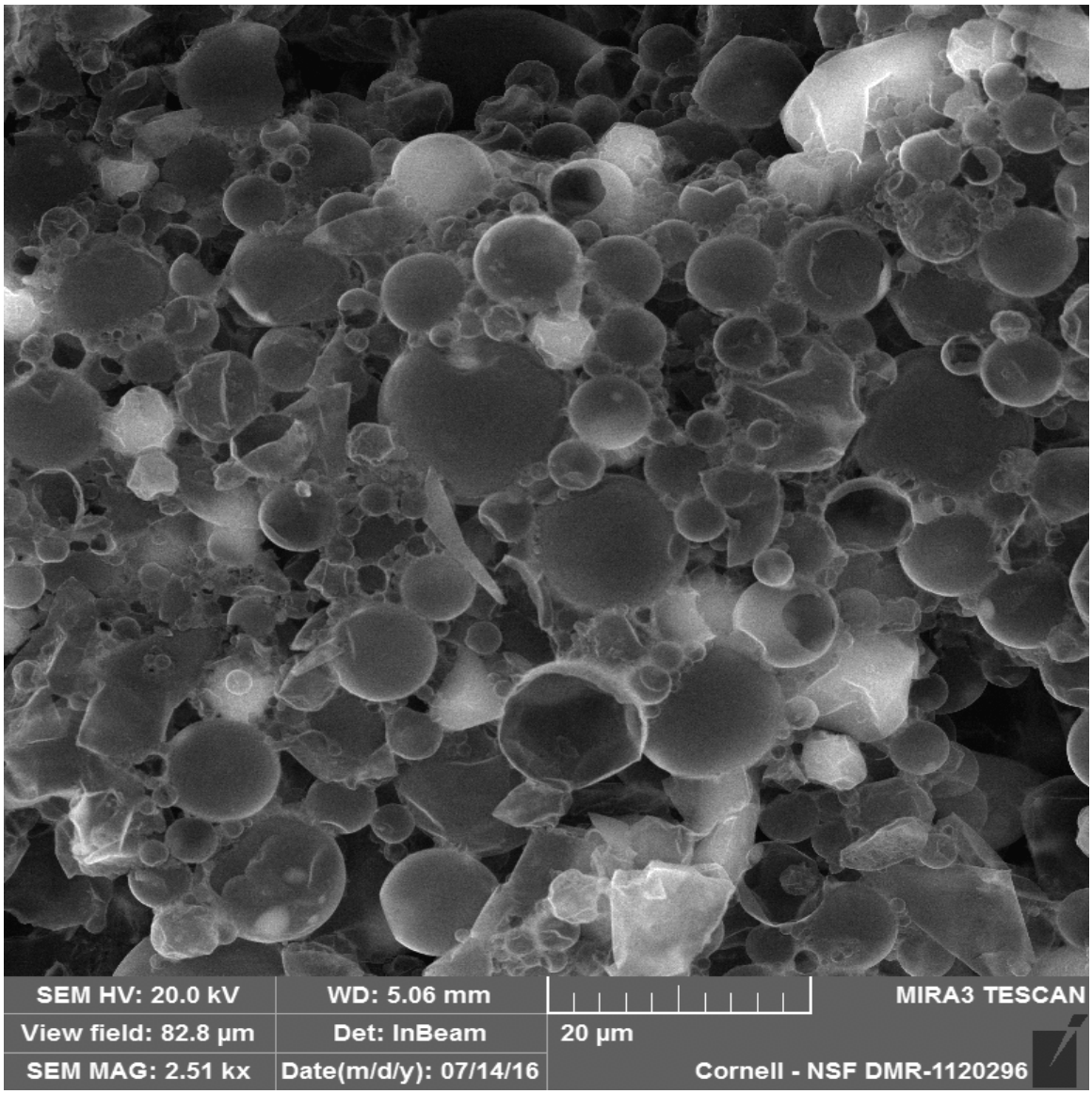

Figure 43. SEM Images of capsules created after stirring with a magnetic stir bar

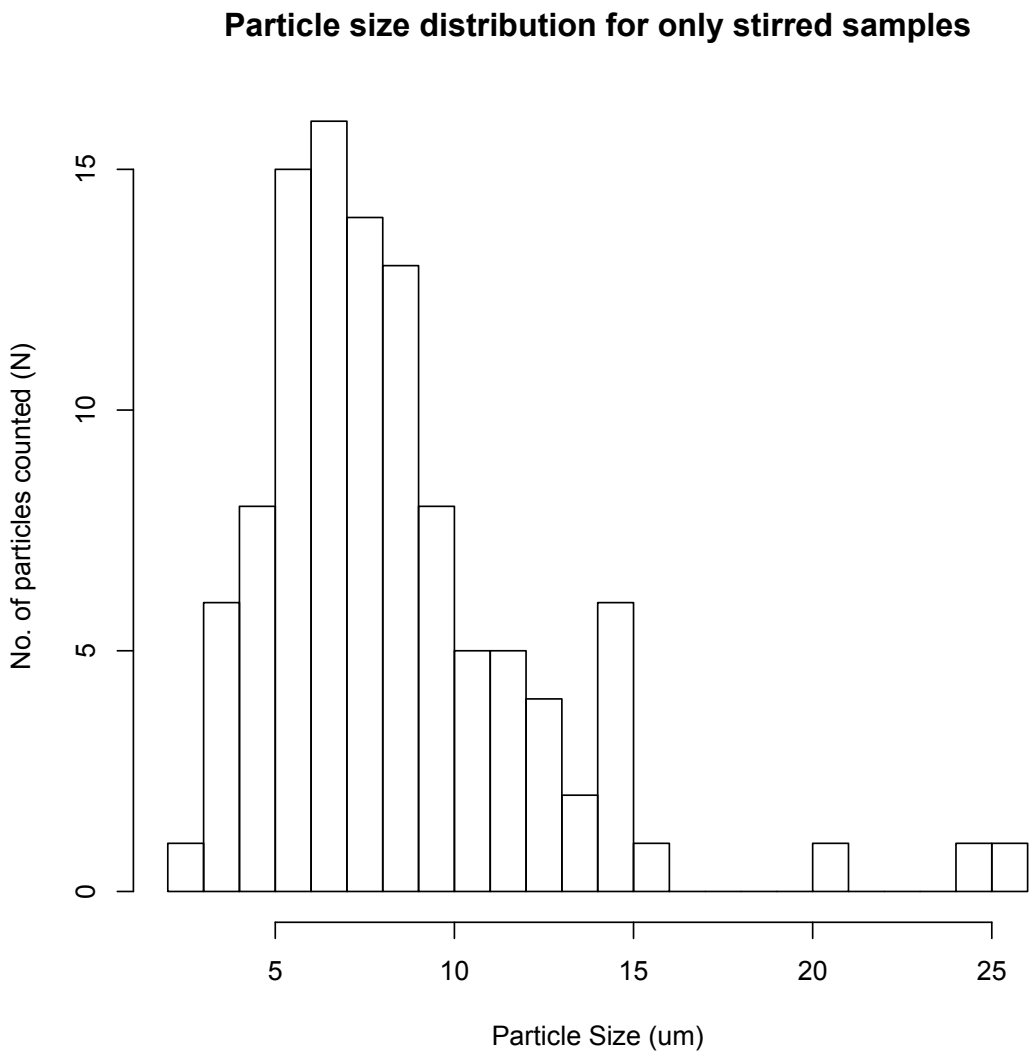

Figure 44. Particle size distribution for stirred samples

The average particle size for the distribution is 8.37 μm with a standard deviation of 4 μm for the distribution. As seen from the histogram the particle sizes and distributions are much larger than that obtained after ultrasonication and there is therefore scope of using a device such as the Couette cell to

decrease particle size distribution and narrow down the range of the particles to obtain more uniform particles.

EDS Spectra for one sample shows that the surface is made out of silica due to the signal for both silicon and oxygen being obtained from the capsules. Some capsules also show the presence of Carbon because of the hexadecane that is filled inside them. This confirms that encapsulation is taking place inside the particles, but there is some amount of breakage among the particles as seen from the EDS images where most of the capsules have no Carbon signal.

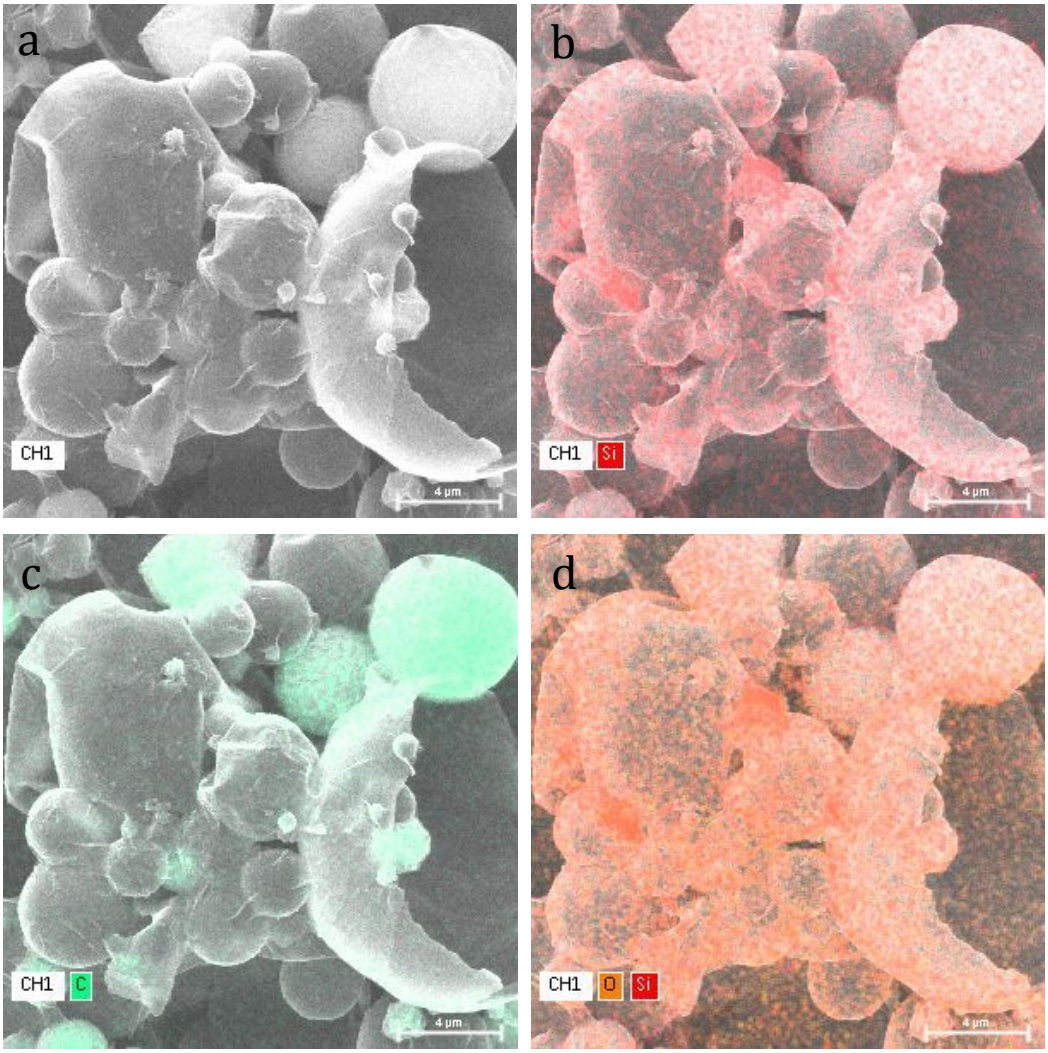

Figure 45. EDS images for silica nanocapsules, a. Original Image b. Silicon c. Carbon d. Silicon and Oxygen

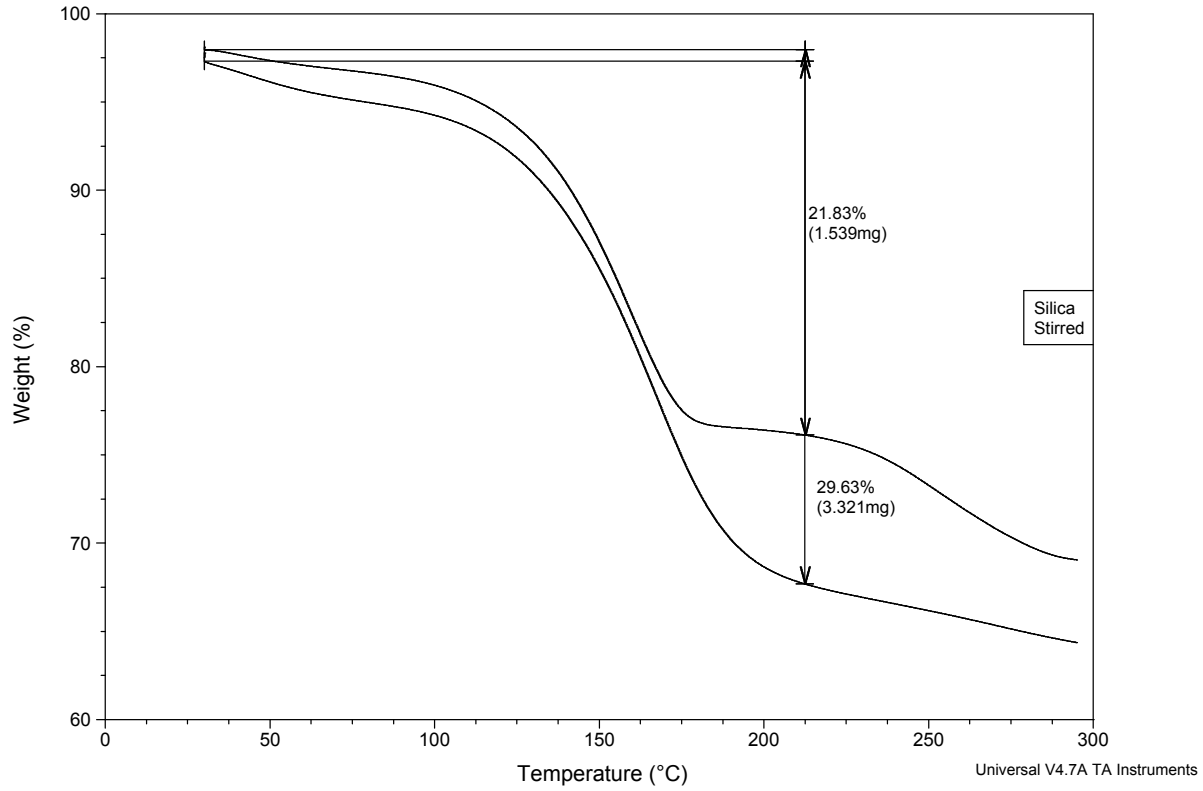

Figure 46. TGA data shows low encapsulation of 8% of hexadecane in the particles.

4.3 Taylor Couette Emulsifier

Using the Taylor-Couette as an emulsifier has been proposed in this thesis. Creating a uniform distribution of droplets that are then influence by the surfactant is done in the Taylor Couette setup in our laboratory. Once droplets are stabilized by the surfactants, repulsion between the aliphatic surfactant chains would minimize coalescence between the particles and the shear force due to the rotation as well as turbulent eddies within the vortices would break up larger particles till they reach a size distribution consistent with the length scales associated with the reactor. For the purpose of testing this hypothesis,

we used a Taylor-Couette contactor in which axial flow could also be induced with the use of a peristaltic pump. The physical dimensions of the cell are listed below

$\boldsymbol{L_C}$	$15 \pm 0.1\ cm$	$\boldsymbol{R_2}$	$2.537 \pm 0.01\ cm$
$\boldsymbol{R_1}$	$2.279 \pm 0.01\ cm$	$\boldsymbol{d}$	$0.258\ cm$
$\boldsymbol{\eta}$	0.898	$\boldsymbol{T}$	58.14

Table 4. Dimensions of the couette cell used for emulsifying the reaction mixture.

Deionized water was used in all experiments and a concentration of 1mg ml-^{1} of CTMA-Br was used. The density and viscosity of the continuous phase I.e. the phase with the surfactant was the same as that of water since the concentration of the surfactant is not large enough to change it. The viscosity of the dispersed phase was measured using a parallel plate viscometer operated in constant shear mode. The measured viscosity was 0.836 mPa.s (or 0.836 cP) and the measured density of the mixture was 900 kg/m^{3}.

The surface tension between the liquid pairs was measured using the method previously described in Chapter 2 by Rashidnia et al. [45] and was found to be 0.00023 N/m. The surface tension between the two liquids was extremely low and therefore it would have been easy to break the boundary between the two fluids and induce segregated and banded flow. 4 different rotation rates were

studied in the process coupled with 3 different axial flow rates. The rotation rates were – 200, 500, 800 and 1100 RPM and the axial flow rates used had Reynolds' Numbers of $Re_z = 19.3, 36\ and\ 72.9$.

Nandi et al. [44] have shown earlier that a couette cell operated in the laminar regime acts as a stabilizer and prevents coalescence of particles. Smoluchowski's classic theory [51] assumed that on contacting, two droplets would merge together to form a larger droplet. Based on that, he computed the coalescence rate to be

$$C_s(v, v') = \frac{\gamma}{\pi}\left((v)^{\frac{1}{3}} + (v')^{\frac{1}{3}}\right)^3 n(v)n(v')$$

In reality, the rate is lower than this as the concept of merging on contact is not valid and the actual rate is represented as a fraction of this

$$C(v, v') = \kappa C_s(v, v')$$

Where the prefactor κ relates to the droplet population and the shear rate applied to the emulsion.

$$\kappa = \alpha_0 \left[\frac{4q}{1+q^2}\right]^5, \qquad q = \left(\frac{v}{v'}\right)^{\frac{1}{3}}$$

The critical capillary number dictating droplet breakup is 0.7, which means that any droplet above a certain size for a certain shear rate will be broken down to a smaller droplet due to shear forces acting on the droplets.

$$Ca^* = \frac{\gamma^* a_{max} \mu_c}{\sigma} = 0.7$$

Apart from this there are also two other length scales in the system determined by the turbulent eddies and the droplet breakup due to viscous, inertial and surface forces. These are the size distribution obtained through the Haas correlation [39] and also a secondary length scale associated with the vortices

$$d_p = 150We^{-0.65}Re^{-0.2}\left(\frac{\mu_d}{\mu_c}\right)^{0.5}\left(\frac{d}{R_1}\right)^{0.5}, from\ the\ Haas\ correlation$$

4.4 Results and discussion

Particle size distributions obtained from analyzing SEM images of the dispersions as well as performing DLS experiments on dilute suspension clearly indicate the presence of 2 length scales in the sample. In terms of population of particles about each of these length scales, the number of particles counted for the smaller length scale is higher than that counted for the larger length scale. There are also some particle that are much larger than the length scales shown above, but they are very few in number and are formed as they have not been emulsified within the Taylor-Couette reactor. A standard particle size distribution histogram looks like Figure. **(insert number here)**

The general size trend observed with increasing axial flow rates for all rotation rates is that the length scale does decrease. The lower length scale, is the turbulence microscale and is a function of the dissipated energy in the system and addition of axial flow increases the energy dissipation in the system. Therefore the trend of observing smaller particles at higher axial flow rates could be explained.

The larger length scale is a function of the shear forces acting on the system, due to the rotation of the inner cylinder. The correlation put forward by Haas [39], was valid only for turbulent flows without any induced axial flow.

The general observed trend for these particles is also that they decrease in size with increasing axial flow rates. It implies that addition of axial flow rates to a certain extent destabilizes the droplet and overcomes the energy of cohesion to break the droplets into even smaller droplets. The change in length from $Re_z = 19.3$ to $Re_z = 72.9$ is not appreciable across all rotation rates and therefore there would seem to be a limiting effect the axial flow rate has on the droplet size.

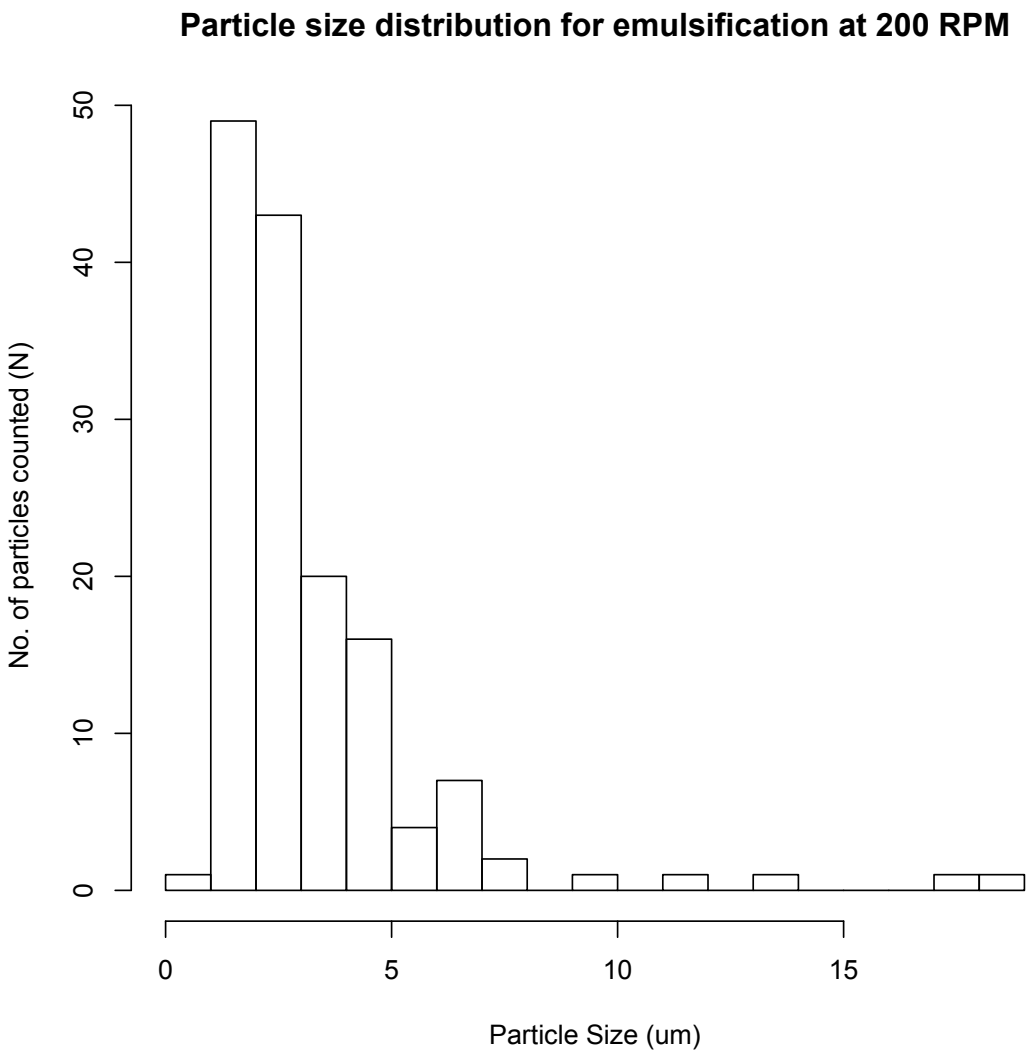

Figure 47. Histogram for particle sizes measured for a sample only emulsified at 200 RPM

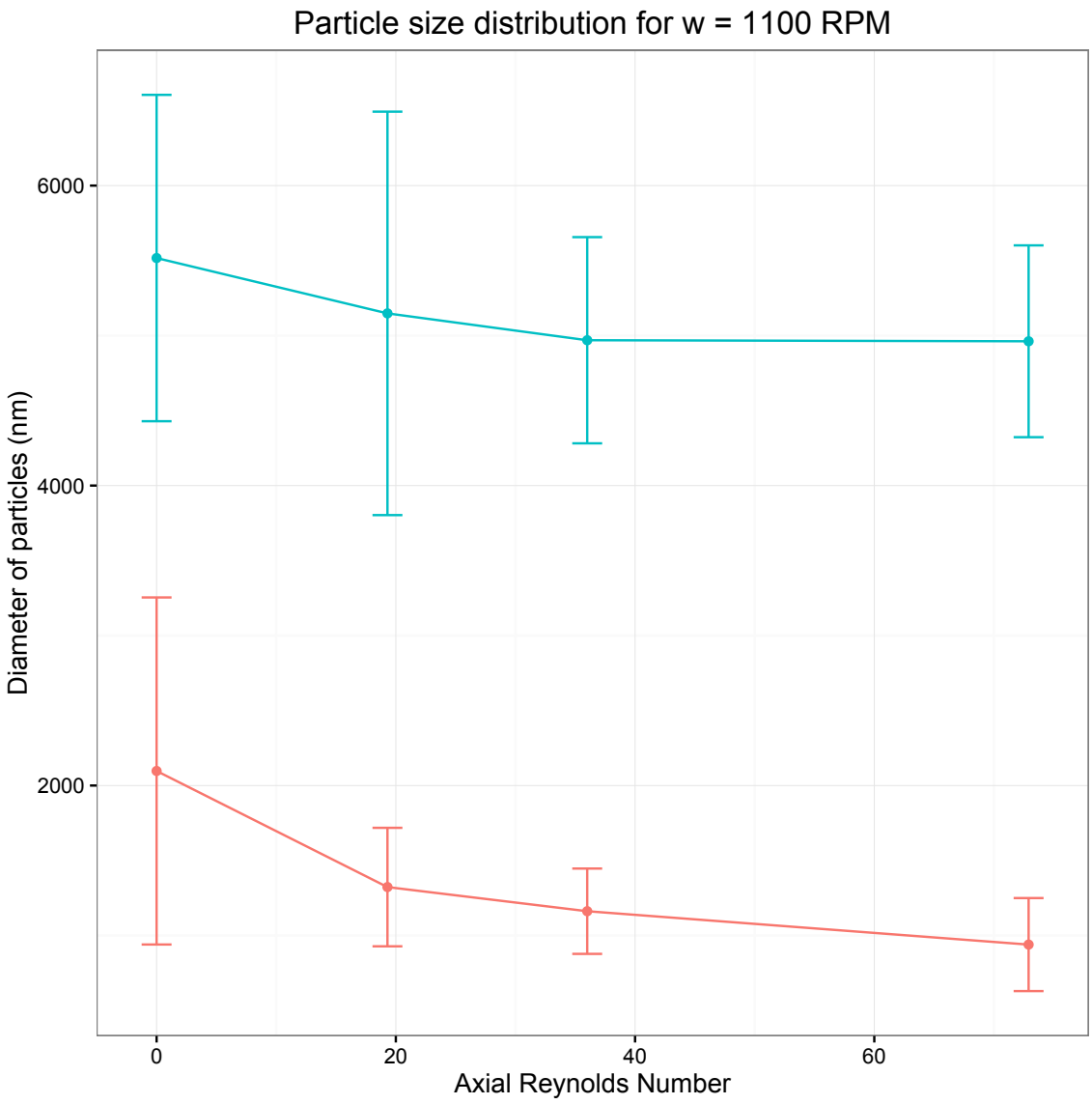

Figure 48. Changes in particle sizes with increase in Axial flow rate for

Re_θ = 6800

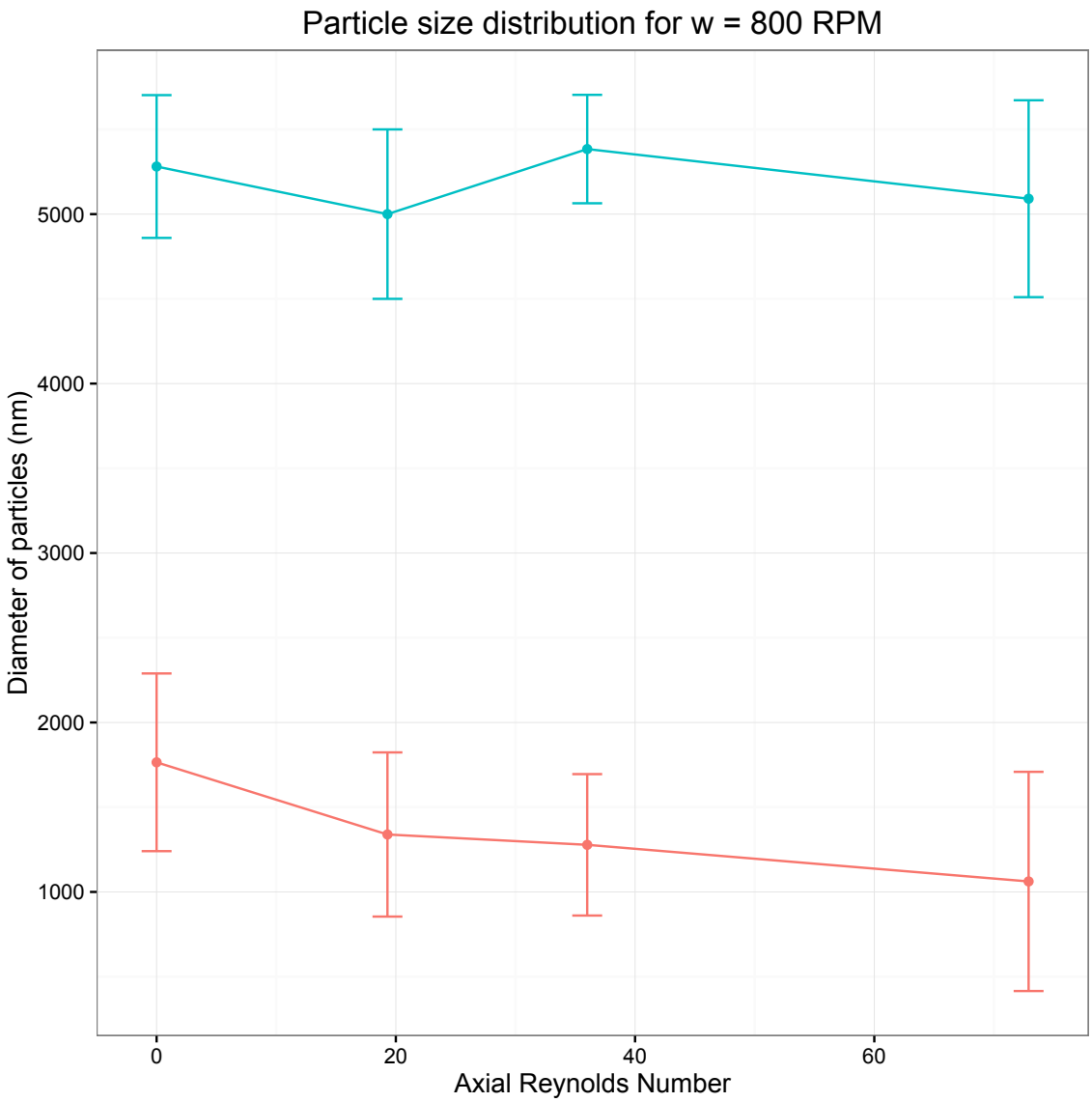

Figure 49. Changes in particle sizes with increase in Axial flow rate for

$\boldsymbol{Re_\theta}$ = 4945

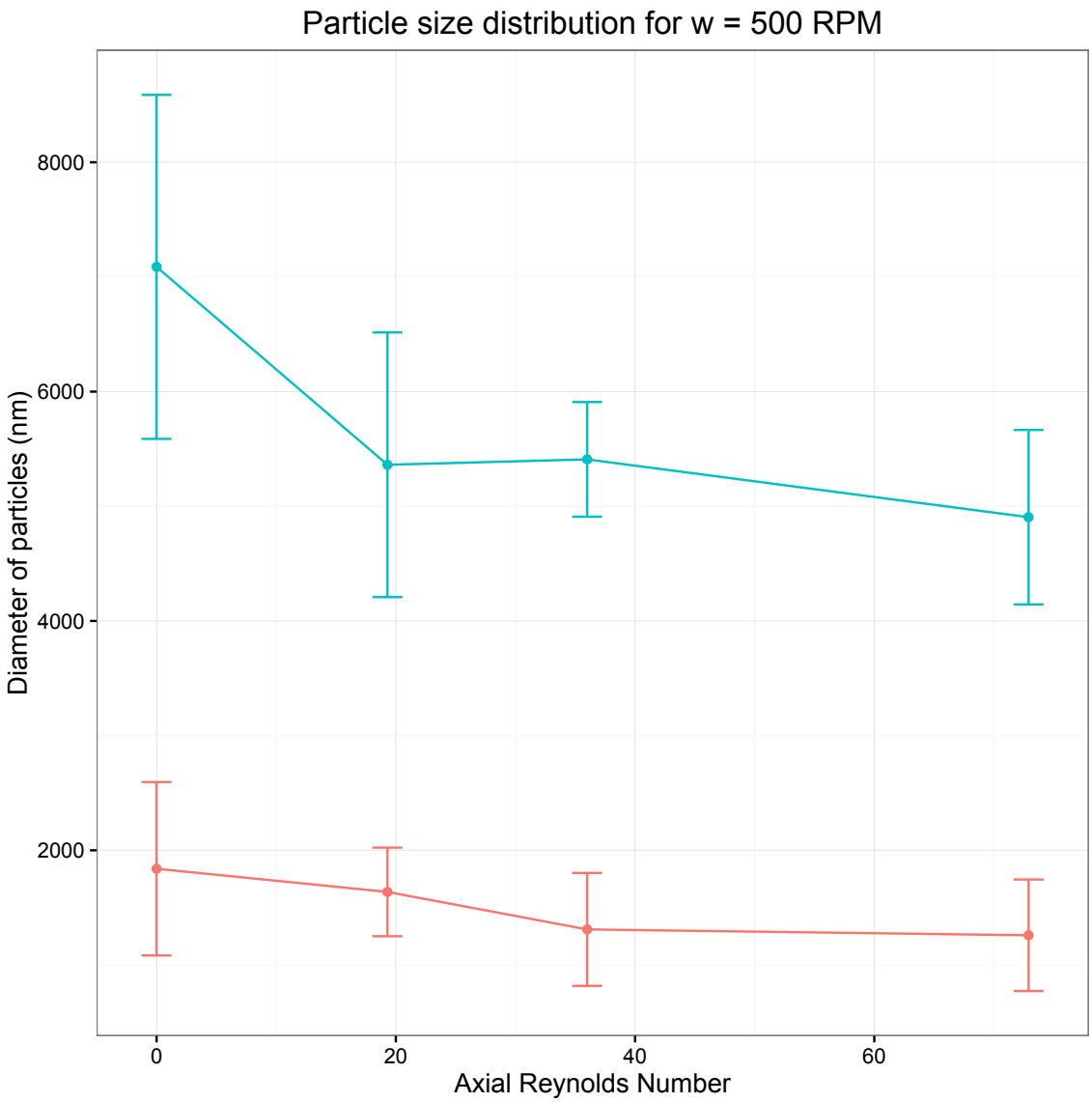

Figure 50. Changes in particle sizes with increase in Axial flow rate for $\boldsymbol{Re_\theta}$ = 3090

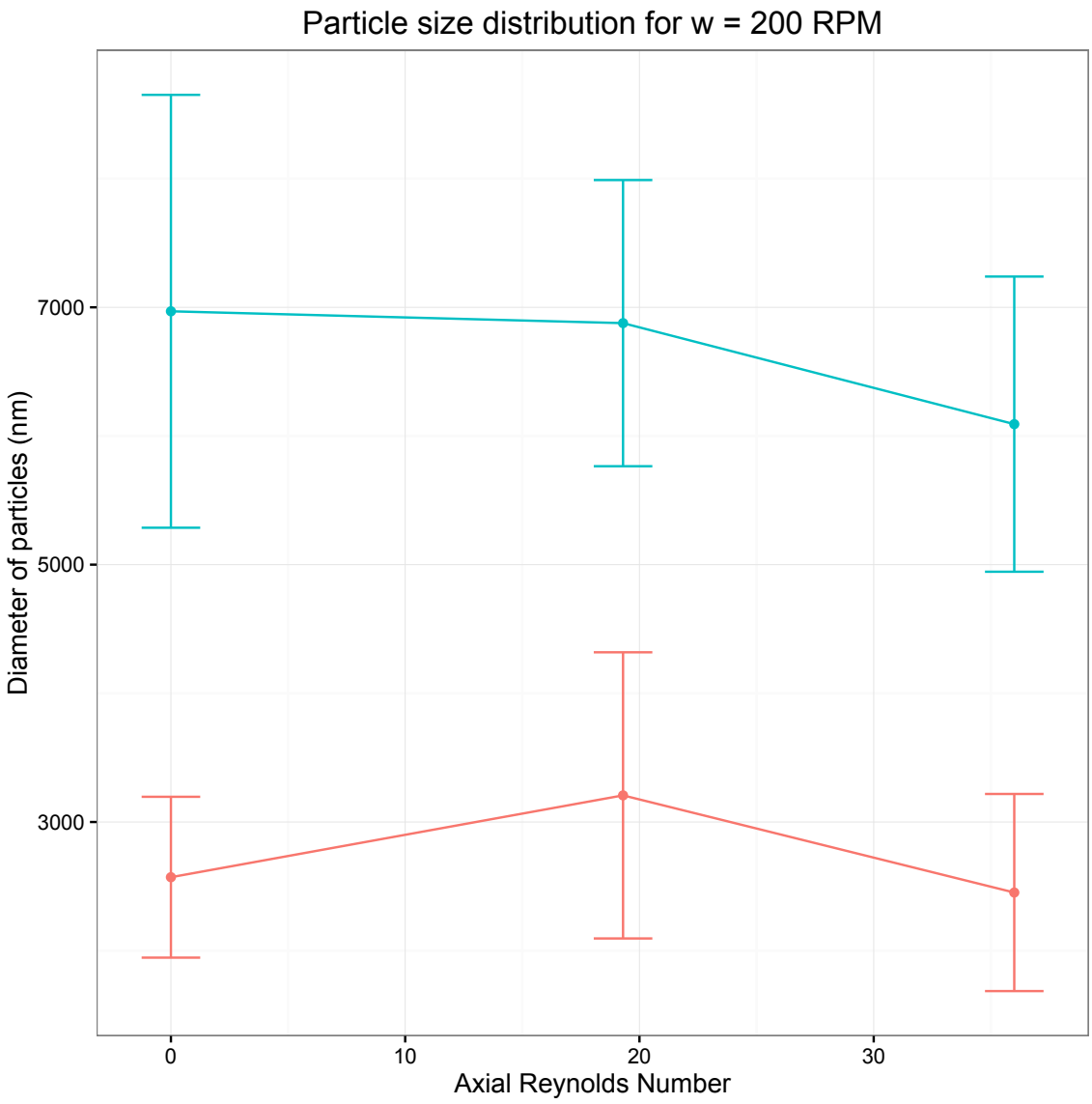

Figure 51. Changes in particle sizes with increase in Axial flow rate for

Re_θ = 1236

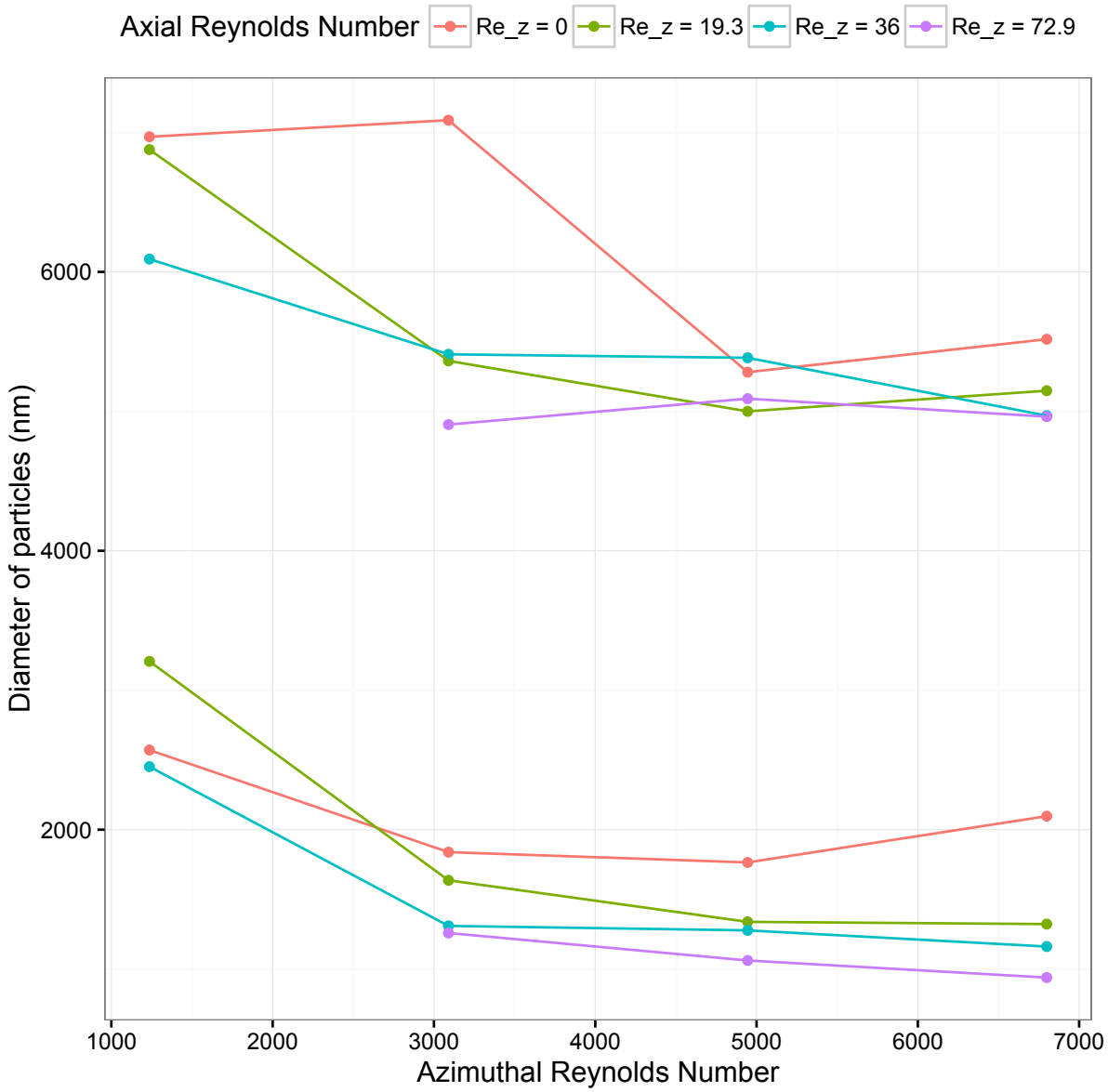

Figure 52. Size evolution at different axial flow rates for different rotation rates

The general size trend for all axial flow rates is that the particle size decreases with increasing rotation rate at a given axial flow rate. At the highest flow rate studied, this effect is not as pronounces as at lower flow rates where the size of the particles remains nearly constant at all rotation rates, within the standard deviation of the measurement at that point.

The additional benefit gained by increasing the axial flow from $Re_z = 36$ to $Re_z = 72.9$ is not substantial and it indicates the fact that there is a possible limit to how much any induced axial flow rate can influence the system. Size distributions for a rotation rate of 200 RPM is much larger than the sizes at 1100 RPM for all axial flow rates due to higher particle sizes. These higher particle sizes are due to lower energy dissipation and lower shearing rate that does not substantially break the droplets. The flow structure at this point of time is that of segregated flow, where larger droplets still remain relatively unaffected by the turbulent vortices. Which is why apart from the 2 length scales, we also observe much larger macroscopic particles as seen from the particle size distributions shown below for 200 RPM

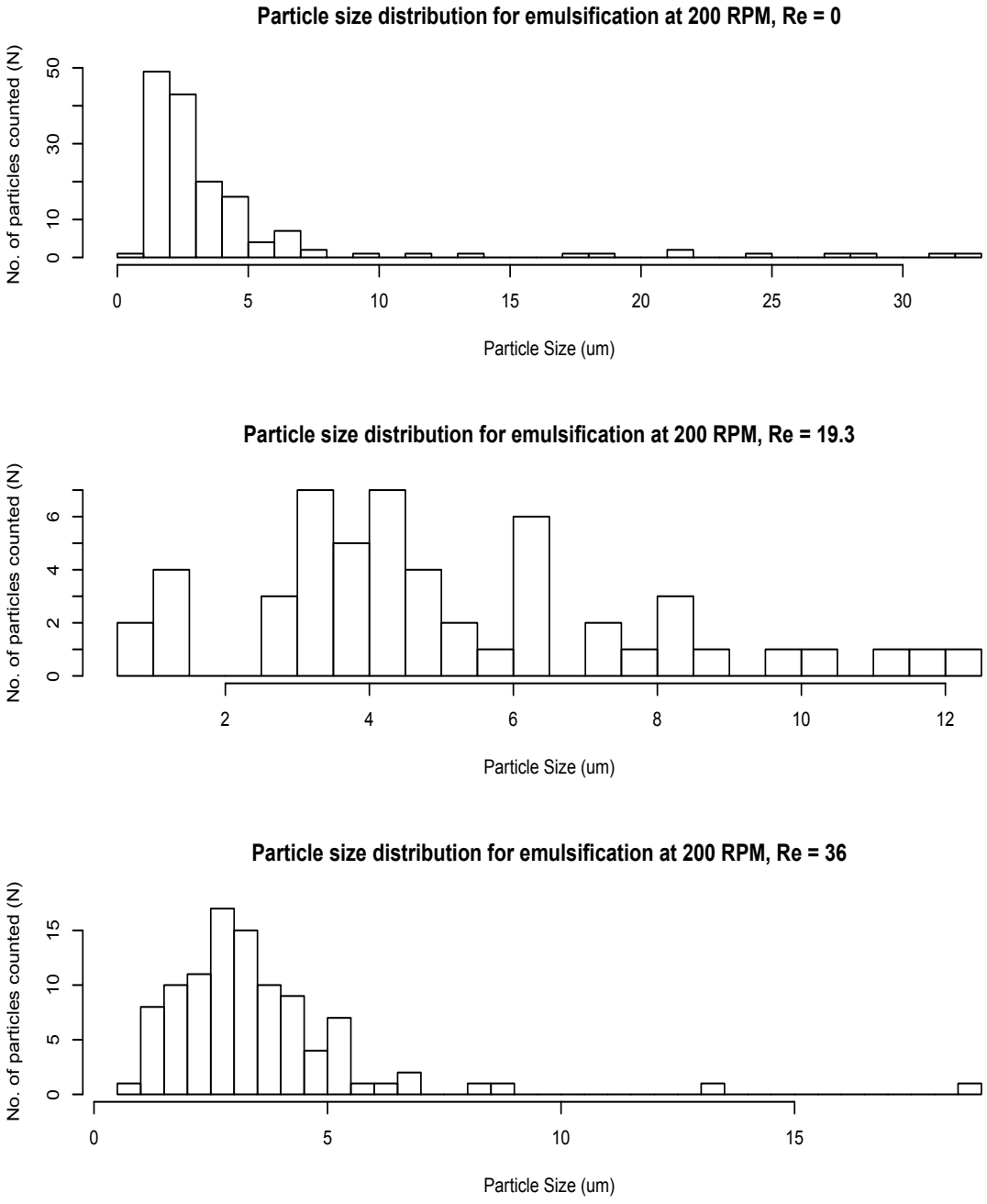

Figure 53. Particle size distributions for Reynolds Numbers of 0,19.3 and 36 at a rotation rate of 200 RPM

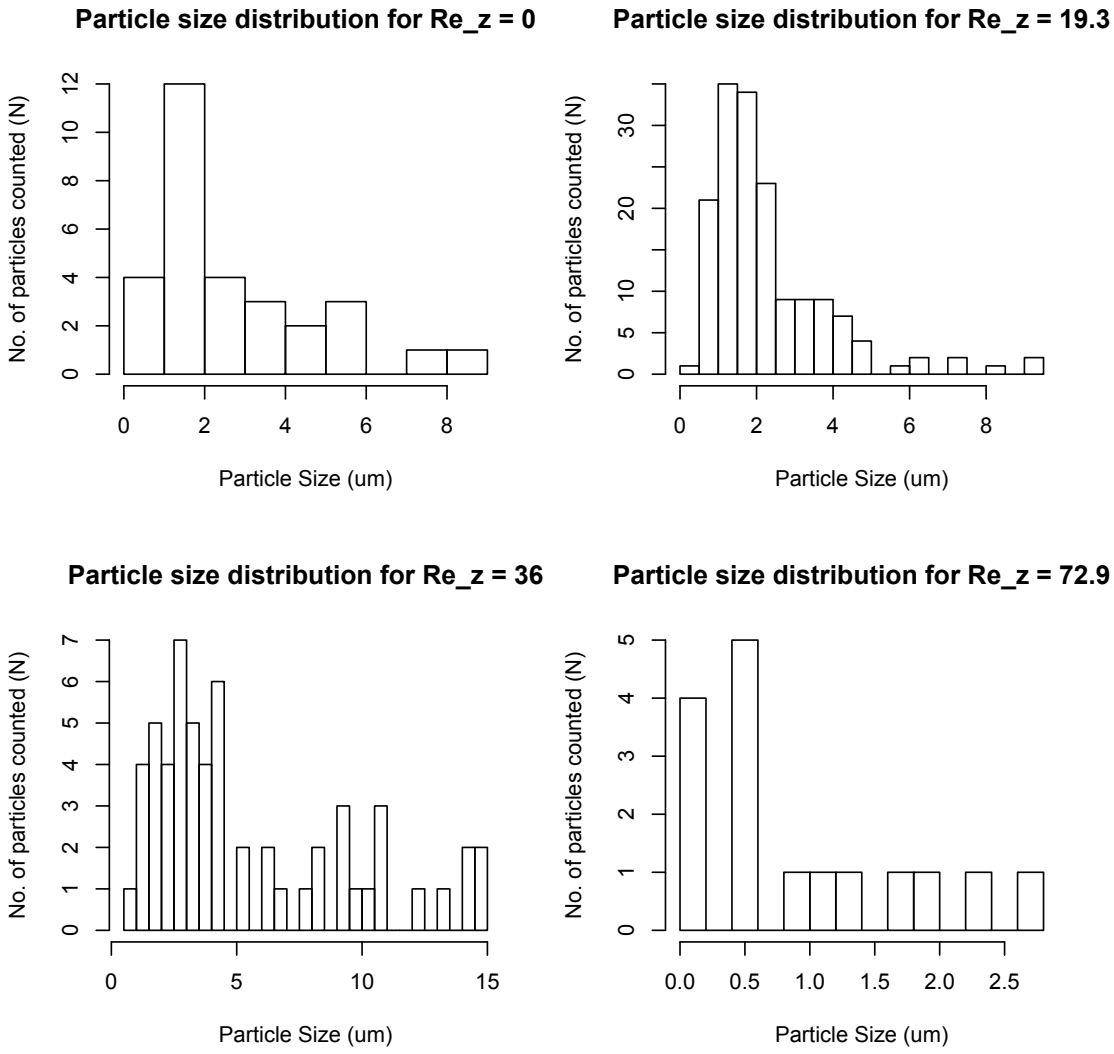

Figure 54. Particle size distributions for axial Reynolds numbers of 0, 19.3, 36 and 72.9 at a rotation rate of 1100 RPM

The maximum particle sizes for a rotation rate of 1100 RPM for different axial flow rates show much smaller and narrower distribution of particles which

would be expected at the higher amount of shear force and dissipated energy present in the system.

How much encapsulation takes place?

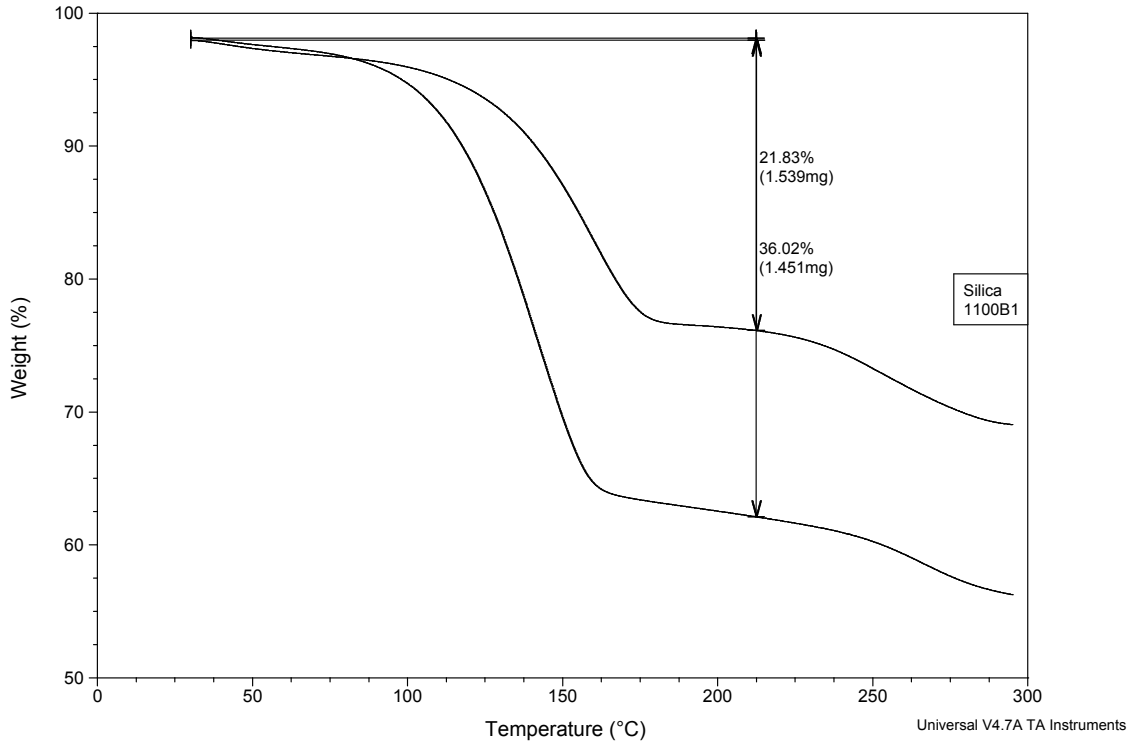

Figure 55. TGA of microcapsules synthesized at 1100 RPM with no axial flow.

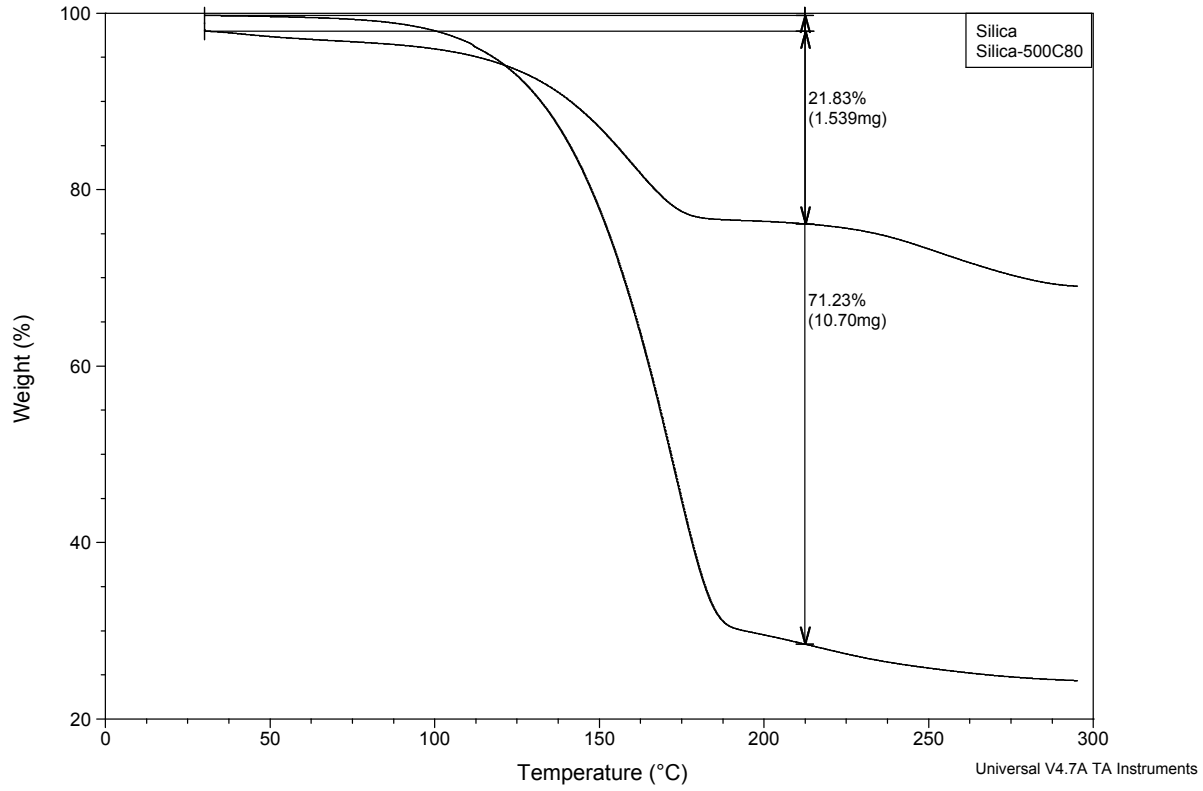

Figure 56. TGA of microcapsules created at a rotation rate of 500 RPM and $Re_z = 19.3$

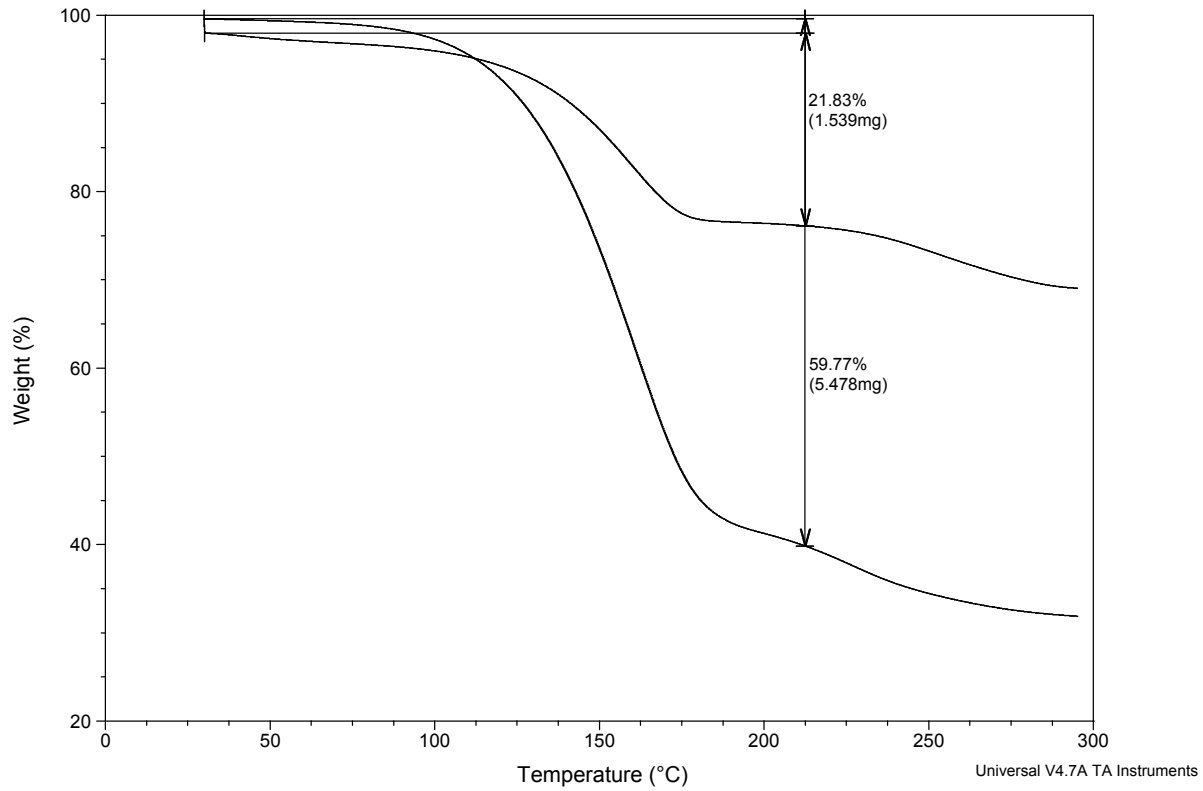

Figure 57. TGA of microcapsules created at a rotation rate of 800 RPM and $Re_z = 36$.

Each different reaction conditions create microcapsules with different shell thickness and therefore a different percentage by weight of the hexadecane encapsulated inside the microcapsules. At this stage it is not possible to say if there is a trend to how much of the organic phase is actually encapsulated inside the silica capsules, but more detailed analysis of particles for the other conditions will reveal if there is a trend to the amount of organics encapsulated inside.

FTIR Spectra for these capsules

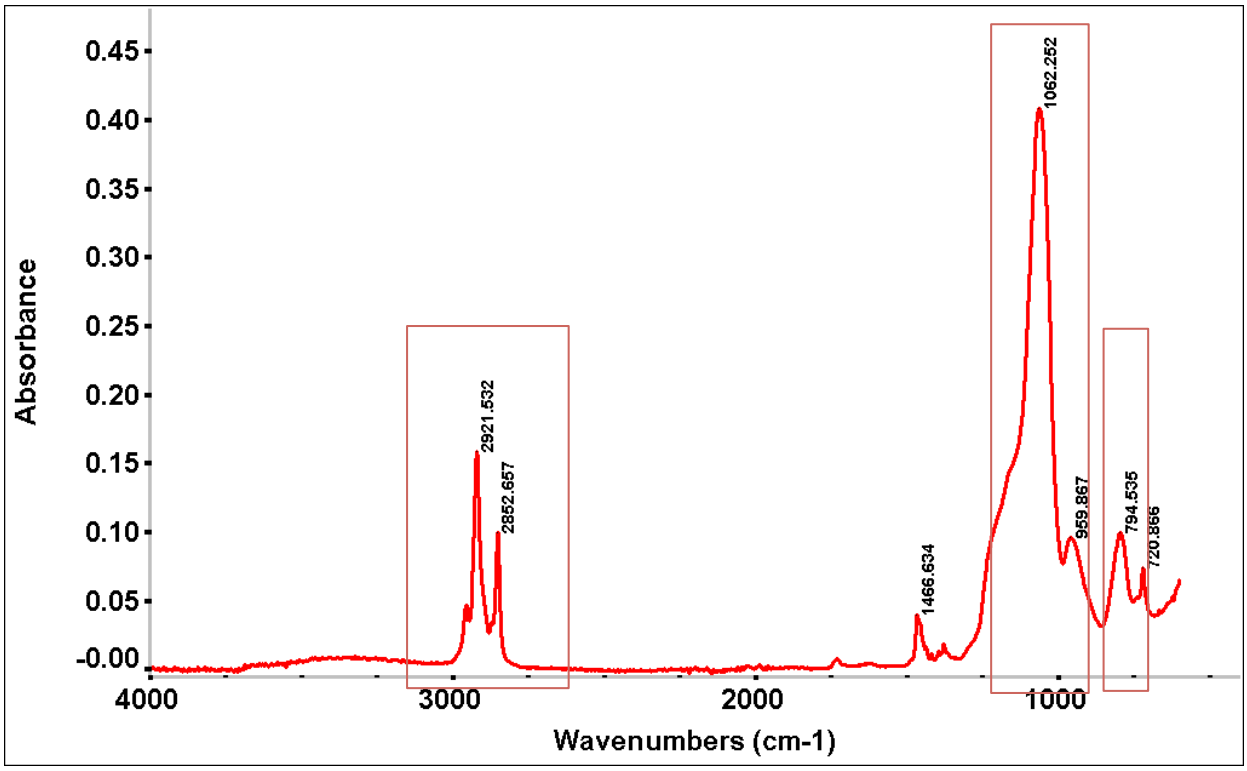

Figure 58. FTIR Spectra taken after crushing microcapsules

Bond type	Spectra
Si-O-Si linkages	1062 cm^{-1}
Methylene stretch	2920 cm^{-1}
Methyl stretch	2852 cm^{-1}
Methylene and methyl C-H bend	1466 cm^{-1}
Methylene rocking	744 cm^{-1}

Table 5. Assignment of FTIR peaks to different characteristics in the sample.

Smaller length scale dominates

There are more number of particles at the smaller secondary length scale compared to the larger droplet length scale. This indicates that the turbulence microscale is the more dominant length scale. It is possible that the droplets when they migrate to the core of the vortices interact with these eddies and are split into smaller particles. This indicates that given a sufficiently large time all particles will interact with these vortices and be broken down into the smaller particles observed in the distribution.

This smaller length scale indicates the presence of eddy vortices or secondary vortices in the system, that act on the droplets locally and break up the droplets into smaller droplets, lower than the size of the primary length scale governed by the primary droplet size.

CHAPTER 5

FUTURE WORK

Information about vortices and wave numbers

How the number and spacing of vortices develops in the system can also be characterized using the wave number. The wave number is defined as

$$a_c = \frac{2\pi}{\frac{\lambda_c}{d}}$$

Where λ_c is the spacing between a counter-rotating pair of vortices. This wave number defines the number of vortices present in the system and is used as a measure of the size of the vortices as experiments have shown that the vortices are circular in shape.

Initial experiments show that, on reaching banded flow, irrespective of the volume fraction, the number of vortices remain the same for the system at all rotation rates for operation without any axial flow.

Heavier liquid as the dispersed phase

Most of the data presented here is when the lighter liquid is dispersed in a denser liquid irrespective of the viscosity. When the opposite happens, a

different set of flow structures are observed apart from the ones already studied. Experiments were done using a 50 wt% mixture of water and glycerol in kerosene. The flow structures observed are

1. Rolling flow, where the denser phase flows along with inner cylinder like a sheath that insulates the continuous phase from the cylinder.
2. Regions where the kerosene is dispersed in the aqueous phase i.e. a form of phase inversion
3. Homogenous systems are observed more readily than for the previous setup.

Properties and dynamics of these systems need to be studied as well to complete the understanding of liquid-liquid Taylor Couette flow.

Three phase systems – immiscible liquids and solids

Systems involving reactions using immiscible liquids often require the use of solid catalysts to accelerate reactions. Since the total contact surface area is enhanced greatly in the dispersed state of flow, it also becomes important to see how solid particles would orient themselves in these flows so as to maximize catalyst efficacy. Ideally, we would like them to align at the surface to be in contact with both simultaneously. If a fixed bed system is being used, locating the catalyst particles at the location where it would be most likely to

contact the liquids is important. Some laser induced fluorescence imaging showed that the spatial orientation of the dispersed phase is dependent on the dominant force in the system. Such a study needs to be extended to banded flows as well to understand how their orientation would determine catalyst location in the system.

Complete encapsulation within the reactor

Currently the reactor has been employed as an emulsification device with the complete reaction taking place elsewhere. Coalescence of droplets means that we observe the large standard deviations around particle sizes as observed in the results in the previous chapter. Earlier, Taylor-Couette vortices have been shown to produce uniform monodisperse particle sizes for crystallization studies and therefore it should be possible to achieve similar results for such an application also. The uniformity of the forces on the system would enable us to obtain more uniform distributions without compromising on particle sizes obtained. Indeed, some experiments done at the batch scale verify this with particle sizes being clustered very narrowly i.e. low standard deviation about the mean. Also as the duration of the reaction in the reactor is longer, all particles have sizes near the turbulent microscale and there is only one length scale involved in the system.

Also, there is a limit to the particle sizes that could be obtained through the system due to the surface tension between the system and the turbulence length scales involved. Decreasing the surface tension through the addition of more surfactants would eventually collapse the two length scales in the system into 1 length scale that would enable us to get a near monodisperse distribution of capsules.

$$d_p = 150We^{-0.65}Re^{-0.2}\left(\frac{\mu_d}{\mu_c}\right)^{0.5}\left(\frac{d}{R_1}\right)^{0.5}, from\ the\ Haas\ correlation$$

The droplet size correlation is depended on the surface tension and therefore decreasing that number would decrease the effective droplet size.

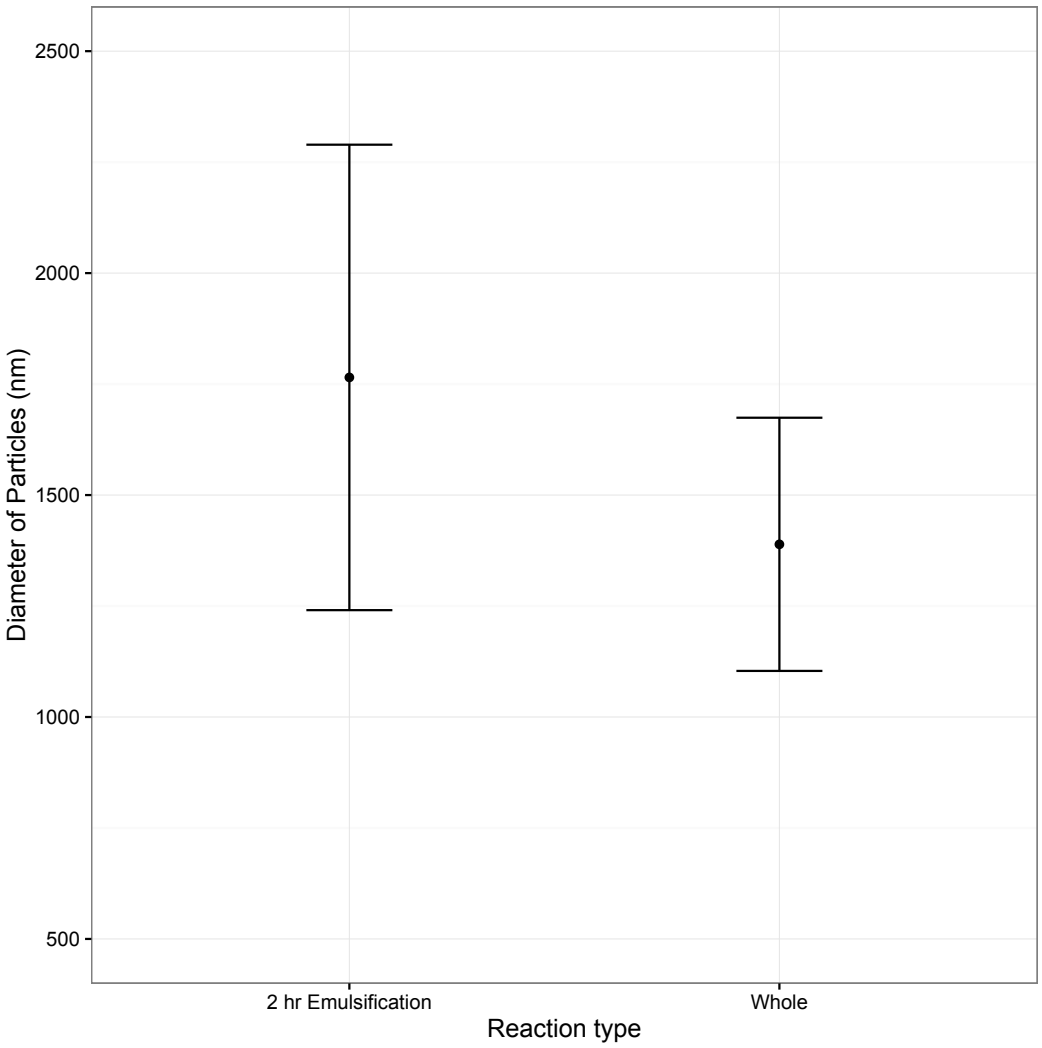

Figure 59. Size distribution at the turbulent length scale for 2 types of emulsifications studied

CHAPTER 6

CONCLUSIONS

In conclusion, the following observations were made that are critical to understanding how transitions in these flows could be understood and how we could possibly predict properties of the system.

Surface energy is critical to understanding liquid-liquid flows

How transitions develop for a two-liquid system is a function of the interfacial energy between the two fluids. The lower the interfacial energy, the faster is the onset of instability given that all other physical parameters remain the same for the system. This was observed when the continuous aqueous phase was doped with a small amount of surfactant that enabled us to change **only** the interfacial energy of the system.

Azimuthal Reynolds Number is the dimensionless number that best describes the system

Based on a mixture viscosity and density as determined by the volume fraction of the dispersed phase in the continuous phase, the azimuthal Reynolds' number was shown to describe the system the best. The Reynolds' number

and the Taylor number are both a measure of the inertial and viscous forces present in the system, but the Reynolds' number is a better fit due to it being of lower order of magnitude. In reality, either the Taylor or Reynolds number should be sufficient without any loss in generality of the terms discussed in this thesis.

Addition of axial flow destabilizes the system

This observation is in stark contrast to the observations for single fluid Taylor-Couette flow where addition of axial flow stabilizes the system and delays the onset of instability. The reverse phenomenon is observed for this system, where increasing intensity of axial flow destabilizes the system much earlier than before. Our hypothesis is that the additional energy dissipated within the reactor due to the axial flow is the mechanism that destabilizes it further.

Predicting Transitions between the primary flow structures is possible

Predicting when a transition will take place for a system is possible knowing the surface energy of the system. This is true when the heavier phase is dispersed in the lighter phase and does not hold true for the opposite case. Also, analyzing the data collected and correlating it to surface energy reveals

that the surface energy is more important for the first transition as compared to the second transition.

Silica Encapsulation utilizes the length scales in the reactor to create microcapsules

Utilizing the mixing properties afforded by the Taylor Couette reactor was the primary aim of this project. Studying droplet breakup and emulsification within the reactor show that there are 2 length scales within the reactor that govern the size of the capsules. Increasing the rotation rate and the axial flow rate both lead to a drop in the primary size of the particles. Therefore it is possible to design systems where we could obtain 2 different particle distribution sizes for applications involving liquid-liquid Taylor Couette flow.

APPENDIX

Viscometry data

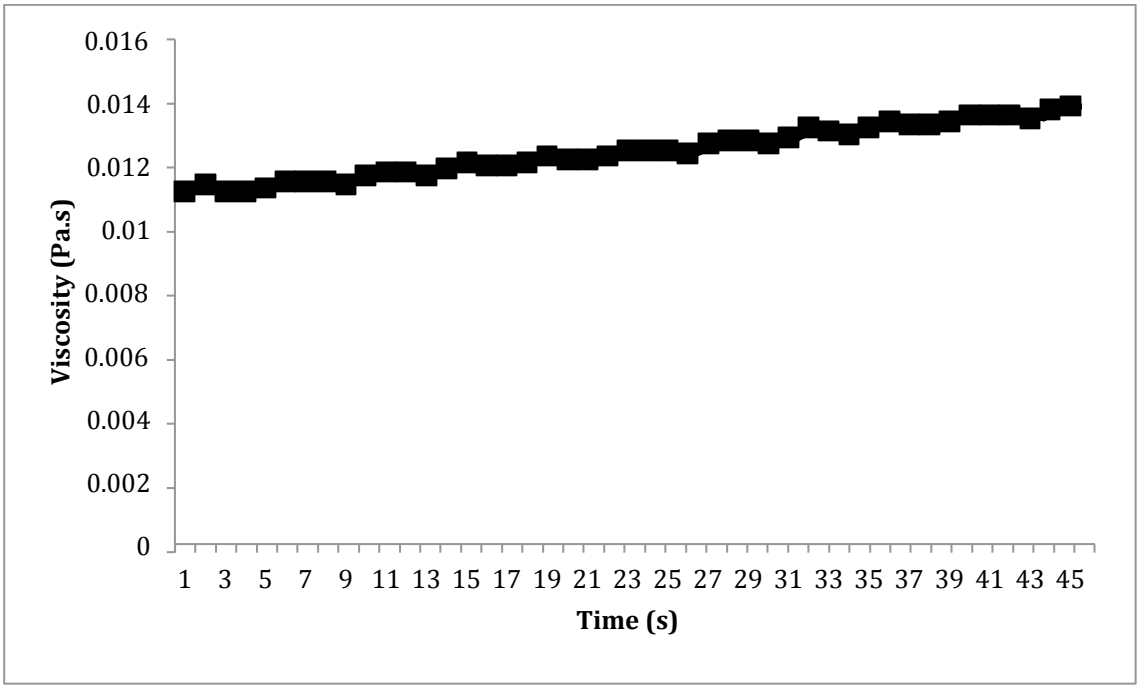

Figure 60. Viscosity of Sodium Iodide/Glycerol and Water solution at a shear rate of 100 s^{-1}

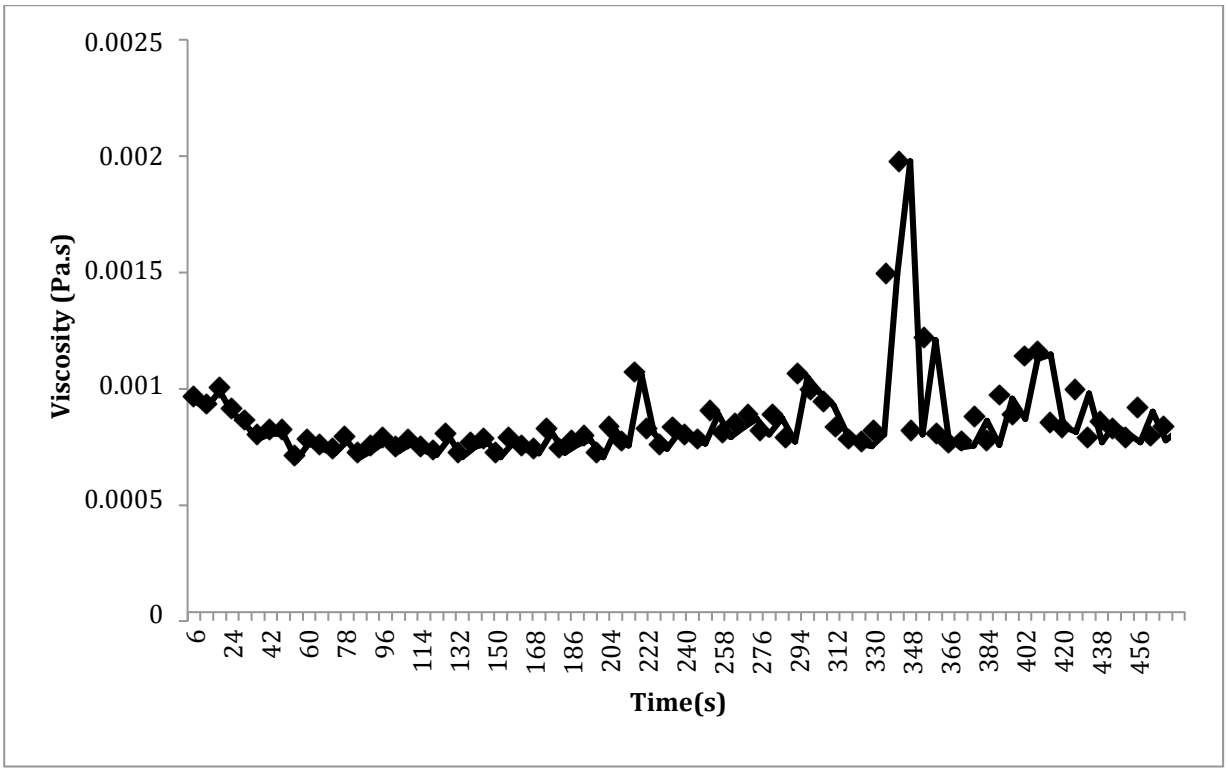

Figure 61. Viscosity of TEOS and Hexadecane solution at a shear rate of

100 s^{-1}

SEM Images for silica microcapsules

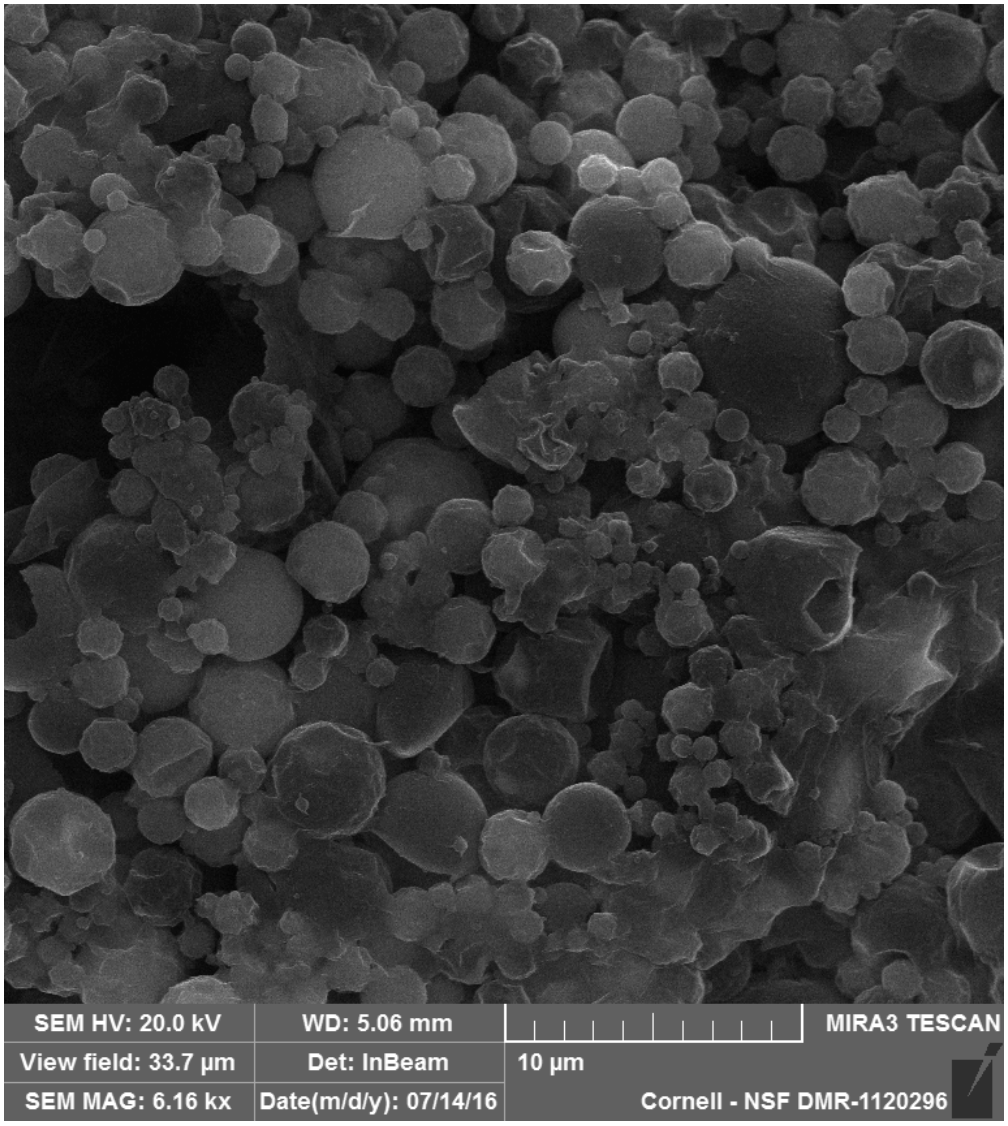

Figure 62. SEM Image for silica microcapsules created at 500 RPM with no axial flow.

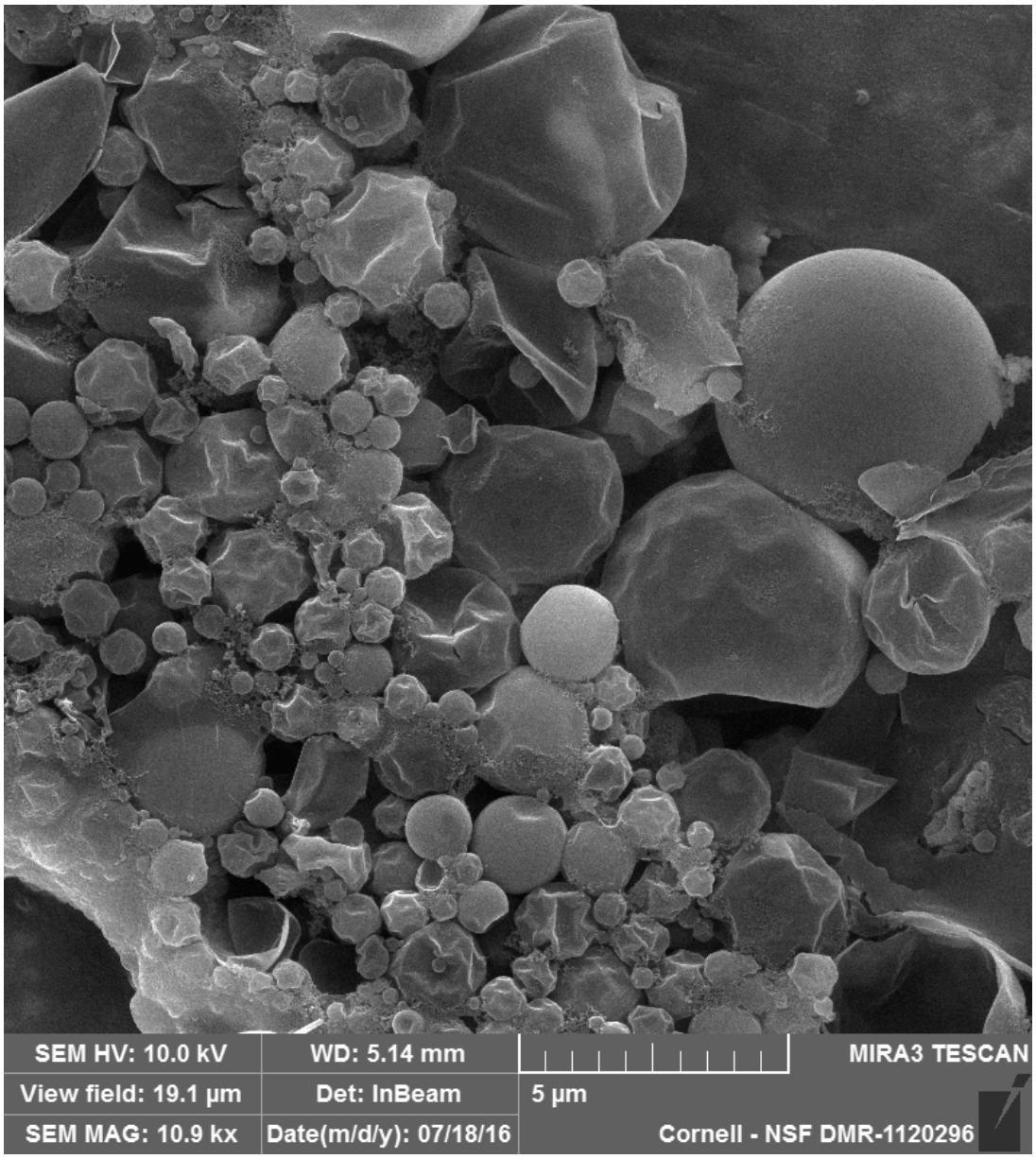

Figure 63. SEM images of microcapsules created using 800 RPM and an axial flow rate of Rez = 36

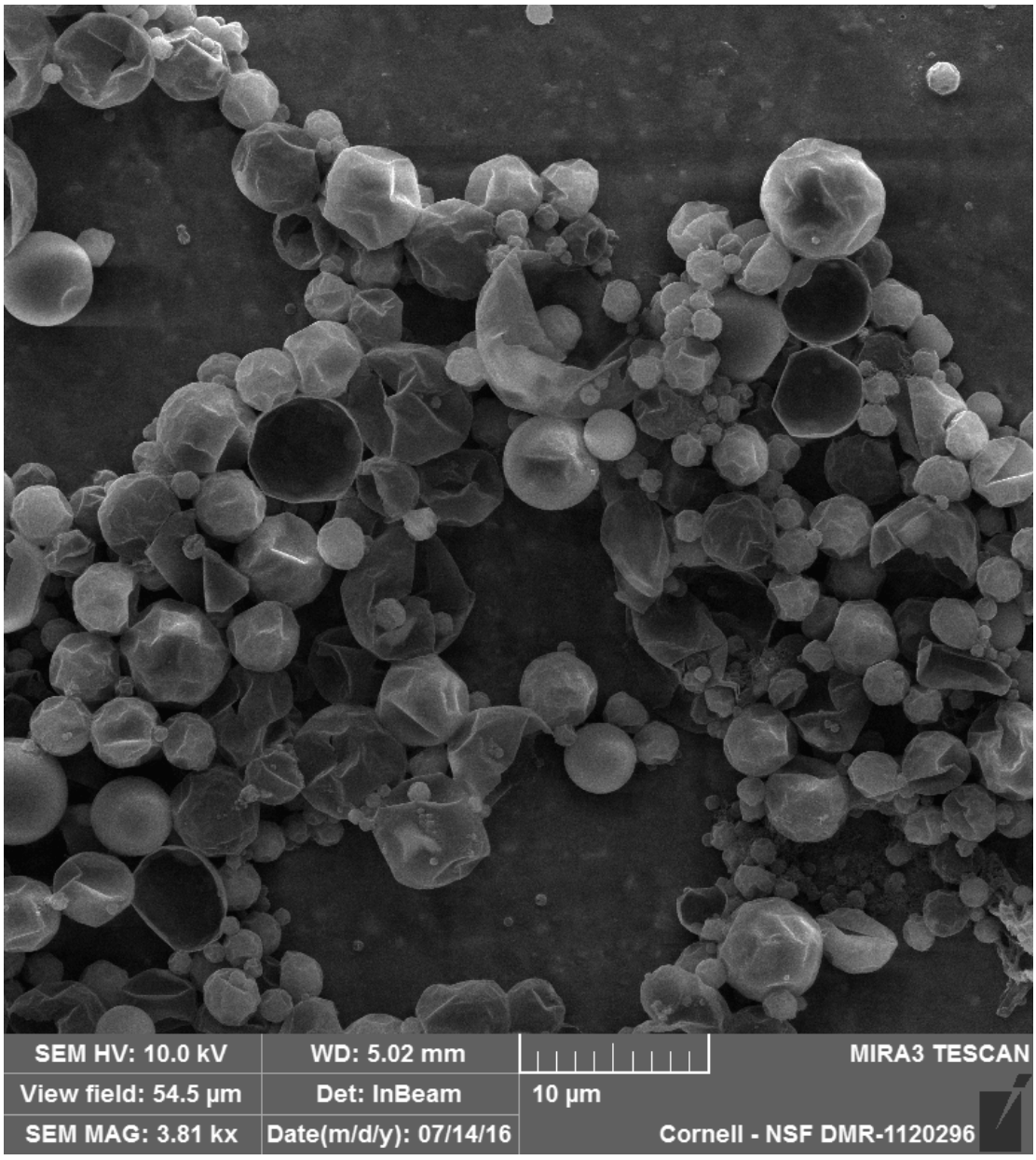

Figure 64. SEM image of microcapsules created using 500 RPM and an axial flow rate of Rez = 72.9

EDS Images for silica microcapsules

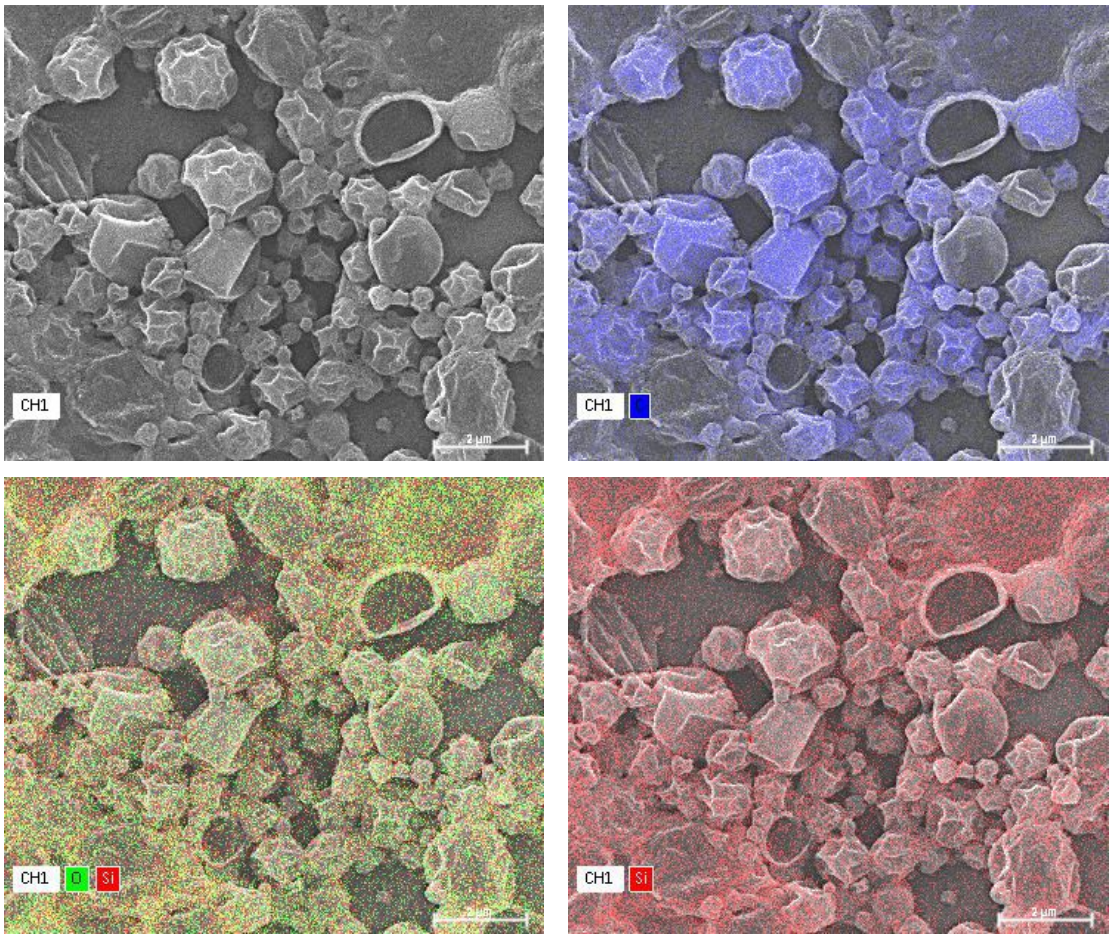

Figure 65. EDS images showing encapsulation for 200 RPM, Rez = 36

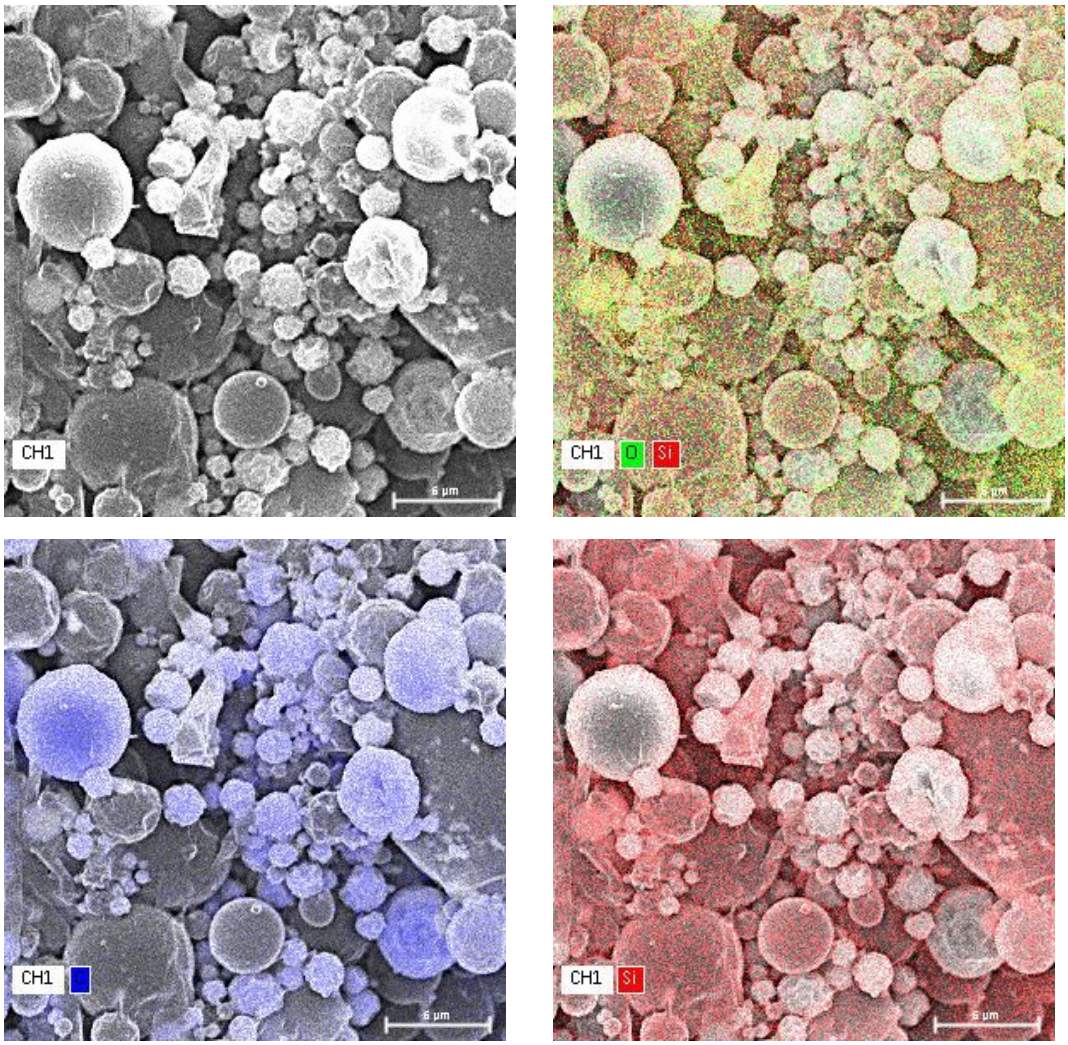

Figure 66. EDS Images showing encapsulation for 1100 RPM, Rez = 19.3.

REFERENCES

[1] Taylor, G.I. “Stability of a Viscous Liquid Contained between Two Rotating Cylinders.” *Philosophical Transactions of the Royal Society of London* 223 (1923): 289–343. Print.

[2] Couette, Maurice. “Études Sur Le Frottement Des Liquides.” *Annales de Chimie et de Physique* VI (1890): 433–510. Print.

[3] Rayleigh, L. “On the Dynamics of Revolving Fluids.” *Proceedings of the Royal Society A: Mathematical, Physical and Engineering Sciences* 93.648 (1917): 148–154. Web. 21 July 2016.

[4] Mallock, A. “Experiments on Fluid Viscosity.” *Philosophical Transactions of the Royal Society A: Mathematical, Physical and Engineering Sciences* 187.0 (1896): 41–56. Web. 21 July 2016.

[5] Donnelly, Russell J. “Taylor-Couette Flow: The Early Days.” *Physics Today* 44.11 (1991): 32. Web. 21 July 2016.

[6] Woliński, J., and S. Wroński. “Interfacial Polycondensation of Polyarylate in Taylor-Couette-Reactor.” *Chemical Engineering and Processing: Process Intensification* 48.5 (2009): 1061–1071. Web.

[7] Aljishi, Mohammad Fuad et al. “Effect of Flow Structure at the Onset of Instability on Barium Sulfate Precipitation in Taylor–Couette Crystallizers.” *Journal of Crystal Growth* 373 (2013): 20–31. Web.

[8] Judat, Bernd, Anna Racina, and Matthias Kind. "Macro-and Micromixing in a Taylor-Couette Reactor with Axial Flow and their Influence on the Precipitation of Barium Sulfate." Chemical engineering & technology 27.3 (2004): 287-292.

[9] Marchisio, Daniele L., Antonello A. Barresi, and Mirko Garbero. "Nucleation, growth, and agglomeration in barium sulfate turbulent precipitation." AIChE Journal 48.9 (2002): 2039-2050.

[10] Sczechowski, Jeffrey G., Carl A. Koval, and Richard D. Noble. "A Taylor vortex reactor for heterogeneous photocatalysis." Chemical Engineering Science 50.20 (1995): 3163-3173.

[11] Giordano, Raquel LC, Roberto C. Giordano, and Charles L. Cooney. "Performance of a continuous Taylor–Couette–Poiseuille vortex flow

enzymic reactor with suspended particles." Process biochemistry 35.10 (2000): 1093-1101.

[12] Baier, Gretchen. Liquid-liquid extraction based on a new flow pattern: two-fluid Taylor-Couette flow. University of Wisconsin, Madison, 1999.

[13] Fischel, Richard J., and Robert C. Brumfield. "Couette membrane filtration apparatus for separating suspended components in a fluid medium using high shear." U.S. Patent No. 4,755,300. 5 Jul. 1988.

[14] Ameer, G. A., et al. "Regional heparinization via simultaneous separation and reaction in a novel Taylor-Couette flow device." Biotechnology and bioengineering 63.5 (1999): 618-624.

[15] Kang, Sung Hoon et al. “Effect of Taylor Vortices on Calcium Carbonate Crystallization by Gas-Liquid Reaction.” *Journal of Crystal Growth* 254.1-2 (2003): 196–205. Web.

[16] Jung, Wang Mo et al. “Precipitation of Calcium Carbonate Particles by Gasliquid Reaction: Morphology and Size Distribution of Particles in Couette-Taylor and Stirred Tank Reactors.” *Journal of Crystal Growth* 312.22 (2010): 3331–3339. Web.

[17] Jung, Wang Mo et al. “Particle Morphology of Calcium Carbonate Precipitated by Gas-Liquid Reaction in a Couette-Taylor Reactor.” *Chemical Engineering Science* 55.4 (2000): 733–747. Web.

[18] Kataoka, Kunio, et al. "Emulsion polymerization of styrene in a continuous Taylor vortex flow reactor." Chemical Engineering Science 50.9 (1995): 1409-1416.

[19] Dluska, E., and A. Markowska. “One-Step Preparation Method of Multiple Emulsions Entrapping Reactive Agent in the Liquid–liquid Couette–Taylor Flow.” Chemical Engineering and Processing: Process *Intensification* 48.1 (2009): 438–445. Web.

[20] Kim, Jong-Min, et al. "Agglomeration of nickel/cobalt/manganese hydroxide crystals in Couette–Taylor crystallizer." Colloids and Surfaces A: Physicochemical and Engineering Aspects 384.1 (2011): 31-39.

[21] Marcus, Philip S. "Simulation of Taylor-Couette flow. Part 1. Numerical methods and comparison with experiment." Journal of Fluid Mechanics 146 (1984): 45-64.

[22] Wereley, Steven T., and Richard M. Lueptow. "Spatio-temporal character of non-wavy and wavy Taylor–Couette flow." Journal of Fluid Mechanics 364 (1998): 59-80.

[23] Andereck, C. David, S. S. Liu, and Harry L. Swinney. "Flow regimes in a circular Couette system with independently rotating cylinders." Journal of Fluid Mechanics 164 (1986): 155-183.

[24] Wu, Mingming, and C. David Andereck. "Phase dynamics in the Taylor–Couette system." Physics of Fluids A: Fluid Dynamics (1989-1993) 4.11 (1992): 2432-2445.

[25] Wu, Mingming, and C. David Andereck. "Phase dynamics of wavy vortex flow." Physical review letters 67.10 (1991): 1258.

[26] Lim, T. T., Y. T. Chew, and Q. Xiao. "A new flow regime in a Taylor–Couette flow." Physics of Fluids (1994-present) 10.12 (1998): 3233-3235.

[27] Fenstermacher, P. R., Harry L. Swinney, and J. P. Gollub. "Dynamical instabilities and the transition to chaotic Taylor vortex flow." Journal of fluid mechanics 94.01 (1979): 103-128.

[28] Di Prima, R. C., and Harry L. Swinney. "Instabilities and transition in flow between concentric rotating cylinders." Hydrodynamic instabilities and the transition to turbulence. Springer Berlin Heidelberg, 1981. 139-180.

[29] Gu, Z. H., and T. Z. Fahidy. "Visualization of flow patterns in axial flow between horizontal coaxial rotating cylinders." The Canadian Journal of Chemical Engineering 63.1 (1985): 14-21.

[30] Thoroddsen, Sigurdur T., and J. M. Bauer. "Qualitative flow visualization using colored lights and reflective flakes." Physics of Fluids (1994-present) 11.7 (1999): 1702-1704.

[31] Chandrasekhar, S. Hydrodynamic and Hydromagnetic Stability. New York: Dover Publications, 1981. Print.

[32] Snyder, H. A. “Experiments on the Stability of Spiral Flow at Low Axial Reynolds Numbers.” Proceedings of the Royal Society A: Mathematical, Physical and Engineering Sciences 265.1321 (1962): 198–214. Web. 21 July 2016.

[33] KATAOKA, KUNIO, et al. "Ideal plug-flow properties of Taylor vortex flow." Journal of Chemical Engineering of Japan 8.6 (1975): 472-476.

[34] Adrian, Ronald J., and Jerry Westerweel. Particle image velocimetry. No. 30. Cambridge University Press, 2011.

[35] Meeuwse, Marco, John van der Schaaf, and Jaap C. Schouten. "Multistage rotor-stator spinning disc reactor." AIChE Journal 58.1 (2012): 247-255.

[36] Joseph, Daniel D., et al. "Stability of rigid motions and rollers in bicomponent flows of immiscible liquids." Journal of Fluid Mechanics 153 (1985): 151-165.

[37] Joseph, D. D., K. Nguyen, and G. S. Beavers. "Non-uniqueness and stability of the configuration of flow of immiscible fluids with different viscosities." Journal of Fluid Mechanics 141 (1984): 319-345.

[38] Baier, Gretchen, and Michael D. Graham. “Two-Fluid Taylor–Couette Flow: Experiments and Linear Theory for Immiscible Liquids between Corotating Cylinders.” Physics of Fluids 10.12 (1998): 3045. Web. 16 May 2016.

[39] Haas, P. a. “Turbulent Dispersion of Aqueous Drops in Organic Liquids.” AIChE Journal 33.6 (1987): 987–995. Web.

[40] Sathe, Mayur J. et al. “Computational Fluid Dynamics Simulation and Experimental Investigation: Study of Two-Phase Liquid–Liquid Flow in a Vertical Taylor–Couette Contactor.” Industrial & Engineering Chemistry Research 49.1 (2010): 14–28. Web. 16 May 2016.

[41] Campero, Richard John, and R. Dennis Vigil. “Spatiotemporal Patterns in Liquid-Liquid Taylor-Couette-Poiseuille Flow.” Physical Review Letters 79.20 (1997): 3897–3900. Web. 16 May 2016.

[42] Zhu, Xiaoyan, and R. Dennis Vigil. “Banded Liquid–liquid Taylor-Couette-Poiseuille Flow.” AIChE Journal 47.9 (2001): 1932–1940. Web. 16 May 2016.

[43] Zhu, Xiaoyan, Richard John Campero, and R.Dennis Vigil. “Axial Mass Transport in Liquid–liquid Taylor–Couette–Poiseuille Flow.” Chemical Engineering Science 55.21 (2000): 5079–5087. Web. 16 May 2016.

[44] Nandi, Arup, Anurag Mehra, and D. Khakhar. “Suppression of Coalescence in Surfactant Stabilized Emulsions by Shear Flow.” Physical Review Letters 83.12 (1999): 2461–2464. Web.

[45] Rashidnia, N, R Balasubramaniam, and D Del Signore. “Interfacial Tension Measurement of Immiscible Liquids Using a Capillary Tube.” AIChE Journal 38.4 (1992): 615. Web.

[46] Nur, Hadi, Shigeru Ikeda, and Bunsho Ohtani. "Phase-boundary catalysis of alkene epoxidation with aqueous hydrogen peroxide using amphiphilic zeolite particles loaded with titanium oxide." Journal of Catalysis 204.2 (2001): 402-408.

[47] Pfister, G., et al. "Bifurcation phenomena in Taylor-Couette flow in a very short annulus." Journal of Fluid Mechanics 191 (1988): 1-18.

[48] Golubitsky, M., and W. F. Langford. "Pattern formation and bistability in flow between counterrotating cylinders." Physica D: Nonlinear Phenomena 32.3 (1988): 362-392.

[49] I. F. Sbalzarini and P. Koumoutsakos. Feature Point Tracking and Trajectory Analysis for Video Imaging in Cell Biology, Journal of Structural Biology 151(2):182-195, 2005.

[50] Schindelin, Johannes, et al. "Fiji: an open-source platform for biological-image analysis." Nature methods 9.7 (2012): 676-682.

[51] M.V. Smoluchowski, Z. Physik. Chem. (Liepzig), 92 (1917), p. 129

[52] Fickert, Johannes et al. “Design and Characterization of Functionalized Silica Nanocontainers for Self-Healing Materials.” Journal of Materials Chemistry 22.5 (2012): 2286–2291. Web.

[53] Aljishi, Mohammad Fuad, Mayank Jhalaria, and Yong Lak Joo. *Influencing Surface Functionalization of Aluminum Fillers with 3-Methacryloxypropyltrimethoxysilane through the Onset of Instability in Taylor Couette Flow*. N.p., 2015. (In progress).